THE UNIVERSITY OF CHICAGO

FLAVIVIRAL ANTAGONISM OF RIG-I-LIKE RECEPTOR-BASED IMMUNITY

A DISSERTATION SUBMITTED TO
THE FACULTY OF THE DIVISION OF THE BIOLOGICAL SCIENCES
AND THE PRITZKER SCHOOL OF MEDICINE
IN CANDIDACY FOR THE DEGREE OF
DOCTOR OF PHILOSOPHY

COMMITTEE ON MICROBIOLOGY

BY
WILLIAM RIEDL

CHICAGO, ILLINOIS
AUGUST 2020

TABLE OF CONTENTS

LIST OF FIGURES

ACKNOWLEDGEMENTS

I am grateful to my mentor, Michaela Gack, for her guidance and support during my time at the University of Chicago. Without her training, I would lack (amongst many things) the focus and perseverance to have furthered this science. I am especially thankful for her unique ability to respect me as a colleague, yet understand me as a trainee.

I would additionally like to thank my thesis committee–Dominique Missiakas, Glenn Randall, and Raymond Roos–for their questions, their knowledge, their curiosity, their support, and their interest in my success.

Daunting personal endeavors undertaken by oneself can only be completed, and only have meaning, with the support and community given by friends and family. Thank you for the laughs, the smiles, and the gas money.

CHAPTER 1

INTRODUCTION

1.1 Flaviviruses

The genus Flavivirus is a group of vector-borne viruses of the family *Flaviviridae*, primarily transmitted to vertebrate hosts by arthropod vectors including species of mosquitoes and ticks. The family encompasses a number of important human pathogens, including Yellow Fever (YFV), Tickborne encephalitis (TBEV), Japanese encephalitis (JEV), Zika (ZIKV), dengue (DENV), West Nile (WNV) viruses, and the more distantly related Hepatitis C virus (HCV)[1]. The name flavivirus, derived from the Latin "*flavus*" for "yellow", originates from the jaundice symptoms associated with YFV, the prototypical flavivirus[2]. Flaviviruses primarily cause two distinct disease types based on the tropism of the infection: encephalitic symptoms arise due to neurotropic infection, while non-encephalitic symptoms occur due to viscerotropic infection and are often associated with hemorrhagic symptoms[3]. Despite divergent tissue tropisms within this genus, these viruses share a common genome construction; their positive sense, single-stranded RNA (ssRNA) genome (~10-13kb) has a 5′ type I cap structure as well as a 3′ end which lacks a poly A tail, instead terminating in a stable stem-loop structure. The genome encodes 10 genes that are translated into a single polyprotein. The polyprotein is cleaved, both co- and post-translationally, into individual proteins—3 structural and 7 non-structural (NS)—by host proteases as well as the viral protease, NS3, in conjunction with its cofactor NS2B, referred henceforth to as "NS2B-3". NS2B-3 then cleaves itself to generate distinct NS2B and NS3 proteins. Flaviviral NS proteins (NS1, NS2A, NS2B, NS3, NS4A, NS4B, and NS5) have several functions including ones to replicate the viral genome and co-opt or evade host pathways such as the translation machinery or the innate immune system, while the structural proteins (C, prM, E) function to produce infectious virions. Infectious virions are coated in a cell-derived lipid membrane decorated with E and M structural proteins inserted via their transmembrane domains. The mature form of the flaviviral E protein functions as a determinant of cell and tissue tropism, as it coordinates interactions between susceptible host cells and their cognate viral receptor expressed on the cell

surface[2].

The viral receptor and attachment factor(s) expressed on the cell surface differs between flaviviruses. For example, the C-type lectin CD209 antigen (DC-SIGN) enables attachment of DENV and WNV particles to dendritic cells, while the mannose receptor has been described as a bona fide receptor of DENV in macrophage cells[4]. ZIKV entry into glial, placental, and fibroblast cells is mediated by the phosphotidylserine receptor, Axl[5,6].

Upon binding to its cellular receptor, flaviviral virions enter the host cell via receptor-mediated endocytosis, and the viral capsid protein dissociates from the RNA genome in concert with the acidification of the endosome. The genomic material then enters the cytosol and is translated by host ribosomes into a single polyprotein, which is cleaved by host proteases and the viral protease NS3 within convoluted membrane structures derived from the endoplasmic reticulum[7,8]. The virus replicates within vesicle packets composed of membranes associated with host endoplasmic reticulum (ER), and nascent genomic RNA is complexed with capsid protein in the lumen of the ER. The virion assembles and prM undergoes maturation to form the M protein through cellular furin-mediated cleavage as it transits through the trans-golgi network and the secretory pathway, until the virus is released from the host cell[6,7].

1.1.1 Zika virus epidemiology and disease

ZIKV was first identified in 1947 after being isolated from a sentinel rhesus monkey in the Zika forest of Uganda[9]. Prior to the 2000s, sporadic human ZIKV infections emerged along the equator in Africa and Asia. In time, two lineages of ZIKV were identified: the African lineage strain, first discovered in Uganda in 1947, and the Asian lineage strain, first documented in Malaysia in 1966[3]. In 2007, the virus caused an epidemic on the island of Yap, an island of Micronesia in the Pacific Ocean. During this outbreak, ZIKV-associated disease was primarily linked to mild fever and rash[10]. In French Polynesia in 2013, the virus caused a second epidemic[3]. While ZIKV disease primarily manifested as

febrile during this epidemic, a number of cases involving neurological complications were retrospectively linked to ZIKV infection, including Guillain-Barré syndrome in adults[3]. ZIKV was introduced to Brazil between 2013 and 2014, and reached vast public attention when it made its way through the Americas to cause a wide-spread epidemic[3,11]. This third epidemic peaked in 2016, and was cited as an international public health emergency due to the high number of infections and the link to congenital neurodevelopmental defects. Historically, ZIKV infection has been associated with a self-limiting, mild febrile illness that manifests in roughly 20% of infections; primary symptoms are considered to be fever, rash, headache, and conjunctivitis that resolve within a week. In recent epidemics these more mild symptoms have been well documented, but whether due to the scale of outbreak, or novel genetic features of the virus or susceptible population, ZIKV infection has also been associated with severe symptoms in adults including multi-organ failure, meningitis and encephalitis, thrombocytopenia, and Guillain-Barre syndrome[12]. By early 2017 and within 52 countries, there were more than 580,000 suspected cases of ZIKV, and over 2,300 confirmed cases of congenital ZIKV syndrome[3]. During 2017, the epidemic slowed dramatically; likely due to protective herd immunity in afflicted communities[12]. However, it is projected that over 2 billion people live in areas that are hospitable to ZIKV transmission, where a large portion of this population is naïve to ZIKV[13]. For these reasons, ZIKV remains a significant hazard to human health.

The two extant lineages of ZIKV, the African and Asian lineages, differ by 10% at the nucleotide level[12]. Strains circulating in the Americas responsible for the most recent epidemics are descended from the Asian lineage. Both lineages of the virus are primarily spread by the bite of infected *Aedes* spp. mosquitos, namely *Aedes aegypti* and *Aedes albopictus*[14], but ZIKV has also been spread by blood transfusion. In contrast to other flaviviruses, ZIKV can be spread via direct human-to-human transmission, i.e. vertical spread and sexual contact[15–17]. In recent epidemics, vertical intrauterine infection has been linked to a group of congenital malformations termed congenital ZIKV syndrome: namely, microcephaly and cerebral calcification[12]. One recent study used mathematical

modeling to estimate that transmission of the virus via sexual contact accounts for approximately 3% of total ZIKV transmission[18].

ZIKV has been shown to infect a number of different human cell types. In the nervous tissue, ZIKV infects neural progenitor cells (NPCs) and astrocytes in cell culture, as well as NPCs and mature neurons in embryonic mouse models[16,19,20]. In human samples, ZIKV RNA has been isolated from multiple human placental cell types, blood from the umbilical cord, and embryonic human brain tissue[21]. *In vitro*, placental Hofbauer and trophoblast cells sustain ZIKV infection. Viral RNA has been recovered in a number of human sample types, suggesting even greater tissue tropism; mouse studies have revealed that ZIKV is shed in tears, and viral RNA can be recovered from human conjunctival fluid[16]. Furthermore, ZIKV RNA can be detected in the sperm or semen of infected males as well as within female cervical mucus, and male-to-female as well as female-to-male transmission has been documented[16].

Of the unique ZIKV traits associated with the virus in recent epidemics, perhaps the most distinct is the incidence of microcephaly in newborns infected with the virus *in utero*. One explanation for the incidences of ZIKV-associated microcephaly is inhibition of differentiation and apoptosis of neural progenitor cells by ZIKV in the fetal brain[16,19]. This idea is supported by increased cell death upon infection of human neurosphere organoid models, as well as cortical thinning and microcephaly upon intraventricular inoculation of embryonic mice with an Asian lineage strain of ZIKV[19,22].

1.1.2 Dengue virus epidemiology and disease

DENV is considered to be the world's most prevalent arbovirus, accounting for as many as 390 million infections per year worldwide and for more disease than any other arbovirus[23,24]. Like ZIKV, DENV is spread by the bite of infected *Aedes aegypti* and *Aedes albopictus* mosquitos in tropical and subtropical environments[24,25]. *Aedes* mosquito species act as vectors for the spread of DENV between and among its primary non-human

primate and human hosts[23]. Four serotypes of DENV currently co-circulate—serotypes 1, 2, 3, and 4—and many regions have multiple strains circulating at once, an occurrence termed hyperendemicity[23,26]. While primary infection with DENV leads to long-lasting immunity against the serotype responsible for the primary infection, immunity to other serotypes of DENV is not necessarily gained. In fact, secondary heterologous infection may lead to enhanced disease severity due to a phenomenon termed antibody dependent enhancement (ADE)[27], wherein sub-neutralizing levels of heterotypic antibody bind to and facilitate uptake of infectious virions into permissive immune cells. It is thought that ADE thereby promotes a hyperactive immune response and subsequent severe disease as described below[26,27].

DENV primarily infects monocytes, macrophages, and dendritic cells[28]. In its search for subdermal blood vessels, a DENV-infected mosquito can transmit the virus to skin-resident macrophages and dendritic cells[25]. These cell types recruit monocytes and dendritic cells to the dermis, where they are infected with the virus[29]. DCs and macrophages travel to lymph nodes which act as secondary sites of infection, leading to a high viral titer in the blood (viremia)[25].

Infection with DENV has an incubation period of 4-10 days, and symptomatic infection can cause dengue fever, an acute febrile disease with symptoms of fever, joint pain, and rashes[23,25]. The symptomatic phase of dengue fever typically lasts between 2-7 days. During some infections (<1%), the disease advances to a more severe state—dengue hemorrhagic fever (DHF)—characterized by a sudden high fever, hepatitis, thrombocytopenia, and hemorrhagic manifestations[25,26]. DHF can progress to dengue shock syndrome (DSS), characterized by vascular leakage and subsequent sudden drop in blood pressure. Disease manifestation is thought to be driven by immunopathogenesis in response to viral infection, rather than directly by viral replication[30].

1.1.3 West Nile virus epidemiology and disease

West Nile virus (WNV) was first isolated from an infected woman with a febrile illness in 1937 in the West Nile district of northern Uganda[31]. Minor and infrequent outbreaks of mild WNV disease occurred throughout the 1900s in Africa and Europe. In the mid to late 1990s, WNV began to cause outbreaks of enhanced disease severity in Africa, Europe, North America, and the Middle East, signaling a shift in the pathogenesis of the disease. In particular, in 1999, WNV spread to New York state and caused significant morbidity, including 78 cases of encephalitic infection in New York City, and overall caused 132 non-fatal cases and 18 fatal cases of WNV infection. Furthermore, retrospective serological surveys suggest that a significant number of asymptomatic cases went undetected at the time[31]. Because of the high incidence of morbidity and mortality caused during this outbreak, the strain isolated, NY99, is classified as a BSL3 pathogen. Following its introduction in New York, the virus spread throughout the United States and is now endemic to North America, as well as parts of South and Central America. In 2003, it was estimated that there were roughly 750,000 undiagnosed infections in the US alone[32]. In 2018, the CDC reported more than 2,600 cases of symptomatic WNV infection in the US.

WNV is primarily transmitted by the bite of an infected *Culex* species mosquito (e.g. *C. univitattus, C. pipiens*). Bird species of the Corvidae family (e.g. jays and crows) are thought to be primary reservoirs of WNV in the US[31]. Humans and horses are considered terminal hosts—i.e. hosts in which the virus causes low level, transient viremia, and are not considered able to sustain the virus in a population for extended periods of time. Because avian species support high levels of viremia, human and horse disease incidence correlates with increased avian infection. Accordingly, crow mortality is an established epidemiological indicator used to predict imminent increased incidence of disease in humans[33].

Following initial transmission of the virus from an infected mosquito to a human, WNV proliferates in Langerhans dendritic cells[34]. These immune cells then drain to nearby

lymph nodes, from which the virus disseminates via the blood to the spleen and kidneys[32]. In instances of severe encephalitic disease, WNV crosses the blood brain barrier and infects the CNS, replicating primarily within neuronal and glial cells. Following successful neuronal invasion, WNV utilizes axonal transport machinery to traffic through the long neuronal axoplasm, and then infects neighboring neurons transsynaptically[35]. The probability of WNV neuronal invasion is thought to be correlated to the level and duration of viremia[31].

Despite being terminal hosts of WNV with generally low levels of viremia, infection with the virus leads to symptoms in about 20-30% of cases of human infection. Symptomatic infections typically manifest 2-14 days after the mosquito bite as a non-specific self-limiting febrile illness with symptoms including fever, muscle and joint pain, headache, and fatigue. A subset of these symptomatic cases (about 1 in 150) can progress to enhanced disease severity caused by neuroinvasive infection, and is characterized by acute flaccid paralysis, meningitis, encephalitis, and respiratory failure[31].

1.1.4 Powassan virus epidemiology and disease

Powassan virus (POWV) was first identified in 1958 after being isolated from the brain tissue of a child from Powassan, Ontario, who died from encephalitis caused by the virus[36]. POWV is a member of the tick-borne encephalitis serocomplex—a group of serologically similar tick-borne flaviviruses (TBFVs). However, POWV is the only tick-borne flavivirus that circulates naturally in North America. The virus also circulates in parts of Russia[37]. POWV causes sporadic disease in humans—there were 27 cases between 1958-1998, and 98 cases between 1999-2016[38]. Although infrequent, the incidence of disease appears to be increasing in North America, and POWV disease has a case fatality rate of 20-30%, and long-term neurological sequelae are common in survivors[37,38].

Similar to WNV, TBFVs like POWV infect humans only as terminal hosts, due to transient and low-levels of viremia. In mouse models of infection, POWV is spread from the

tick to the host within 3 hours after the bite has occurred, but can occur as quickly as 15 minutes[39–41]. This is in contrast to the many hours required for successful transmission of the etiologic agent of Lyme disease, *Borrelia burgdorferi*. There are three major tick species which are thought to transmit POWV strains in the US: *Ixodes scapularis, Ixodes cookie*, and *Ixodes marxi*[38]. These three ticks have divergent vertebrate host preferences, and POWV strains differ along these lines of preference[37]. In fact, POWV strains are classified into two lineages, I and II. Lineage I circulates in North America and Russia, while lineage II circulates only in the US and Canada, and has also been called Deer tick virus (DTV)[37,41,42]. Lineage II strains are therefore called DTV-like. Serologically similar, the two lineages of POWV differ in the length of the 3′-UTR, and have some amino acid substitutions at cleavage sites. Lineage I strains also have two initiation codons for the C protein[37,43]. The first identified strain of POWV, strain LB, is a lineage I strain. Lineage I strains of POWV are carried by *I. cookie* and *I. marxi* species of ticks, which display specific host preferences for the groundhog and skunk, or the red squirrel, respectively. Lineage II strains are primarily carried by *I. scapularis*, which has a broader range of hosts and is considered more aggressive in biting humans, and is considered to be a major source of human infections with POWV[37]. Over their 2 to 3 year lifespan, *Ixodes* spp. ticks will infect one to three hosts[38].

POWV, like other vector-borne flaviviruses, replicates near the site of infection before being disseminated to draining lymph nodes. In a mouse model, the virus was shown to replicate in macrophages and fibroblast cells proximal to the tick bite[41]. POWV is thought to behave similarly to TBEV, which is carried to nearby draining lymph nodes by macrophage and dendritic cells, thereby seeding lymph nodes with virus and causing subsequent viremia[37]. During the viremic stage, neurotropic flaviviruses (including WNV and POWV) cross the blood-brain barrier to infect the central nervous system (CNS). Immunohistochemistry of human brain tissue staining following autopsy has demonstrated that POWV infects neurons, although the full range of cell types infected by POWV in the CNS requires further investigation[44,45].

Serological data from endemic areas during the period of 1958-1998 demonstrated a low number of silent infections with POWV, but incidence of symptomatic infection has increased over the past two decades[38,44]. Symptomatic infection may manifest 8-34 days after infection typically as a febrile illness (prodrome phase), but can progress to more severe neurological symptoms where the most common symptom is encephalitis[38,44]. The exact percentage of patients whose symptoms advance to this state is unclear, but in a recent case study of 9 patients, 7 had encephalitis and one case was fatal. Therefore, the case fatality rate is estimated to be approximately 10%. However, roughly 50% of those survivors had long-term neurological sequelae[44,45].

1.1.5 Treatment of flaviviruses and vaccine outlook

A significant portion of the world is at risk for flavivirus infection. Moreover, in much of the world, multiple flaviviruses are circulating endemically at once. Therefore, the control of these viruses—through vector control and prophylactic measures—and enhanced treatment of viral disease remains of paramount importance to the global community.

Flaviviruses are not the only arboviruses and pathogens spread by mosquito vectors; Alphaviruses, including Chikungunya and Eastern / Western equine encephalitis viruses, and members of the *Bunyaviridae*, including La Crosse and Rift Valley fever viruses, as well as malaria-causing *Plasmodium* spp. parasites can all be transmitted by the bite of an infected mosquito[46]. Furthermore, ticks are capable of transmitting a number of flaviviruses (TBEV and POWV included), as well as non-viral disease, namely, Lyme disease in the U.S. Therefore, mosquitos and ticks represent a significant threat to human health through a capacity to transmit myriad diseases. It follows that vector control should remain an important aspect of the fight against arboviruses and other arthropod-borne pathogens. Vector control efforts encompass a wide range of techniques, including screens to enclose rooms and larval source reduction[23], to more advanced techniques like biological control programs (e.g. sterile insect technique and cytoplasmic incompatibility through *Wolba-*

chia species). However important as well as promising, these efforts have been detailed elsewhere[46,47] and will not be discussed further.

Several flaviviruses have been successfully controlled through the utilization of vaccines, including YFV, TBEV, and JEV. The most successful of these vaccines is the 17D vaccine strain of YFV, a virus that had been passaged 128 times in chicken embryo tissue, resulting in a loss of pathogenicity and mosquito transmissibility. This highly immunogenic vaccine results in lifelong immunity with minimal symptoms and adverse events[48]. While there is not a licensed vaccine for use in humans, vaccination against WNV in horses has been another successful endeavor—a formalin-inactivated vaccine and a canarypox chimeric vaccine were introduced in the early 2000s and have effectively decreased WNV disease incidence in horses. ChimeraVax, a chimeric vaccine against WNV utilizing the YFV 17D backbone (an approach used with success in JEV vaccination) is a live-attenuated vaccine which has passed phase II clinical trials in humans[48]. Vaccination against DENV has proved a more complex problem due to the 4 serotypes which circulate, and the additional risk of ADE. Dengvaxia, a quadrivalent vaccine consisting of four monovalent chimeric attenuated viruses expressing the DENV prM and E proteins with YFV 17D NS backbone, has been licensed in Mexico, Brazil, El Salvador, Paraguay, and the Philippines. After a 3 dose regimen in a phase III trial, Dengvaxia provided only a 60% efficacy against the four serotypes of DENV overall after a one-year period[48–50]. Due to the challenges associated with ADE in secondary heterologous DENV infection, this figure is insufficient to provide the necessary protection, especially given that better outcomes were seen for non-naïve DENV vaccinees[48]. Therefore, other DENV vaccines are currently in clinical trials. No vaccines have been licensed for use against ZIKV infection, although a number of candidates are in clinical trials using various platforms of delivery—DNA-based vaccines, mRNA-based vaccines, as well as live-attenuated and formalin-killed ZIKV vaccines are in development[48]. Due to shared antigenicity of their E protein, it has been demonstrated that immune-plasma against WNV and DENV enhanced ZIKV infection in a mouse model, suggesting that there may be further complications in immunization cam-

paigns in areas where these flaviviruses co-circulate[51].

1.2 Innate immune recognition of intracellular RNA: Mechanisms, regulation, and viral evasion thereof

1.2.1 The type I interferon (IFN-I) system

The human innate immune system has evolved to swiftly counter viral infection and trigger a highly-specific adaptive immune response. Viral infection is detected by a variety of intracellular sensors that act to induce the production of type I interferons (IFN-I). IFN-I are cytokines which, when secreted, activate the innate immune response through the production of viral restriction factors and also help with the recruitment of innate and adaptive immune cells, effectively creating an antiviral state within infected and nearby cells. Rampant and unregulated innate immune activation and signaling can be exceedingly detrimental to the host, and responses to viral infections are therefore meticulously controlled.

The human genome encodes for a number of different IFN-I cytokines, including IFNβ and 13 types of IFNα, which are secreted by infected and neighboring cells during viral infection. Secreted IFN-I cytokines signal in an autocrine or paracrine mode by binding to and activating the interferon-α/β receptor (IFNAR), which then amplifies signaling through the JAK-STAT pathway. JAK-STAT signaling leads to the formation of the IFN-stimulated gene factor 3 (ISGF3) transcriptional complex, which binds to the IFN-stimulated response elements in the genome to induce the expression of antiviral genes termed IFN-stimulated genes (ISGs)[52,53]. ISGs are more than 300 genes that have a wide array of antiviral activity. Some cellular sensors of microbes (e.g. RIG-I and MDA5) are themselves ISGs, thereby enhancing cell sensitivity to viral infection. Other ISGs, such as *OAS, RNase L, MX1*, and *ISG54* (IFIT2) have direct antiviral activity and target steps of the viral life cycle. Others, such as *CCL5, IL-6*, and *IL-8* are cytokines and chemokines that enhance antiviral

signaling to other cell types[54].

1.2.2 Detection of viral PAMPs and IFN induction mechanisms

The expression of IFN-I is induced after detection of pathogen-associated molecular patterns (PAMPs) by pattern recognition receptors (PRRs). PAMPs are conserved features of microbial genomes, proteins, or other molecules that are distinct from host features in either their appearance or localization. Furthermore, PAMPs are inherent to molecules essential to the life cycle of the microbe. For example, viral genomic material (DNA or RNA) can be detected based upon its unique appearance in comparison to host genomic material (e.g. lacking a 5′ cap structure and displaying an exposed 5′ triphosphate moiety (ppp) or based upon its localization (e.g. within endosomes or the cytosol). PRRs act to detect these conserved features and activate convergent signaling pathways that induce IFN-I gene expression.

Intracellular viral genomic material is the primary PAMP detected during viral infection, and is largely detected by three classes of pattern recognition receptors—Toll like receptors (TLRs), the cGAS-STING pathway, and the RIG-I-like receptors (RLRs).

The TLRs detect many different classes of PAMPs—including PAMPs of both bacteria and viruses—and are primarily expressed in innate-like lymphocytic cells, such as neutrophils and macrophages[55]. The major TLRs that sense viral nucleic acid derivatives are TLR3 (dsRNA), TLR7 (U-rich ssRNA), TLR8 (GU-rich ssRNA), and TLR 9 (unmethylated CpG DNA)[52,56]. TLR3, -7, -8, and -9 transition along the endocytic pathway to detect nucleic acids within acidified endolysosomes[52,56]. TLRs signal through the adaptor molecules MyD88 (TLR7, TLR8, TLR9) or TRIF (TLR3) to trigger the gene expression of IFN-I[56].

cGMP-AMP (cGAMP) synthase (cGAS) was only recently identified as a bona fide sensor of cytosolic, intracellular DNA[57]. Upon binding to ds- or ssDNA, cGAS gener-

ates the small cyclic di-nucleotide cGAMP, which then binds to and activates the ER-resident protein STING, resulting in subsequent IFN-I induction[58,59]. Although a sensor of DNA, the cGAS-STING pathway has been implicated in the detection of flavivirus infection, namely through the detection of mislocalized host DNA during DENV infection[60–63].

The RIG-I-like receptors (RLRs) are comprised of three RNA helicases—retinoic acid inducible gene I (RIG-I), melanoma differentiation-associated protein 5 (MDA5), and laboratory of genetics and physiology 2 (LGP2)–that recognize RNA within the cytosol. Upon binding to dsRNA, RIG-I and MDA5 become activated and are relocalized to the mitochondrial-associated membrane, where they interact with the mitochondrial antiviral-signaling (MAVS) protein. MAVS is localized to the outer mitochondrial membrane, the mitochondrial- associated membrane (MAM) of the ER, as well as peroxisomes. At these membranes, MAVS acts as a signaling platform to amplify RLR signaling pathways. Upon activation through interactions with RIG-I or MDA5, MAVS forms higher-order oligomeric structures to recruit members of a signaling complex including TBK1 and IKKϵ[52,64]. This signalosome complex in turn recruits and activates the cytosolic and nuclear-localizing transcription factors IRF3 and IRF7, as well as NFκB which upregulate genes encoding IFN-I and antiviral signaling molecules[53].

1.2.3 RLR structure, ligands, and signaling

The three RLRs are structured similarly, each consisting of a central helicase domain that recognizes RNA flanked by a carboxy-terminal regulatory domain (CTD or RD). RIG-I and MDA5 also have an N-terminal domain that is comprised of tandem caspase-activation recruitment domains (CARDs), which are important for conferring signaling. LGP2 lacks these N-terminal CARDs and is therefore thought to regulate the activation of RIG-I and MDA5, rather than directly signal to downstream IFN activation pathways. Despite a similar structure, RIG-I and MDA5 display divergent binding preferences for RNA ligands, and can therefore sense distinct groups of viruses. However, in some cases, RIG-I and MDA5

are capable of sensing the same virus. For example, many flaviviruses are detected by both RIG-I and MDA5[52,53].

In terms of RLR-specific ligands, RIG-I binds to short stretches of dsRNA (between 10 and 300bp) with marked characteristics of viral RNA, including exposed 5′ tri- or di-phosphate ends. In most cases, RNA-ligand recognition is believed to be sequence-independent; however, certain viral RNAs with an enrichment of poly-U/UC or AU sequences showed efficient RIG-I activation ability[52,65,66]. This diverse set of binding parameters enables RIG-I to interact with RNA of multiple viral species, including the panhandle structure of influenza A virus (IAV) genomic RNA harboring a non-methylated 5′ triphosphate[66–68]; transcription products from measles virus (MeV) and Sendai virus (SeV)[69]; as well as polyU/UC rich regions of hepatitis C virus (HCV) genomic RNA[52,70].

RIG-I does not exclusively bind to viral RNA, as recent studies have shown that host RNA can also directly activate RIG-I. For example, the ISG oligoadenylate synthase (OAS) detects viral nucleic acids and produces an RNA species, 2′, 5′-linked adenylate. RNaseL cleaves these self-RNA species, and the cleavage products can bind to and activate RIG-I[71]. RIG-I has also been shown to bind to a host 5S ribosomal RNA pseudogene (*RNA5SP141*) transcript during herpes simplex virus 1 (HSV-1), Epstein-Barr (EBV), and IAV virus infection. Infection with these viruses promotes shuttling of *RNA5SP141* from the nucleus to the cytosol, and virus-mediated host shutoff of protein synthesis leads to rapid turnover of *RNA5SP141*-interacting proteins. Exposed *RNA5SP141* then binds to RIG-I and triggers IFN-I induction[72]. Altogether, RIG-I can be activated by a distinct array of cytoplasmic RNA during viral infection.

Although activation of MDA5 is less well understood than RIG-I, it is thought to bind long stretches of dsRNA (>1000bp) at internal positions, where the best understood ligand of MDA5 is the synthetic dsRNA polyriboinosinic:polyribocytidylic acid (polyI:C)[52,73]. Initially, MDA5 was characterized as a sensor of *Picornaviridae* infection. MDA5-deficient

mice are highly susceptible to encephalomyocarditis virus (EMCV) infection and unable to initiate IFN-I induction following infection[69,73]. Furthermore, cells deficient in MDA5 had a delayed IFN-I induction upon infection with Newcastle disease virus (NDV) and SeV, two paramyxoviruses[74].

After detecting an RNA ligand, activation of and signaling through the RIG-I pathway are tightly coordinated through protein-protein interaction as well as reversible post-translational modification of key molecules. In the inactivated state, RIG-I is phosphorylated at two residues within the CARD domain, S8 and T170, and three residues in the CTD/RD, T770, S854, and S855 which hold RIG-I in an autorepressed state and prevent it from interacting with downstream binding partners[75,76]. Upon binding to dsRNA, RIG-I is dephosphorylated at S8 and T170 by PP1α or PP1γ and is further dephosphorylated in its CTD, enabling RIG-I to adopt an open conformation[77,78]. RING finger protein leading to RIG-I activation (Riplet) then mediates the K63-linked ubiquitination of RIG-I at K788 in the C-terminal RD, thereby promoting an interaction between RIG-I and TRIM25 essential for RIG-I signaling activity. TRIM25 is activated by binding RNA, and thereafter mediates K63-ubiquitination of RIG-I K172 in the CARDs to enable a conformational change of the CARDs, ultimately allowing CARD-CARD interactions with other proteins and RIG-I mediated signaling[79–83]. In addition to promoting the RIG-I-TRIM25 interaction, release of the RD-mediated auto-repressed state promotes an interaction between the RIG-I CARD domain and the scaffold protein 14-3-3ϵ[84]. Together with TRIM25, RIG-I and 14-3-3ϵ form a ternary translocon complex necessary for the relocalization of active RIG-I from the site of infection to the downstream site of signaling, primarily the outer membrane of the mitochondria and MAM[85]. The formation of this ternary complex is essential for the downstream interaction between RIG-I and MAVS that further develops the nascent antiviral signaling[84].

In resting cells, MDA5 is held in an inactivated state by phosphorylation at S88. Upon binding to ligand RNA, MDA5 is dephosphorylated by PP1-α or PP1-γ, which is critical for

subsequent MDA5 filament oligomerization and downstream activation of MAVS[78]. Upon dephosphorylation, MDA5 binds to 14-3-3η and is re-localized to the mitochondria and MAM where it can interact with and initiate signaling through MAVS. Interaction with 14-3-3η is crucial for the re-localization of activated MDA5 to the mitochondria and downstream MAVS-mediated IFN-I induction[86].

1.2.4 14-3-3 proteins are involved in diverse intracellular processes

The respective RIG-I and MDA5 scaffold proteins 14-3-3ϵ and 14-3-3η are part of the 14-3-3 protein family—in humans, this family has 7 members (β, γ, ϵ, η, σ, θ, ζ). This family of proteins forms homo- or heterodimers to act as adapter and chaperone proteins. 14-3-3 proteins can impart multiple effects on their target proteins and their signaling by altering the conformation of a target protein, by masking localization signals on the target protein, by linking two target proteins, or by blocking interactions between proteins[87]. 14-3-3 proteins largely bind to phosphorylated cellular proteins at the consensus motif Rxx(pT/pS)xP, although a number of variations of this motif have been found to coordinate binding to 14-3-3 proteins[88]. Despite the fact that this family of proteins shares a consensus binding motif on phosphorylated target proteins, 14-3-3 proteins bind to distinct and unique target proteins to regulate an assortment of cellular processes, including cellular metabolism, protein trafficking, DNA replication, innate immunity, and autophagy[84,86,88,89].

1.2.5 RLR detection of flaviviruses

RIG-I and MDA5 share some overlap in the viral pathogens they detect, given the range of RNA species present during distinct phases of the viral life cycle. RIG-I has been shown to be critical in the detection of infection by ssRNA viruses with negative strand genomes (influenza viruses, rhabdoviruses, and arenaviruses) and positive strand genomes (HCV, JEV)[52,53]. MDA5 was first found to be essential in the detection of picornaviruses like EMCV, but has also been shown to be important in detecting MeV, a

paramyxovirus[52,69,90,91]. However, some groups of viruses can be detected by both sensors—including paramyxoviruses, reoviruses, and some flaviviruses[52].

Our understanding of how RIG-I and MDA5 both contribute to establishing antiviral states in flavivirus-infected cells is still evolving. Early characterizations of RLR involvement in specific antiviral responses revealed that RIG-I, but not MDA5, is essential for induction of IFN-I during JEV infection in mouse models[69]. However, loss of both RIG-I and MDA5 expression results in a loss of IFN-I induction during DENV infection, while the single loss of either sensor only moderately attenuates induction of IFN-I[74]. Moreover, it was later shown that both RIG-I and MDA5 are essential for the antiviral response against WNV infection in mice[92]. In human trophoblasts, both RIG-I and MDA5 contribute to ZIKV detection, while in A549 human lung epithelial cells, induction of IFN-I through RIG-I is the dominant signaling mode[93–96]. Because of the multitude of cell types involved in human ZIKV infection, a deeper understanding of how these two sensors contribute to IFN-I induction during natural ZIKV infection is required.

Being that both RIG-I and MDA5 recognize dsRNA and induce signaling through MAVS, it remains enigmatic as to how both sensors are non-redundant and crucial during flaviviral infection. One theory suggests that these two sensors act temporally; RIG-I acts early during infection resulting in an initial wave of IFN-I, which subsequently upregulates MDA5 expression, and MDA5 acts later in infection to amplify this antiviral signaling. This is supported by evidence collected during infection of RIG-I$^{-/-}$ and MDA5$^{-/-}$ mouse embryonic fibroblasts: RIG-I expression was shown to be important for IFN-I induction early in infection, and MDA5 expression appeared more crucial after 24 hours of WNV infection[92]. Exactly how these two sensors participate in concert during the antiviral response during flaviviral infection is still under scrutiny, and the relative roles each sensor plays may differ depending on the cell type as well as the specific flavivirus in question.

Despite the fact that RIG-I and MDA5 are important for controlling many flaviviral in-

fections, the PAMP or PAMPs responsible for activating RIG-I or MDA5 during flaviviral infection is still under investigation. Extensive research has defined the features of RNA that bind to RIG-I, including an exposed 5′ triphosphate moiety. Flaviviruses encode a methyltransferase (NS5) in their limited genome which coordinates capping of the 5′ end. This methyl-guanosine cap therefore prevents activation of RIG-I during infection. However, a recent study utilized RNAseq to demonstrate that RIG-I recognizes the 5′ end of nascent DENV and ZIKV genomic RNA during viral replication, prior to being capped[97]. How RIG-I detects this RNA species while replication occurs in viral-induced membranous compartments remains to be determined. Furthermore, this study was unable to detect flaviviral genomic RNA in complex with MDA5 during infection.

1.2.6 Immune evasion of RLR signaling by flaviviruses

Flaviviruses have evolved a number of unique mechanisms to evade detection by sensors of intracellular RNA, as well as mechanisms to evade downstream IFN-I signaling pathways. Several of these evasion mechanisms are inherent to the flavivirus lifecycle. Many flaviviruses—including DENV, WNV, ZIKV—sequester their replication components inside vesicle packets during active replication. This serves several purposes: to concentrate replication components to increase replication efficiency, as well as to effectively hide RNA replication intermediates from intracellular cytosolic sensors of RNA. JEV does not conceal its dsRNA in human cells, and thereby activates RLRs and subsequent production of IFN-I[98]. Cellular mRNA is preceded by a methyl cap structure, which protects 'self' RNA from degradation by cellular antiviral enzymes. In turn, flaviviruses have evolved to modify their genomes, adding a 2′-*O*-methyl cap to the 5′ end of their genomic material. Viral genomic RNA is modified by the 2′-*O* methyltransferase activity of flavivirus NS5. Loss of this NS5-mediated methyltransferase activity attenuates WNV, DENV, and YFV infection due to an enhanced innate immune response and recognition by IFN-induced proteins with tetricopeptide repeats (IFIT) proteins, a group of ISG protein products with direct antiviral activity[99,100].

Due to their importance in activation of antiviral mechanisms during flavivirus infection, many flaviviruses have evolved mechanisms through which they antagonize RLR signaling—either through direct targeting of RLRs themselves or proteins that RLRs interact with[101]. For example, DENV NS3 was demonstrated to antagonize RIG-I signaling by interacting with the 14-3-3ϵ chaperone protein via a phosphomimetic motif to compete for the RIG-I-14-3-3ϵ interaction, thereby blocking the re-localization of activated RIG-I to the mitochondria. Mutation of the phosphomimetic 64-RxEP-67 motif in DENV NS3 to encode 64-KIKP-67 abrogated the 14-3-3ϵ interaction. WNV NS3 was also shown to bind to 14-3-3ϵ and antagonize RIG-I signaling. Infection of monocytic cells with a mutant DENV deficient in binding 14-3-3ϵ, DENV(KIKP), elicited a markedly enhanced induction of antiviral signaling molecules in comparison to the WT virus. Together, these data indicate that DENV NS3 antagonizes RIG-I signaling by binding to 14-3-3ϵ[102]. Multiple studies have demonstrated that overexpression of DENV and ZIKV NS4A proteins antagonize RLR signaling pathways by antagonizing the RLR-MAVS interactions. Specifically, DENV NS4A was shown to bind and thereby sequester MAVS from an interaction with RIG-I[103]. Similarly, overexpression of ZIKV NS4A in HEK293T cells reduced IFN-I induction upon overexpression and stimulation with RIG-I 2CARD, and antagonized the RIG-I-MAVS and RIG-I-MDA5 interaction[95]. The contributions that DENV and ZIKV NS4A proteins make in evading innate immunity in virally infected cells has yet to be fully understood. Furthermore, mechanisms by which flaviviruses antagonize MDA5 directly are not understood. Given that MDA5 is capable of detecting DENV, WNV, and ZIKV, it stands to reason that these viruses have evolved mechanisms to directly antagonize MDA5. The HCV protease, NS3-4A, cleaves MAVS between its N-terminal signaling domain and the C-terminal transmembrane domain, thereby antagonizing RLR signaling by dissociating MAVS from the mitochondrial membrane[64,104].

Evasion of intracellular immunity is not limited to gene products of flaviviruses, in fact some subgenomic flaviviral RNA (sfRNA) species formed during replication have been shown to antagonize RIG-I signaling. During replication, sfRNA forms via cleavage of the

flaviviral 3′-UTR by the cellular endoribonuclease XRN1. The sfRNA of an epidemic DENV strain was found to bind directly to TRIM25 and prevent efficient RIG-I signaling [105]. sfRNA generated during JEV, WNV, and ZIKV infection have also been found to antagonize IFN-I induction [106–108].

In some cases, flaviviral NS proteins target the machinery responsible for some post-translational modifications of RLRs, which are essential for downstream signaling. HCV NS3-4A, in addition to its role in cleaving MAVS for the mitochondria, targets the E3 ubiquitin ligase Riplet for cleavage and thereby prevents K63-linked ubiquitination of the RIG-I C-terminal domain RD and blocks full-fledged activation of RIG-I [82].

Several flaviviral NS proteins antagonize signaling downstream of the RLR pathways, where multiple antiviral signaling pathways converge. For example, overexpression of ZIKV NS1 and NS4B, DENV NS2A and NS4B, and NS4B of WNV antagonizes signaling at the level of TBK1 [109–111]. Overexpression of the DENV protease, NS2B-NS3, binds to IKKϵ to prevent IFN-I induction [112], while ZIKV NS5 binds to IRF3 to block IFN-I induction [111].

Altogether, flaviviruses are viral pathogens that cause severe disease, in part because they encode within their genomes a wide range of mechanisms to antagonize the RLR-MAVS signaling axis to promote their replication. However, whether these mechanisms are shared between certain members, or whether other flaviviruses encode novel and unique evasion mechanisms requires greater study. Furthermore, an understanding of how POWV evades innate immune signaling is entirely non-existent. The following dissertation aims to elucidate some of these ideas, in the hopes that this research may be used to enhance our treatment of these arthropod-borne pathogens.

CHAPTER 2

ZIKA VIRUS NS3 MIMICS A 14-3-3ϵ BINDING MOTIF TO ANTAGONIZE RIG-I-MEDIATED INNATE IMMUNITY

This chapter is adapted from: Riedl, W.; Acharya, D.; Lee, J.H.; Liu, G.; Serman, T.; Chiang, C.; Chan, Y.K.; Diamond, M.S.; Gack, M.U. Zika Virus NS3 Mimics a Cellular 14-3-3-Binding Motif to Antagonize RIG-I- and MDA5-Mediated Innate Immunity. Cell Host Microbe 2019, 26, 493–503.e6

Attributions: WR performed and analyzed all experiments with the exception of the following: D.A. performed and analyzed Figures 2.1 A, 2.7 B and C, 2.8 B and C. J.-H. L. and D.A. performed and analyzed Figures 2.1 C and D. C.C. generated the MAVS *KO* SVGA cells used in Figure 2.8 B and C.

2.1 Abstract

Mosquito-transmitted flaviviruses, including the recently emergent Zika virus (ZIKV), represent a major human health concern. Detection of viral infection by cellular pattern recognition receptors (PRRs) is a critical first step in generating a type-I interferon (IFN)-mediated antiviral program. RIG-I and MDA5, the PRRs responsible for detecting cytosolic RNA, bind to viral nucleic acid and initiate downstream signaling by interacting with the downstream adaptor protein MAVS. Translocation of RIG-I from the cytosolic site of RNA detection to the mitochondria is mediated by binding to the cellular chaperone 14-3-3ϵ. ZIKV NS3 encodes a phosphomimetic 14-3-3ϵ binding motif (64-RLDP-67) that mediates an interaction between NS3 and 14-3-3ϵ. In the context of viral infection, mutational perturbation of the 14-3-3ϵ interaction site in NS3 spurs an enhanced production of cytokines and impairs ZIKV infection. Our results demonstrate that ZIKV NS3 evades RIG-I-mediated innate immunity through an NS3-14-3-3ϵ interaction, and loss of this evasion ability attenuates viral replication.

2.2 Introduction

ZIKV was first identified in 1947 in Uganda and caused sporadic disease in Africa and Asia in the latter half of the 20th century[3,9]. Similar to DENV, a related flavivirus, ZIKV is transmitted by *Aedes* spp. mosquitos, primarily *Aedes aegypti*. Historically, the virus has caused mild, self-limiting febrile disease. However, recent epidemics of ZIKV disease have been characterized by severe symptoms including encephalitis, thrombocytopenia, and Guillain-Barre syndrome in adults, as well as a suite of symptoms termed congenital Zika syndrome (CZS) in newborn babies. Accordingly, ZIKV has a broad tissue tropism, having been shown to replicate in epithelial tissue in fibroblasts, placental tissue in trophoblasts, neural tissue in astrocytes and microglial cells, and in immune cells including monocytes and dendritic cells[16]. Despite epidemics of increasing size in the recent past, there is no treatment or vaccine available targeting ZIKV.

ZIKV is a member of the *Flaviviridae* family of viruses, a group of positive sense, single stranded RNA viruses transmitted by arthropod vectors. The ~10.8kb genome encodes a single polyprotein cleaved by host and viral proteases into 10 proteins—7 non structural (NS) (NS1, NS2A, NS2B, NS3, NS4A, NS4B, and NS5) and 3 structural proteins (C, M, E). Replication of the virus occurs in the cytosol within membranous structures associated with the endoplasmic reticulum[3]. Recent work has suggested that the genomic material of ZIKV is recognized by a cellular sensor of RNA, RIG-I, during replication prior to the nascent genome becoming capped by the viral methyltransferase[97]. RIG-I, a DEAD-box helicase and innate immune PRR, is activated to induce antiviral signaling after binding to dsRNA in the cytosol[52]. Once activated, RIG-I undergoes a series of activating and reversible post-translational modifications (PTMs) that enable binding to the cellular chaperone protein 14-3-3ϵ, which mediates the re-localization of activated RIG-I to the mitochondria[84]. Mitochondrial membranes act as an antiviral signaling platform by hosting MAVS, the downstream signaling partner of RIG-I. MAVS amplifies RIG-I signaling by recruiting tank binding kinase 1 (TBK1) and activating IFN signaling via IRF3 and IRF7[64,85]. IRF3 and IRF7 act as transcription factors to induce the expression of IFN and pro-inflammatory cytokines, which are secreted from the infected cell. Ultimately, the IFN response induces expression of a suite of interferon stimulated genes (ISGs) to create an antiviral state[54].

Flaviviruses have evolved mechanisms to evade this antiviral IFN response. The specific mechanisms that ZIKV utilizes are not yet fully understood. Here, we demonstrate a mechanism by which ZIKV evades RIG-I-mediated innate immune induction. We show that ZIKV NS3 binds to 14-3-3ϵ to preclude the 14-3-3ϵ-mediated RIG-I cytosol-to-mitochondria translocation, thereby inhibiting downstream induction of IFN, cytokines, and downstream ISGs through the RIG-I pathway. Generation of a mutant ZIKV deficient in this 14-3-3ϵ binding ability further demonstrated that the NS3-14-3-3ϵ interaction is a critical component of the ZIKV innate immune subversion toolkit.

2.3 Results

2.3.1 ZIKV is attenuated by 14-3-3 protein-mediated antiviral gene expression

Members of the 14-3-3 protein family have essential roles in various intracellular pathways, including cell cycling, transcription, apoptosis, and immunity[113]. 14-3-3ϵ is a critical element in the RIG-I-mediated innate immune response to Sendai virus (SeV) and hepatitis C virus (HCV)[84], while 14-3-3η promotes MDA5-mediated innate immune signaling against HCV infection[86]. Therefore, we reasoned that these 14-3-3 proteins would restrict ZIKV replication via their roles in RLR signaling. Ectopic expression of either 14-3-3ϵ or 14-3-3η restricted the replication of ZIKV in human fetal astrocytes (SVGA), while 14-3-3σ did not (Figure 2.1 A). Similarly, expression of 14-3-3ϵ and 14-3-3η in human lung epithelial cells (A549) mirrored the capacity of RIG-I and MDA5 to inhibit ZIKV infection, suggesting that 14-3-3ϵ and 14-3-3η attenuate ZIKV in their roles in RLR signaling (Figure 2.1 B). To formally test this, we silenced 14-3-3ϵ, 14-3-3η, RIG-I, MDA5, and 14-3-3σ in SVGA cells, and then infected these cells with ZIKV. Knockdown of either 14-3-3ϵ or 14-3-3η potently diminished IFNB1, CCL5, IFIT2, and RSAD2 transcript abundance 24 and 48 h post ZIKV infection. Accordingly, silencing of RIG-I or MDA5, but not 14-3-3σ, depleted antiviral gene induction (Figure 2.1 D). Together, these data indicate that 14-3-3ϵ and 14-3-3η promote RLR signaling and are critical for IFN induction during ZIKV infection.

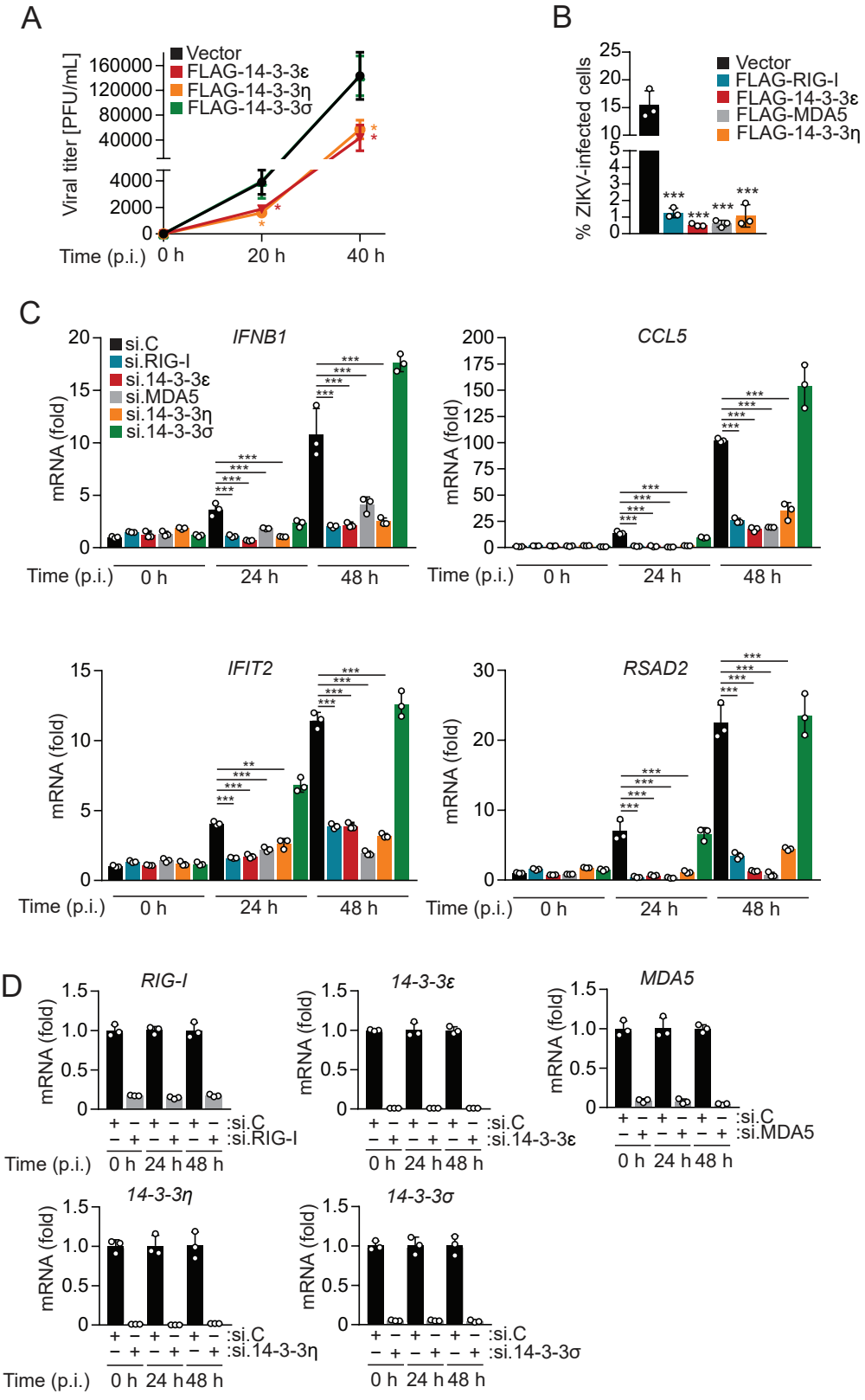

Figure 2.1 14-3-3 proteins inhibit ZIKV replication by mediating antiviral gene expression

Figure 2.1 *(continued)* 14-3-3 proteins inhibit ZIKV replication by mediating antiviral gene expression.
(A) Viral titers, as determined by plaque assay (presented as PFU/mL), in the supernatant of SVGA cells transfected for 30 h with vector or the indicated FLAG-14-3-3 proteins infected at MOI 0.1 with ZIKV (BRA/2015) for the indicated times.
(B) Percentage of ZIKV-infected A549 cells transfected for 42 h with the indicated plasmid, then infected with ZIKV at MOI 0.2 for 48 h, assessed by flow cytometry using α-ZV-2 antibody.
(C) Analysis of the levels of indicated transcripts in siRNA-transfected cells infected with ZIKV at MOI 1 for 24 or 48 h by qRT-PCR.
(D) Knockdown efficiency of the indicated genes for the experiment shown in (C), determined by qRT-PCR and normalized to cellular GAPDH.
Data are expressed as means ± SD (n = 3). *p < 0.05, **p < 0.01, ***p < 0.001 (Student's t test in A); *p < 0.01, **p < 0.001, ***p < 0.0001 (ANOVA in B and C).

2.3.2 ZIKV NS3 encodes a phosphomimetic 'RLDP' motif to bind to 14-3-3ϵ

RIG-I is essential in generating an antiviral response to ZIKV as well as other flaviviruses[92–95,102,114]. It stands to reason that flaviviruses have evolved mechanisms to antagonize RIG-I signaling, whether via targeting RIG-I itself or components of the RIG-I pathway. Indeed, recently published work from our laboratory demonstrated that DENV and WNV NS3 antagonize the RIG-I pathway by targeting the RIG-I-14-3-3ϵ interaction. DENV and WNV NS3 proteins encode phosphomimetic 'Rx(E/D)P' motifs which enable binding and sequestering of cellular 14-3-3ϵ, thereby enabling NS3 to antagonize RIG-I signaling[102]. We compared the analogous 'Rx(E/D)P' region of NS3 in a number of different flaviviruses—interestingly, ZIKV NS3 encodes a conserved phosphomimetic motif matching the 14-3-3ϵ-binding motif in WNV NS3, and similar to that of DENV NS3, which harbors a phosphomimetic Glu (E66) residue instead of D66 (Figure 2.2 A). Furthermore, the 'RLDP' motif of ZIKV is conserved in the NS3 proteins of all ZIKV strains analyzed (a total of 673 strains) (Figure 2.2 B). In contrast, the NS3 proteins of Yellow Fever (YFV), Japanese encephalitis (JEV), Tick-borne encephalitis (TBEV), and the distantly related

Hepatitis C (HCV) viruses do not encode a phosphomimetic motif at the corresponding location (Figure 2.2 A). Accordingly, YFV and HCV NS3 proteins do not bind to 14-3-3ϵ [102].

A

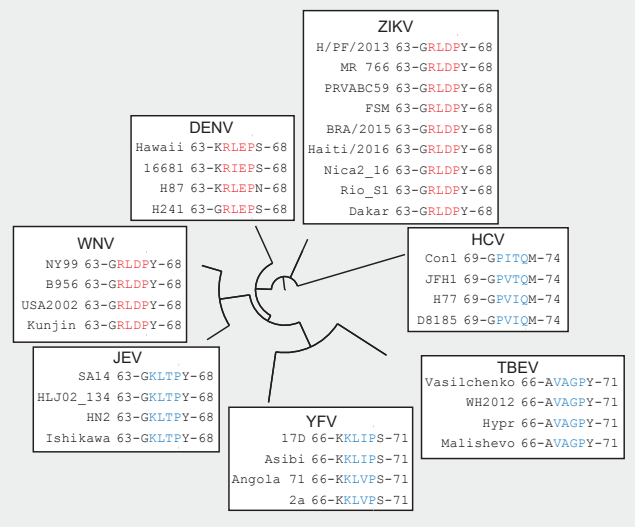

B

Virus	# Sequences analyzed	# Sequences encoding (E/D) in position 3
ZIKV	673	673
WNV	1,798	1,797
DENV	3,280	3,279
HCV	2,132	0
TBEV	199	0
YFV	155	0
JEV	327	0

Figure 2.2 Zika virus NS3 encodes a phosphomimetic 'RLDP' motif.
(A) Cladogram of Flaviviridae family members displaying viral strains and corresponding regions of NS3 encoding the phosphomimetic Rx(E/D)P motif. Phosphomimetic motifs of ZIKV, DENV, and WNV are highlighted in red, while the associated regions of *Flaviviridae* family members JEV, YFV, TBEV, and HCV are highlighted in blue. The cladogram is not to scale.
(B) Summarized sequence analysis of the indicated flaviviral NS3 proteins for the presence or absence of a phosphomimetic (E or D) amino acid in position 3 of the Rx(E/D)P motif at amino acid 64-67 in ZIKV NS3, or the corresponding position in other NS3 proteins, using only complete genomes of viruses from the NIAID Virus Pathogen Database and Analysis Resource (ViPR).

The presence of a potential 14-3-3ϵ-interaction motif in ZIKV NS3 led us to hypothesize that ZIKV NS3 may interact with 14-3-3ϵ and antagonize the RIG-I signaling pathway. Indeed, we found that ZIKV NS3 binds to 14-3-3ϵ in a manner similar to DENV NS3 (Figure 2.3 A), and that mutation of the 'RLDP' motif to 'KIKP', analogous to the DENV KIKP mutant[102] results in a loss of binding to 14-3-3ϵ (Figure 2.3 B). As the prototypical African strain MR 766 differs in pathogenesis from more recent epidemic ZIKV isolates, we next asked if the NS3 proteins from different strains also differ in their 14-3-3ϵ-binding capacity. In contrast to YFV NS3, which does not encode a 14-3-3ϵ-binding motif and thus served as a control, the NS3 proteins of all three ZIKV strains tested (MR 766, H/PF/2013 and BRA/2015) efficiently bound to 14-3-3ϵ and with similar affinity (Figure 2.3 C), suggesting that 14-3-3ϵ binding is a conserved feature of multiple ZIKV strains, even those not associated with severe pathogenesis. In support of these findings, NS3 from the BRA/2015 strain also readily bound to endogenous 14-3-3ϵ during authentic infection of SVGA astrocytes (Figure 2.3 D), and this interaction increased over time (Figure 2.3 E). We found that the presence of ZIKV NS3 obstructed the RIG-I-14-3-3ϵ interaction in a dose-dependent manner, indicating that ZIKV NS3 competes for the RIG-I-14-3-3ϵ interaction (Figure 2.4 A).

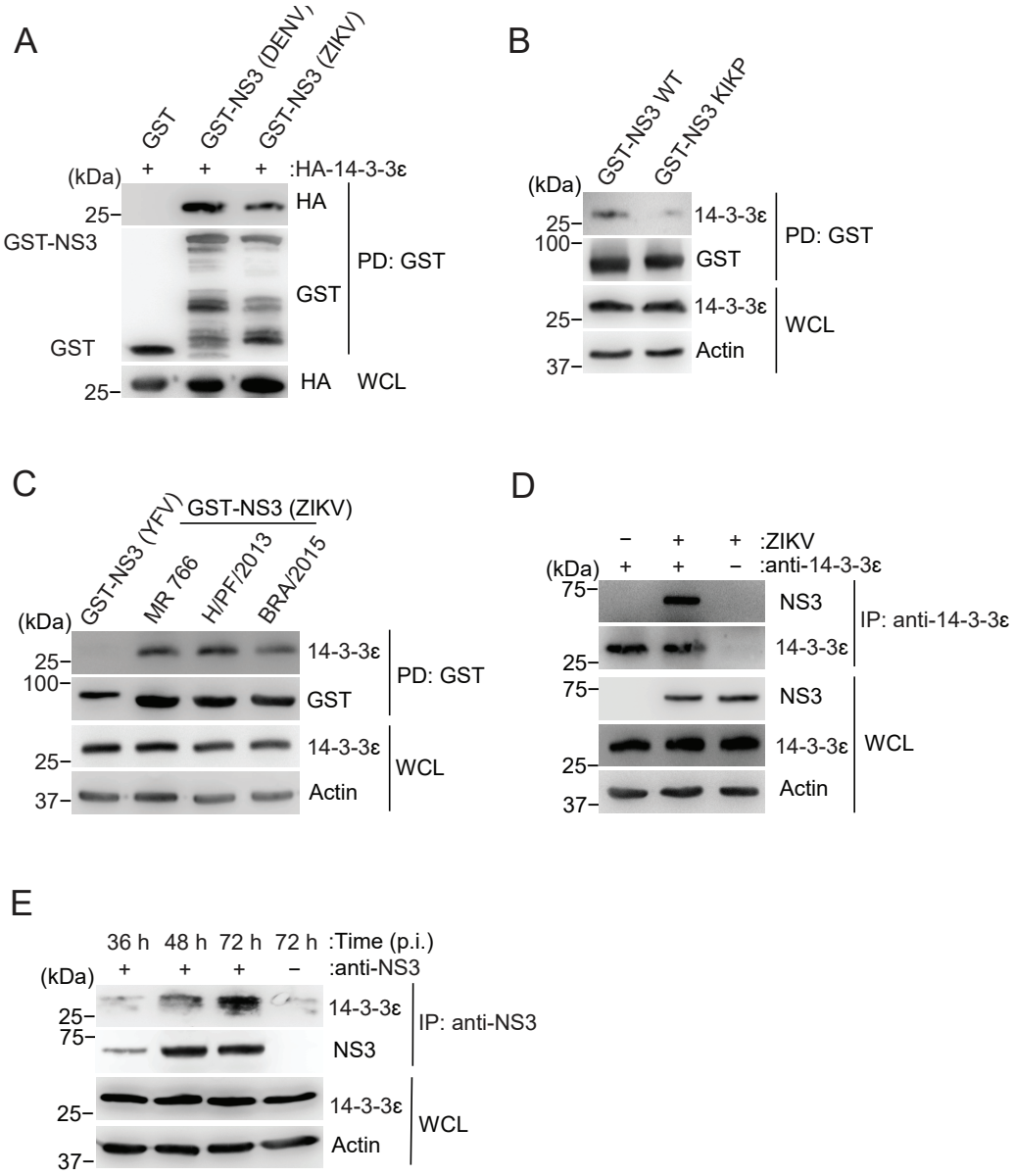

Figure 2.3 ZIKV NS3 binds to 14-3-3ϵ via a phosphomimetic 'RLDP' motif.
(A) GST pull-down of HEK293T cells expressing HA-14-3-3ϵ and GST or GST-NS3 (DENV NGC) or GST-NS3 (ZIKV H/PF/2013) for 42 h, assessed by immunoblot and probed with the indicated antibodies.
(B) GST pull-down of HEK293T cells expressing ZIKV (BRA/2015) GST-NS3 (WT) or GST-NS3 (KIKP) for 42 h assessed as in (B).
(C) GST pull-down of HEK293T cells expressing GST-NS3 of YFV (17D), ZIKV (MR 766), ZIKV (H/PF/2013), or ZIKV (BRA/2015) for 42 h assessed as in (B).
(D) 14-3-3ϵ immunoprecipitation of SVGA cells infected with ZIKV (BRA/2015) at MOI 1 for 48 h, assessed as in (B).
(E) anti-NS3 (ZIKV) immunoprecipitation of SVGA cells infected with ZIKV at MOI 1, harvested at the indicated time points and assessed as in (B).

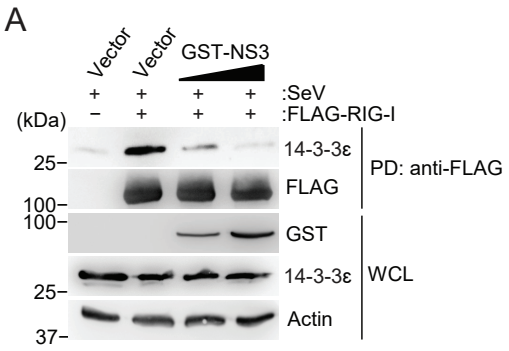

Figure 2.4 ZIKV NS3 competes for the RIG-I-14-3-3ϵ interaction.
(A) anti-FLAG pulldown of HEK293T cells expressing FLAG-RIG-I and increasing amounts of GST-NS3 (BRA/2015) transfected for 42 h then stimulated with SeV (50 HAU/mL) for 22 h. Immunoblot was probed with the indicated antibodies.

2.3.3 ZIKV NS3 antagonizes RIG-I signaling to preclude IFN induction

As 14-3-3ϵ has been shown to bind to RIG-I to mediate its translocation from the cytosol to mitochondria and mitochondria-associated membranes (MAMs) to promote anti-viral signaling[84], we evaluated the frequency of RIG-I mitochondrial translocation in SVGA infected with ZIKV. In cells infected with SeV, RIG-I was localized to the mitochondrial fraction with high abundance. This is in contrast to cells infected with ZIKV where RIG-I presided primarily in the cytosol, and levels of RIG-I at the mitochondria mirrored mock-infected samples (Figure 2.5 A). Therefore, we assessed the effect of ZIKV NS3 on RIG-I-mediated IFN induction through a luciferase reporter assay. In a dose dependent manner, ZIKV NS3 suppressed the induction of IFN when stimulated by SeV, a potent activator of RIG-I (Figure 2.5 B). Similarly, ZIKV NS3 strongly suppressed IFN induction triggered by ectopic expression of RIG-I 2CARD, the constitutively active form of RIG-I[80] (Figure 2.5 C). Moreover, expression of the prototypical African lineage strain (MR 766) NS3 as well as two recently characterized Asian lineage strains of ZIKV (H/PF/2013 and BRA/2015) NS3 proteins were all sufficient to antagonize IFN induction when stimulated by SeV (Figure 2.5 D). Together with the NS3-14-3-3ϵ interaction data, these results suggest that antagonism of the RIG-I signaling pathway is a well-conserved ZIKV evasion mechanism.

In agreement with its ability to block IFN induction, ectopic expression of ZIKV NS3 diminished the SeV-mediated protein expression of ISG15, ISG54, and RIG-I (itself an ISG) (Figure 2.5 E). To further corroborate that ZIKV NS3-mediated antagonism occurs at the level of RIG-I, and not downstream of it, we compared the effect of ZIKV NS3 expression on signaling induced by GST-RIG-I(2CARD) or FLAG-MAVS, which are each sufficient to activate downstream signaling when overexpressed. Ectopic expression of ZIKV NS3 strongly dampened IFN promoter activation (Figure 2.5 C, Figure 2.5 F) induced by RIG-I 2CARD, but had no effect on IFN luciferase activity mediated by FLAG-MAVS (Figure 2.5 F). Taken together, these results indicate that ZIKV NS3 blocks downstream antiviral IFN induction by antagonizing the RIG-I-14-3-3ϵ interaction.

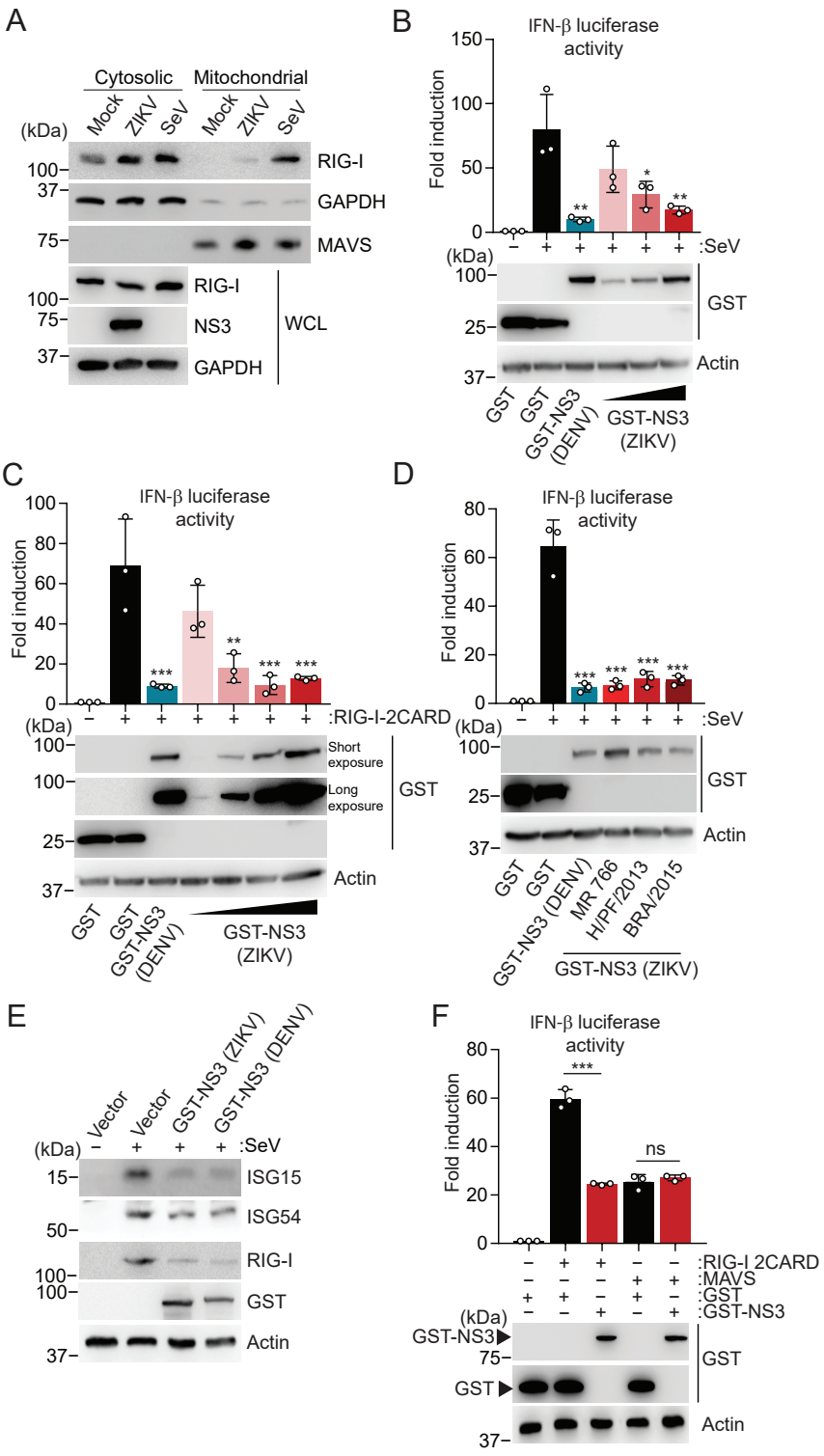

Figure 2.5 ZIKV NS3 antagonizes the RIG-I signaling pathway.

Figure 2.5 *(continued)* ZIKV NS3 antagonizes the RIG-I signaling pathway.
(A) Upper: IB analysis with anti-RIG-I antibody of cytosolic and mitochondrial fractions of SVGA cells mock-infected or infected with SeV (50 HAU/mL) or ZIKV (BRA/2015; MOI 1) for 24 h. Purity of fractions was assessed by IB with anti-GAPDH or anti-MAVS antibodies. Lower: WCL was probed with anti-RIG-I, anti-NS3, and anti-GAPDH.
(B) Upper: IFN-β luciferase activity in HEK293T cells transfected to express a luciferase reporter under control of the IFN- promoter, and GST or GST-NS3 from Dengue virus (NGC) or Zika virus (H/PF/2013) for 40 h, then infected with SeV (50 HAU/mL) for 20 h. Luciferase activity was normalized to the constitutive expression of β-Galactosidase from a plasmid and are represented as relative to untreated GST-expressing cells, set to 1. Lower: IB analysis of WCL with anti-GST and anti-Actin (loading control).
(C) Upper: IFN-β luciferase activity in HEK293T cells transfected for 30 h with a IFN-promoter-driven luciferase reporter and GST-RIG-I-2CARD together with GST or GST-NS3 from Dengue virus (NGC) or increasing amounts of GST-NS3 from Zika virus (H/PF/2013) assessed as in (B) Lower: IB analysis of WCL with anti-GST and anti-Actin (loading control).
(D) Upper: IFN-β luciferase activity in HEK293T cells transfected for 40 h with a IFN-promoter-driven luciferase reporter and GST or GST-NS3 from DENV (NGC) or ZIKV (MR 766, H/PF/2013, or BRA/2015) then infected with SeV (50 HAU/mL) for 20 h and assessed as in (B). Lower: IB probed with anti-GST and anti-Actin (loading control).
(E) Immunoblot analysis of ISG abundance or actin (loading control) of WCL from HEK293T cells transfected with GST or GST-NS3 from ZIKV (H/PF/2013) or DENV (NGC) for 48 h, then infected with SeV (50 HAU/mL) for 24 h, probed with the indicated antibodies.
(F) IFN-β luciferase activity and IB analysis of HEK293T cells transfected with an IFN-promoter-driven luciferase reporter and GST or ZIKV GST-NS3 (H/PF/2013) and either vector, RIG-I-2CARD, or MAVS, assessed as in (B).
Data are expressed as means ± SD (n = 3). *p < 0.01, **p < 0.001, ***p < 0.0001 (ANOVA in B–D), or *p < 0.05, **p < 0.01, ***p < 0.001 (Student's t test in F). ns, not statistically significant.

2.3.4 ZIKV(KIKP) is growth attenuated in A549 cells

Being that the ZIKV NS3 'RLDP' motif is essential for 14-3-3ϵ binding (Figure 2.3 B), and that the RIG-I-14-3-3ϵ interaction is important for RIG-I signaling[84], we reasoned that mutation of this phosphomimetic motif in ZIKV NS3 would result in attenuation of ZIKV due to an inability to sequester 14-3-3ϵ and antagonize the RIG-I antiviral response. We therefore generated a recombinant ZIKV (strain MR 766), termed ZIKV(KIKP), by introducing the mutations R64→K64, L65→I65, D66→K66 into NS3. We first compared the

replication of ZIKV(KIKP) and the parental virus (ZIKV(WT)) in Vero cells, a cell line deficient in type I IFN signaling[115], and found no significant differences between the growth of both viruses over a 72 hour-time course (Figure 2.6 A), ruling out a general growth defect of ZIKV(KIKP). We next assessed replication of ZIKV(WT) and ZIKV(KIKP) in A549 cells, in which RIG-I has been demonstrated to be important in regulating IFN induction in response to ZIKV[93]. We found as much as a 100-fold difference between ZIKV(WT) and ZIKV(KIKP) at 24 hours post-infection, and ZIKV(KIKP) was also attenuated at both 48 and 72 hours. The attenuation of ZIKV(KIKP) was not as strong at 48 and 72 hours post-infection, likely due to saturation of ZIKV(WT) replication by 48 hours in this cell culture assay (Figure 2.6 B). These possibilities were not further explored. This growth attenuation of ZIKV(KIKP) was also demonstrated by flow cytometry, where the percentage of ZIKV-infected A549 cells was significantly lower at 24 and 48 hours post-infection than ZIKV(WT) infected cells (Figure 2.6 C).

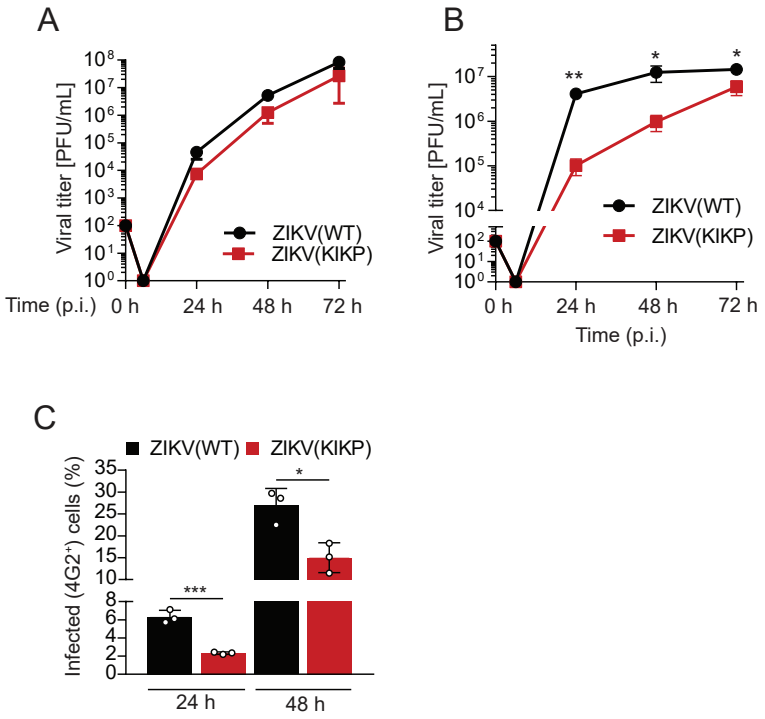

Figure 2.6 ZIKV(KIKP) is growth attenuated in IFN-competent cells.
(A) Viral titer in the supernatant of ZIKV(WT) or ZIKV(KIKP)-infected Vero cells (MOI 0.001). Supernatant was harvested at the indicated time points and viral titer was determined by plaque assay, represented as PFU/mL.
(B) Viral titer in the supernatant of ZIKV(WT) or ZIKV(KIKP)-infected A549 cells (MOI 0.001). Supernatant was harvested at the indicated time points and viral titer was determined by plaque assay, displayed as PFU/mL.
(C) Percentage of ZIKV positive A549 cells infected with ZIKV(WT) or ZIKV(KIKP) (MOI 0.01) for the indicated times, assessed by flow cytometry using an anti-envelope (4G2) antibody.
Data are expressed as means ± SD (n = 3). *p < 0.05, **p < 0.01, ***p < 0.001 (Student's t test).

To formally assess whether the attenuation of ZIKV in A549 and other IFN-competent cell types is due to an enhanced IFN induction, we infected several cell types with ZIKV(WT) and ZIKV(KIKP). In A549, we observed that ZIKV(KIKP) led to greater cytokine transcript expression in comparison to infection with ZIKV(WT), despite the attenuation in growth of ZIKV(KIKP) (Figure 2.6 B; Figure 2.7 A). In particular, expression of *IFNB1* and *CCL5* were significantly upregulated during ZIKV(KIKP) infection, in comparison to ZIKV(WT).

Likewise, we observed enhanced mRNA expression of cytokines *IL-6* and *IL-8*, as well as the ISGs *RSAD2, MX1*, and *IFIT1* during ZIKV(KIKP) infection (Figure 2.7 A). We also assessed induction of antiviral genes in two neuronal cell types—SVGA and HMC3 (microglia). We found that in both cell types, IFN, cytokines, and ISGs were upregulated upon infection with ZIKV(KIKP) in comparison to the parental virus (Figure 2.7 B and C).

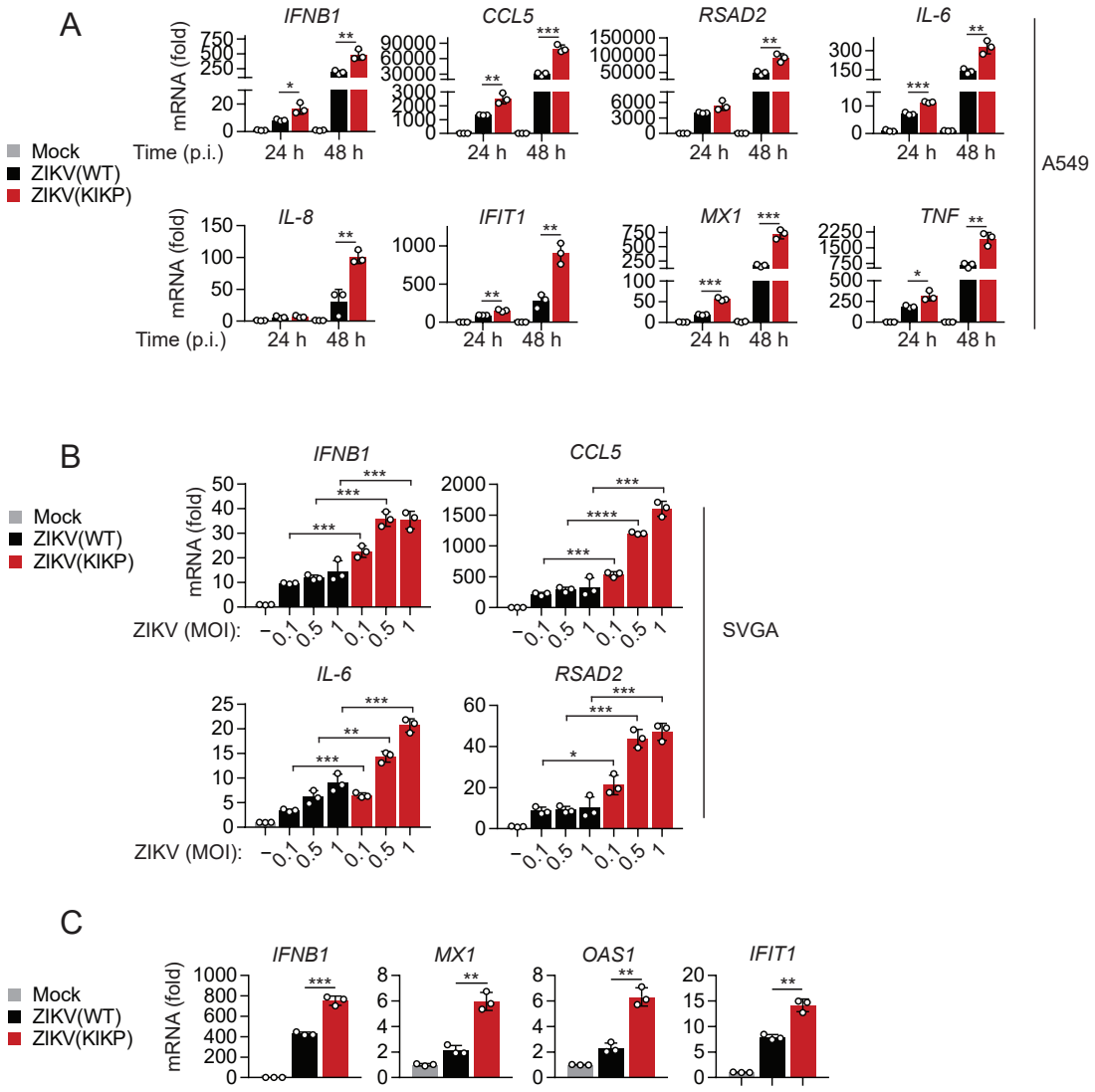

Figure 2.7 ZIKV(KIKP) elicits enhanced immune responses.
(A) IFN, ISG, and cytokine transcript abundance in A549 cells mock-infected or infected with ZIKV(WT) or ZIKV(KIKP) (MOI 0.1) for 24 or 48 h assessed by qRT-PCR and normalized to cellular *GAPDH*.

Figure 2.7 *(continued)* ZIKV(KIKP) elicits enhanced immune responses.
(B) qRT-PCR analysis of indicated transcripts in SVGA cells mock-infected or infected with ZIKV(WT) or ZIKV(KIKP) for 48 h with MOI 0.1, 0.5, or 1. Data are normalized to cellular *GAPDH*.
(C) qRT-PCR analysis of indicated transcripts in HMC3 cells mock-infected or infected with ZIKV(WT) or ZIKV(KIKP) (MOI 0.5) for 48 h, normalized to cellular *GAPDH*.
Data are expressed as means ± SD (n = 3). *p < 0.05, **p < 0.01, ***p < 0.001 (Student's t test).

To address whether this enhanced antiviral response is the result of ZIKV(KIKP) no longer antagonizing the relocalization of RIG-I to the mitochondria, we assessed RIG-I protein abundance at the mitochondria following infection with ZIKV(WT) and ZIKV(KIKP). While cells infected with ZIKV(WT) and mock-infected cells shared similar abundances of RIG-I in mitochondrial fractions, cells infected with ZIKV(KIKP) displayed markedly enhanced levels of RIG-I within the mitochondrial fraction (Figure 2.8 A). Finally, to address whether ZIKV(KIKP) is attenuated by antiviral signaling via the RIG-I-like receptors, we infected SVGA cells in which MAVS—the downstream adaptor of RIG-I—had been knocked out by CRISPR-Cas9 editing, or cells expressing a non-targeting gRNA (NT) (Figure 2.8 B). In NT cells, ZIKV(KIKP) was growth attenuated in comparison to ZIKV(WT), while in *MAVS* KO SVGA cells there was no significant difference between the growth of the two viruses (Figure 2.8 C). Taken together, these data indicate that the mutant virus incapable of binding to 14-3-3ϵ is attenuated by the RIG-I-MAVS signaling axis and subsequent IFN induction.

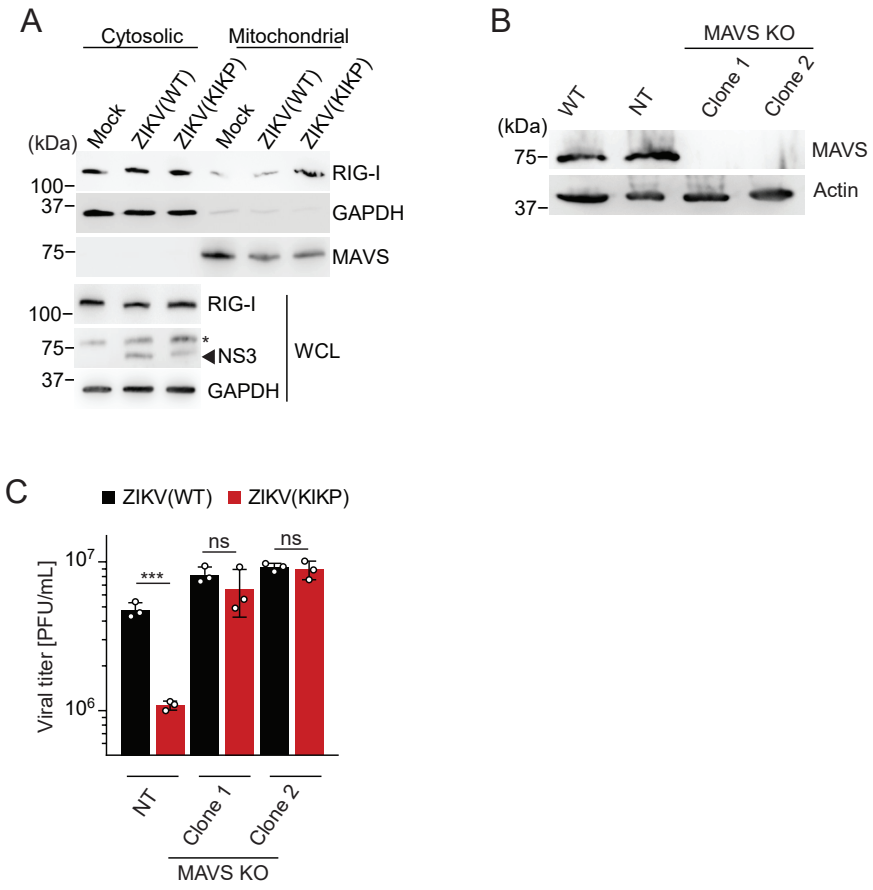

Figure 2.8 ZIKV(KIKP) shows diminished RIG-I antagonism.
(A) Upper: IB analysis with anti-RIG-I antibody of cytosolic and mitochondrial fractions of SVGA cells mock-infected or infected with ZIKV(WT) or ZIKV(KIKP) (MOI 0.1) for 24 h. Purity of fractions was assessed by IB with anti-GAPDH or anti-MAVS antibodies. Lower: WCL was probed with anti-RIG-I, anti-NS3, and anti-GAPDH.
(B) Abundance of endogenous MAVS protein in WCLs of WT, CRISPR nontargeting (NT), or *MAVS* KO SVGA cells (clones 1 and 2) determined by IB with anti-MAVS antibody, used for the experiment shown in (C). WCLs were also probed with an anti-Actin antibody as a loading control.
(C) Viral titers in the supernatant of non-targeting control (NT) or *MAVS* KO SVGA cells infected with ZIKV(WT) or ZIKV(KIKP) (MOI 0.01) for 36 h, presented as PFU/mL.
Data are expressed as means ± SD (n = 3). *p < 0.05, **p < 0.01, ***p < 0.001 (Student's t test). ns, not statistically significant.

2.4 Discussion

The innate immune response is a rapidly acting force designed to counter classes of pathogens and to play an essential role in activating the highly specific adaptive immune response. In fact, multiple studies have determined that the type I IFN response is critical in controlling ZIKV and other flaviviral infections in mammalian hosts. A number of recent studies have identified RIG-I as a primary sensor of and activator of type I IFN signaling during ZIKV infection[93,95,97,114]. In line with these studies, our work demonstrates that ZIKV is sensitive to RIG-I signaling mediated by 14-3-3ϵ, as loss of either RIG-I or 14-3-3ϵ ablated IFN induction in astrocyte cells. Successful evasion of the innate immune system is of paramount importance to effective pathogens. Indeed, flaviviruses have evolved a number of mechanisms to subvert immunity at various steps. Similar to DENV and WNV NS3 proteins, ZIKV NS3 has evolved to antagonize the interaction between RIG-I and 14-3-3ϵ, thereby blocking RIG-I-mediated IFN induction. Importantly, our work found that a recombinant ZIKV deficient in its 14-3-3ϵ-interaction motif was attenuated by RIG-I mediated IFN induction and elicited a greatly enhanced antiviral immune response in cell types relevant to physiological ZIKV infection.

There are two distinct lineages of ZIKV—the first identified strain, MR 766, was an African lineage strain from Uganda, and after expanding westward a second, Asian, lineage of ZIKV was documented[3]. Interestingly, our work has shown that ZIKV of both African and Asian lineages encodes the phosphomimetic 'RDLP' motif to bind to 14-3-3ϵ and antagonize RIG-I-mediated IFN induction. These data suggest that enhanced disease severity in recent Asian-lineage outbreaks of ZIKV disease is not due to the NS3-14-3-3ϵ interaction. Instead, we conclude that the NS3-14-3-3ϵ interaction is an innate immune evasion mechanism fundamental to all strains of ZIKV rather than a determinant of pathogenicity.

An interesting aspect of our conclusions is that ZIKV NS3 targets the adaptor mo-

lecule 14-3-3ϵ rather than directly targeting RIG-I. One explanation for this is that ZIKV NS3 modulates other 14-3-3-driven pathways. In humans, the 14-3-3 protein family is comprised of 7 different members (β, γ, ϵ, η, σ, θ, ζ) that have roles in different intracellular processes, including cell cycling, apoptosis, immunity, and protein trafficking[88,89,113]. Moreover, 14-3-3 proteins share high sequence and structural identity, and bind to cellular proteins displaying the same binding motif, Rxxp(S/T)xP[88]. This suggests that ZIKV NS3 may also bind to other 14-3-3 proteins to modulate other 14-3-3-driven intracellular processes. For example, the related *Flaviviridae* family member HCV modulates activation of the Raf-1 cell cycle kinase via interactions between the HCV core protein and a 14-3-3 protein[116]. Whether ZIKV NS3 interacts with other 14-3-3 proteins necessitates further study. However, our work has demonstrated that loss of the NS3 14-3-3 interaction motif attenuated viral replication primarily through the RLR-MAVS signaling axis. Therefore, a careful examination of other 14-3-3-driven cellular pathways will be needed to better understand the NS3-14-3-3 interactome. Furthermore, studying the loss of the NS3 14-3-3-interaction motif in an IFN-deficient mouse model may provide more clarity as to the importance of NS3 in viral infection outside of evading IFN induction.

Another explanation for why ZIKV NS3 targets 14-3-3ϵ rather than directly targeting RIG-I is that 14-3-3 proteins are conserved in other species. For example, mosquito species encode two 14-3-3 proteins (ϵ, ζ) in their genomes. One recent study identified both proteins as important components of phagocytosis in *Aedes aegypti* cells[117]. It is tempting to speculate that ZIKV NS3 could engage these 14-3-3 proteins in mosquito cells to affect these intracellular processes. However, whether ZIKV NS3 does indeed target 14-3-3 proteins in mosquitos or other host species to modulate intracellular processes is a possibility that has not yet been explored.

A number of mechanisms by which ZIKV evades innate immunity have been suggested by the literature, including many non-structural proteins that attenuate RIG-I signaling upon ectopic expression[95,110,111]. How these evasion mechanisms contribute to

viral replication has largely been untested, and it will be informative to study how multiple mechanisms targeting RIG-I signaling contribute to replication together. Whether these mechanisms are truly redundant deserves further research, as our results indicate that loss of MAVS is sufficient to rescue the KIKP virus, indicating that binding to 14-3-3ϵ is a major evasion mechanism of ZIKV. Moreover, WNV and DENV similarly encode a 14-3-3ϵ interaction capability in their NS3 proteins[102], making this interaction a tantalizing target in designing antiviral therapeutics and rationally designed vaccines against mosquito-transmitted flaviviruses.

2.5 Methods

Cell culture and viruses. HEK293T (ATCC), Vero (ATCC), and A549 (ATCC) cells were cultured in Dulbecco's Modified Eagle's Medium (DMEM, Gibco) supplemented with 10% FBS (v/v) (Gibco) and 1% penicillin-streptomycin (v/v) (Gibco). SVGA (provided by E. Cahir-McFarland; Cambridge, MA,[118]) and HMC3 (ATCC) cells were cultured in Eagle's Minimum Essential Medium (Gibco) supplemented with 10% (v/v) FBS and 1% (v/v) penicillin-streptomycin. All cells were cultured under standard culture conditions.

ZIKV strain Brazil Paraiba 2015 (BRA/2015) (M. Diamond, Washington University in St. Louis;[119]) was propagated in Vero cells as previously described[120]. Briefly, 5E6 Vero cells, seeded into a T-175 culture flask were inoculated 1 day after seeding with ZIKV (MOI 0.001) in 7 mL FBS-free DMEM. 2 h post inoculation, 8 mL DMEM (supplemented with 10% FBS) was added. 72 hours post infection, viral supernatant was removed and clarified by centrifugation at 800 x g for 10 min. SeV (strain Cantell) was purchased from Charles River Laboratories.

ZIKV(KIKP) (strain MR 766) was generated based on a ZIKV strain MR 766 cDNA clone provided by Matthew Evans (Icahn School of Medicine, Mount Sinai) and previously described[121]. Site-directed mutagenesis by PCR was used to generate a mutant MR 766 cDNA clone encoding the substitutions R64K, L65I, D66K in the gene encoding NS3. The WT and mutant infectious clone plasmids were transfected into HEK293T cells using *Trans*IT-LT1 transfection reagent (Mirus Bio) as previously described[121]. Viral supernatant was collected 4 days post transfection, and the WT and mutant viruses were amplified in Vero cells. Supernatants containing amplified recombinant ZIKV(KIKP), or the parental virus were serially diluted and titers were determined by standard plaque assay on Vero cells as described below.

Plasmids and transfections. FLAG-NS3 (ZIKV) (strain MR 766) and FLAG-NS3 (ZIKV) (strain H/PF/2013) were custom-synthesized by Invitrogen in the pcDNA3.1+ vector. GST-

NS3 (ZIKV) (strains MR 766 and H/PF/2013) were subcloned from the pcDNA3.1+ vector into the pEBG vector using KpnI and NotI restriction sites. GST-NS3 (ZIKV) (strain BRA/2015) was generated by introducing two silent mutations (nucleotide base positions 852 A→G, 1734 C →T) into GST-NS3 (ZIKV) (strain H/PF/2013) by site-directed mutagenesis using PCR. Plasmids encoding GST (pEBG), DV2 GST-NS3 (strain NGC), WNV GST-NS3 (strain NY99), YFV GST-NS3 (strain 17D), FLAG-14-3-3σ, FLAG-14-3-3ϵ, HA-14-3-3ϵ, GST-RIG-I (2CARD), FLAG-RIG-I, FLAG-MAVS, IFN- luciferase construct, and pGK–gal have been described previously[102]. All constructs were sequenced to verify 100% agreement with the original sequence. Transfections were performed using the calcium phosphate method, or Lipofectamine and Plus reagent (Life Technologies), or linear polyethylenimine (1 mg/mL solution in 20mM Tris pH 6.8; Polysciences), or *Trans*IT-LT1 (Mirus Bio) following manufacturer's instructions.

Antibodies and reagents. For immunoblot analysis, the following antibodies were used: anti-GST (1:2,000, GST-2, Sigma), anti-FLAG (1:2,000, M2, Sigma), anti-HA (1:2,000, HA-7, Sigma), anti-Actin (1:15,000, AC-15, Sigma), anti-RIG-I (1:2,000, Alme-1, Adipogen), anti-ISG15 (1:1000, F-9, Santa Cruz), anti-ISG54 (1:1,000, 25-735, ProSci), anti-14-3-3ϵ (1:1,500, N1C3, Genetex), anti-SeV (1:2,000 PD029, MBL), anti-GAPDH (1:40,000, CS204254, Millipore), anti-MAVS (1:1,000, 3993S, Cell Signaling Technology). A polyclonal anti-NS3 (ZIKV) antibody was custom-generated by GenScript against the peptide CAALKSFKEFAAGKR and was used for immunoblot analysis (1:1,500). anti-mouse or anti-rabbit-horseradish peroxidase (HRP) conjugated secondary antibodies (both 1:2,000) were purchased from Cell Signaling Technology (7076S and 7074S, respectively). For immunoprecipitation of 14-3-3ϵ, anti-14-3-3ϵ (11648-2-AP, Proteintech) was used. For flow cytometry analysis to determine the percentage of ZIKV-infected cells, hybridoma supernatant containing anti-ZIKV (ZV-2, 1:10, provided by M. Diamond, Washington University in St. Louis[16]) or anti-4G2 mouse monoclonal primary antibody (1:50, Permwash), purified from D1-4G2-4-15 hybridoma cells (ATCC), and goat anti-mouse secondary Alexa Fluor 488 (1:5,000, A-10667, Invitrogen) antibodies were used.

anti-FLAG M2 magnetic beads (Sigma), Glutathione Sepharose 4B resin (GE Life Sciences), protein A/G agarose (Thermo Fisher), or Dynabeads Protein G (Invitrogen) beads were used for respective pull-downs and immunoprecipitations. Protease inhibitor cocktail (P2714) was purchased from Sigma and used at a concentration of 1:500 in all immunoprecipitation experiments.

Immunoblot analysis. Precipitated protein or cell lysates were resolved on 7% or 10% Bis-Tris SDS-PAGE gels (pH 6.4), and then transferred to a Polyvinylidene difluoride (PVDF) membrane (Bio-Rad) using a Novex Semi-Dry Blotter (Invitrogen). Membranes were blocked with 5% (w/v) non-fat dry milk in PBS-T (PBS with 0.05% (v/v) Tween-20) for 30 minutes at room temperature, and then probed with the indicated primary antibody in 2.5% (w/v) non-fat dry milk in PBS-T at 4 °C overnight. Following overnight incubation, membranes were washed in PBS-T for 30 minutes, then probed with HRP-linked secondary antibodies in 2.5% (w/v) non-fat dry milk in PBS-T for 1 h at room temperature and washed in PBS-T again. Proteins were visualized using SuperSignal West Pico or SuperSignal West Femto chemiluminescence reagents (Pierce) and detected by an ImageQuant LAS 4000 Chemiluminescent Image Analyzer (GE).

ZIKV infection and titration. Cell monolayers of SVGA, A549, or Vero cells were first washed with sterile PBS, then inoculated with virus containing FBS-free DMEM at 37 °C for 2 h at the indicated MOI. After 2 h, supernatant was aspirated and cells washed twice with sterile PBS, and media was replaced with DMEM (10% FBS) and incubated at 37 °C for the indicated times. To titrate virus for plaque assay, samples were serially diluted in DMEM with 1% penicillin-streptomycin, then incubated on a confluent monolayer of Vero cells at 37 °C for 2 h. Supernatant was aspirated and replaced with low melting temperature agarose and 2x MEM (Gibco), and incubated for 3 days at 37 °C until plaques formed. Cells were fixed in 1% (w/v) paraformaldehyde for 1 h at room temperature, and then stained with crystal violet (VWR) in 20% ethanol. Plaques were rinsed with water, counted, and virus titers calculated. Plaque-forming units per mL (PFU/mL) was calculated

as (plaque count/well) × (dilution factor) / (volume of inoculum) as previously described [120].

Cell lysis and immunoprecipitation. HEK293T or SVGA cells were lysed in Nonidet P-40 (NP-40) buffer (50 mM HEPES pH 7.4, 150 mM NaCl, 1% (v/v) NP-40, 1 mM EDTA, protease inhibitor cocktail) vortexed and centrifuged at 4 °C, 21,000 × g for 20 minutes. GST or FLAG pull-downs, co-immunoprecipitations and western blot analyses were performed as previously described [80]. Briefly, lysates were subjected to pull-down with GST or FLAG beads for 4 h at 4 °C, or lysates were subjected to immunoprecipitation with 2μg primary antibody overnight at 4 °C followed by incubation with Dynabeads Protein G or protein A/G agarose for 2 h at 4 °C. A portion of the cell lysate was taken prior to pull-down or immunoprecipitation for analysis as a whole cell lysate (WCL) fraction. Elution of precipitated proteins was performed by heating samples in Laemmli SDS sample buffer at 95 °C for 5 minutes.

Luciferase reporter assays. 10^5 HEK293T cells were seeded into 12-well plates, then transfected the next day with 300ng of pGK–gal (β-galactosidase-expression plasmid), 200ng of IFN-β luciferase reporter plasmid, as well as 200ng to 1.5g of plasmid encoding the indicated GST-NS3 constructs, or the GST-expressing pEBG vector. IFN-β luciferase was induced by infecting cells with SeV (50 HAU/mL) 42 h after transfection, or were co-transfected with 2.5 to 5ng of GST-RIG-I 2CARD, 100ng GST-MDA5 2CARD or 30ng of the FLAG-MAVS constructs. At the indicated time points, cells were lysed and luciferase activity was measured (Promega). Luciferase values were normalized to β-galactosidase activity to control for transfection efficiency, and fold luciferase activity was calculated relative to values for control cells, set to 1.

Cytosol-Mitochondria fractionation assay. SVGA cells seeded in 10cm dishes were mock-infected or infected with the indicated ZIKV strain or SeV at the indicated MOIs. 20 to 24 hours post infection, cells were harvested in an isotonic mitochondrial buffer (MIT1000, Merck Millipore), and cytosolic and mitochondrial fractions were prepared ac-

cording to manufacturer instructions. Briefly, a Dounce homogenizer was used to homogenize cells, and WCLs were taken. Lysates were processed by low-speed centrifugation at 600 x g to pellet unbroken cells and nuclei. Next, the supernatant was further processed by high-speed centrifugation at 10,000 x g for 30 min at 4 $^{\circ}$C to pellet the mitochondrial fraction. The two fractions were subjected to a bicinchoninic acid (BCA) assay (Pierce) to normalize protein amounts for SDS-PAGE and immunoblot analysis. Anti-GAPDH and anti-MAVS immunoblot analyses served as quality control for relative cytosolic and mitochondrial fraction purity, respectively.

qRT-PCR. RNA was extracted from A549, SVGA, and HMC3 cells using an RNA extraction kit (OMEGA Bio-Tek) following the manufacturer's instructions. Equal amounts of RNA (25-500ng) were used in a one-step qRT-PCR reaction using the SuperScript III Platinum One-Step qRT-PCR kit with ROX (Invitrogen) and FAM reporter dye primers, from IDT, for the genes analyzed. Gene expression was normalized to cellular *GAPDH*. The comparative CT method ($\Delta\ \Delta$ CT) was used to measure the induction of a target gene relative to its induction in mock-infected samples. Abundance of ZIKV genomic RNA was measured using a previously described primer against mRNA encoding the ZIKV E protein5'-CCACTAACGTTCTTTTGCAGACAT-3' (forward), 5'-CCGCTGCCCAACACAAG-3' (reverse), /56-FAM/AGCCTACCT/ZEN/TGACAAGCAATCAGACACTCAA/3IABkFQ/ (probe)[10]. All qRT-PCR reactions were performed using a 7500 FAST RT-PCR system (Applied Biosystems).

siRNA-mediated knockdown. SVGA cells were seeded (1 x 10^5) in 12 well plates and transfected with 50nM of gene-specific siGENOME SMARTpool siRNAs (Dharmacon) against RIG-I, MDA5, 14-3-3ϵ, 14-3-3η, or 14-3-3σ with RNAiMAX transfection reagent (Invitrogen) according to the manufacturer's instructions. As a control, non-targeting siRNA (siGENOME Non-Targeting siRNA Pool siGENOME Non-Targeting siRNA Pool 2, D-001206-14-05) was transfected. The following siRNAs were used: siRNAs targeting RIG-I (siGENOME SMARTpool M-012511-01-0005), MDA5 (siGENOME SMARTpool M-

013041-00-0005), 14-3-3ϵ (siGENOME SMARTpool M-017302-03-005), 14-3-3η (siGENOME SMARTpool M-010626-01-0005), or 14-3-3σ (siGENOME SMARTpool M-005180-00-0005). Silencing efficiency of these genes was determined by measuring transcript abundance at the indicated times by qRT-PCR using predesigned gene specific primers from IDT.

Flow cytometry analysis. Flow cytometry was used to determine the frequency of ZIKV-positive A549 cells. First, cells were fixed in 1% PFA (Santa Cruz) for 30 m at room temperature followed by saponin-based permeabilization (PermWash, BD Scientific) for 15 minutes. Cells were incubated with anti-ZV2 mouse monoclonal primary antibody [1:10 (in PermWash)], or with anti-4G2 mouse monoclonal primary antibody [1:50 (in PermWash), purified from D1-4G2-4-15 hybridoma cells (ATCC)] for 1 hour at room temperature. After being washed with PBS-T, cells were stained with a goat anti-mouse secondary Alexa Fluor 488 antibody(1:5,000, A-10667, Invitrogen) for 1 h at room temperature, washed with PBS-T and resuspended in PBS. Percentage of ZIKV-infected, single cells was determined with a BD LSRFortessa and assessed using FlowJo software (Tree Star).

Flavivirus NS3 sequence analysis. Alignment tools and flavivirus databases at viprbrc.org were used to align the amino acid sequences of *Flaviviridae* family members, and their NS3 sequences were analyzed for the presence or absence of a potential phosphomimetic 14-3-3 binding motif (RxE/DP) at the region corresponding to amino acids 64-67 in ZIKV NS3. All sequences were gathered from the NIAID Virus Pathogen Database and Analysis Resource (ViPR). A cladogram was generated using anvi'o (version 5.5) with sequences of the NS5 protein of the indicated flavivirus strains.

Statistical analysis. All data were presented as means ± SD and analyzed using GraphPad Prism software (version 7). An unpaired two-tailed Student's t-test ($p < 0.05$ was considered statistically significant), or a one-way ANOVA with Dunnett's multiple comparisons ($p < 0.01$ was considered statistically significant) was used as indicated in the

legends. Pre-specified effect sizes were not assumed, and in general three biological replicates (n) for each condition were used within independent experiments.

CHAPTER 3

ZIKA, DENGUE, AND WEST NILE VIRUS NS3-MEDIATED ANTAGONISM OF MDA5 SIGNALING

This chapter is adapted from: Riedl, W.; Acharya, D.; Lee, J.H.; Liu, G.; Serman, T.; Chiang, C.; Chan, Y.K.; Diamond, M.S.; Gack, M.U. Zika Virus NS3 Mimics a Cellular 14-3-3-Binding Motif to Antagonize RIG-I- and MDA5-Mediated Innate Immunity. Cell Host Microbe 2019, 26, 493–503.e6

Attributions: WR performed and analyzed all experiments with the exception of the following: G.Q. Liu performed and analyzed Figure 3.2 B. D.A. performed and analyzed Figure 3.3 B and C, Figure 3.4 AD. C.C. generated the MAVS KO SVGA cells used in Figure 3.3 B and C.

3.1 Abstract

The innate immune system is critical in detecting and controlling flaviviral infection. The RIG-I-like receptors (RLRs) RIG-I and MDA5 are of particular importance in detecting flaviviruses. Multiple studies have demonstrated the essentiality of both RLRs in controlling DENV, WNV, and ZIKV both *in vitro* and *in vivo*. Recent work has highlighted 14-3-3ϵ and 14-3-3η as necessary mediators of RLR signaling in their roles in re-localizing RIG-I and MDA5 from the cytosol to the mitochondria, where MAVS is located. Our previous work has demonstrated that flaviviruses evade antiviral signaling mediated by 14-3-3ϵ and RIG-I. However, a dearth of evidence has been presented to demonstrate antagonism of the MDA5 signaling pathway by flaviviruses. Here, our data demonstrates that DENV, WNV, and ZIKV NS3 proteins bind to and sequester 14-3-3η to antagonize MDA5-mediated IFN induction. Furthermore, loss of the 14-3-3-binding capacity of ZIKV NS3 results in enhanced re-localization of MDA5 to the mitochondria during ZIKV infection, resulting in greater induction of innate immunity.

3.2 Introduction

Mosquito-transmitted flaviviruses are a significant burden to human health. Dengue virus (DENV) is estimated to cause as many as 390 million infections per year, and about half of the global population is at risk of contracting DENV each year[24]. DENV causes a range of febrile-related symptoms, including hemorrhagic fever[23]. WNV is a mosquito-transmitted flavivirus that can cause encephalitis. Since its introduction in the US in 1999, WNV has caused thousands of deaths, and has become endemic in across the US[31]. ZIKV, a recently emergent mosquito-borne flavivirus, can cause severe congenital birth defects[3]. DENV, WNV, and ZIKV and all flaviviruses are positive-sense single-stranded RNA viruses that can replicate in a broad swath of cell types. For example, DENV primarily replicates in monocytes and macrophages[26]. WNV has a broad tissue tropism, replicating not only in innate lymphoid cells of the blood like DENV, but also has tropism for spleen,

kidney, and neural tissues[32]. ZIKV proliferates in monocytes and macrophages, but also in human trophoblast and other cells of placental origin, as well as within fetal brain tissue[3]. During infection of these cell types, the genomic RNA of flaviviruses is translated into a single polyprotein consisting of 10 proteins, 7 non structural (NS) proteins and 3 structural proteins. The NS3 protein functions in concert with NS2B as the viral protease which, together with host proteases, cleaves the viral polyprotein. Flaviviral NS proteins typically have multiple functions during infection, and accordingly, NS3 also functions as a helicase and has demonstrated roles in evasion of RIG-I innate immunity by binding to and sequestering 14-3-3ϵ[102].

The mammalian type I IFN system is essential for control of flaviviruses both in cell culture and mouse models[92,122,123]. The RIG-I-like receptors RIG-I and MDA5 detect flaviviral infection in the cytosol of infected cells, then activate a signaling pathway to induce type I IFNs. Upon activation, these sensors undergo a series of reversible post-translational modifications, enabling their interaction with 14-3-3ϵ and 14-3-3η, respectively. 14-3-3 proteins share a target interaction motif on cellular proteins, binding to cellular proteins displaying 'Rxx(pS/pT)xP'[88,113]. 14-3-3ϵ and 14-3-3η act as chaperone proteins to mediate the subcellular re-localization of the RLRs to the mitochondria where interactions with MAVS commence antiviral signaling via TBK1, IRF3, and IRF7 to induce the expression of type I IFNs[52,53,84,86]. These IFN molecules are secreted from the infected cell and bind to the IFN receptor (IFNAR) on the infected cell and surrounding cells. Activation of IFNAR results in amplification of the antiviral signal and induction of a group of genes with antiviral effector properties, termed interferon stimulated genes (ISGs)[54].

Due to the importance that type I IFN signaling has in controlling flaviviral replication, these viruses have evolved mechanisms to counter RLR-mediated induction of IFN. For example, a number of studies have suggested that several ZIKV NS proteins inhibit RIG-I-mediated IFN induction upon ectopic expression[94,95,111], although the mechanisms of how these NS proteins evade IFN induction must be further studied. Similarly,

ZIKV and DENV NS4A have been shown to inhibit induction of IFN by inhibiting activation of MAVS[95,103], though how NS4A contributes to viral evasion of IFN induction during infection has yet to be determined. Additionally, the related *Flaviviridae* member Hepatitis C virus (HCV) NS3-4A protein cleaves MAVS from the mitochondria to prevent RIG-I-mediated IFN induction[64]. Along these lines, previous work has demonstrated that ZIKV (Chapter II), DENV, and WNV evade RIG-I-mediated IFN signaling by binding to 14-3-3ϵ, thereby preventing the cytosol-to-mitochondria re-localization of activated RIG-I[102]. However, despite the fact that MDA5 is important in detecting these viruses *in vitro* and *in vivo*, it is not well understood whether DENV, WNV, and ZIKV directly evade signaling through the MDA5 signaling pathway. Here, we demonstrate that DENV, WNV, and ZIKV bind to and sequester 14-3-3η to antagonize MDA5-mediated IFN induction. Generation of a recombinant ZIKV incapable of interacting with 14-3-3η results in attenuated infection due to the 14-3-3η-mediated MDA5 signaling pathway. Furthermore, we demonstrate that both RIG-I and MDA5 are important in controlling ZIKV infection in an astrocyte cell line.

3.3 Results

3.3.1 Flaviviral NS3 proteins bind to 14-3-3η to antagonize MDA5 signaling

Given that DENV, WNV, and ZIKV NS3 proteins encode phosphomimetic motifs which enable binding to 14-3-3ϵ and antagonism of RIG-I signaling, and that 14-3-3 proteins share target interaction motifs on phosphorylated cellular proteins, we reasoned that these flaviviral NS3 proteins could also bind to 14-3-3η. In support of this, ZIKV NS3 bound specifically to 14-3-3η during infection of SVGA cells, but not to 14-3-3σ (Figure 3.1 A). During a 72 hour time-course of ZIKV infection, the NS3-14-3-3η interaction did not increase with time. Rather, as the abundance of NS3 increased, the amount of 14-3-3η bound to NS3 appeared to stay constant (Figure 3.1 B). In previous work, mutation of DENV, WNV, and

ZIKV NS3 from the phosphomimetic 'Rx(E/D)P' motif to encode 'KIKP' resulted in a loss of binding to 14-3-3ϵ. Similarly, we found that mutation of this site in ZIKV NS3 to 'KIKP' resulted in a loss of binding to 14-3-3η (Figure 3.1 C). Therefore our data supports the idea that ZIKV NS3 binds to 14-3-3η via a phosphomimetic 'RLDP' motif, similar to its ability to bind with a degree of specificity to 14-3-3ϵ.

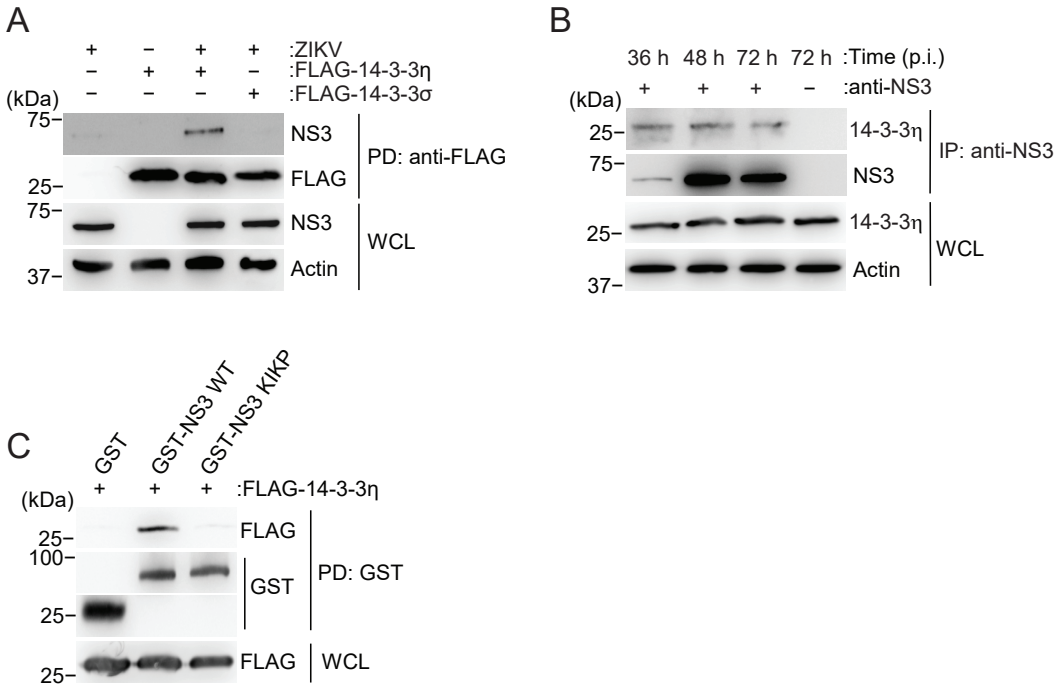

Figure 3.1 ZIKV NS3 binds to 14-3-3η via a phosphomimetic motif.
(A) NS3-14-3-3η interaction in SVGA cells transfected with vector, FLAG-14-3-3η, or FLAG-14-3-3σ for 40 h then infected with ZIKV (BRA/2015, MOI 1) for 48 h, assessed by anti-FLAG pulldown and immunoblot with the indicated antibodies.
(B) Timecourse of NS3-14-3-3η interaction in SVGA cells infected with ZIKV (BRA/2015, MOI 1) for the indicated times assessed by anti-NS3 immunoprecipitation and subsequent immunoblot with the indicated antibodies.
(C) NS3-14-3-3η interaction in HEK293T cells transfected with FLAG-14-3-3η and GST or ZIKV GST-NS3 (WT) or GST-NS3(KIKP), assessed by GST pulldown and subsequent immunoblot with the indicated antibodies.

To evaluate the implication of the NS3-14-3-3η interaction, we asked whether ZIKV NS3 competes for the MDA5-14-3-3η interaction. Indeed, the MDA5-14-3-3η interaction

was lost in a dose-dependent manner in the presence of ZIKV NS3, indicating that ZIKV NS3 binds to and sequesters 14-3-3η (Figure 3.2 A). As a result of this sequestration of 14-3-3η, we found that ectopic expression of ZIKV NS3 blocked the induction of the interferons *IFNB1* and *IFNL1*, and accordingly blocked the expression of the cytokines and ISGs *CCL5, RSAD2, MX1*, and *OAS1* when stimulated by expression of full-length MDA5 (Figure 3.2 B). In particular, ZIKV NS3 downregulated the transcript abundance of CCL5, MX1, and OAS1. We found that the ability of ZIKV NS3 to antagonize the induction of these genes is similar to the measles virus V protein (MeV V), which has been previously identified as a potent inhibitor of MDA5 signaling by targeting the PP1 and PP1 phosphatases[124].

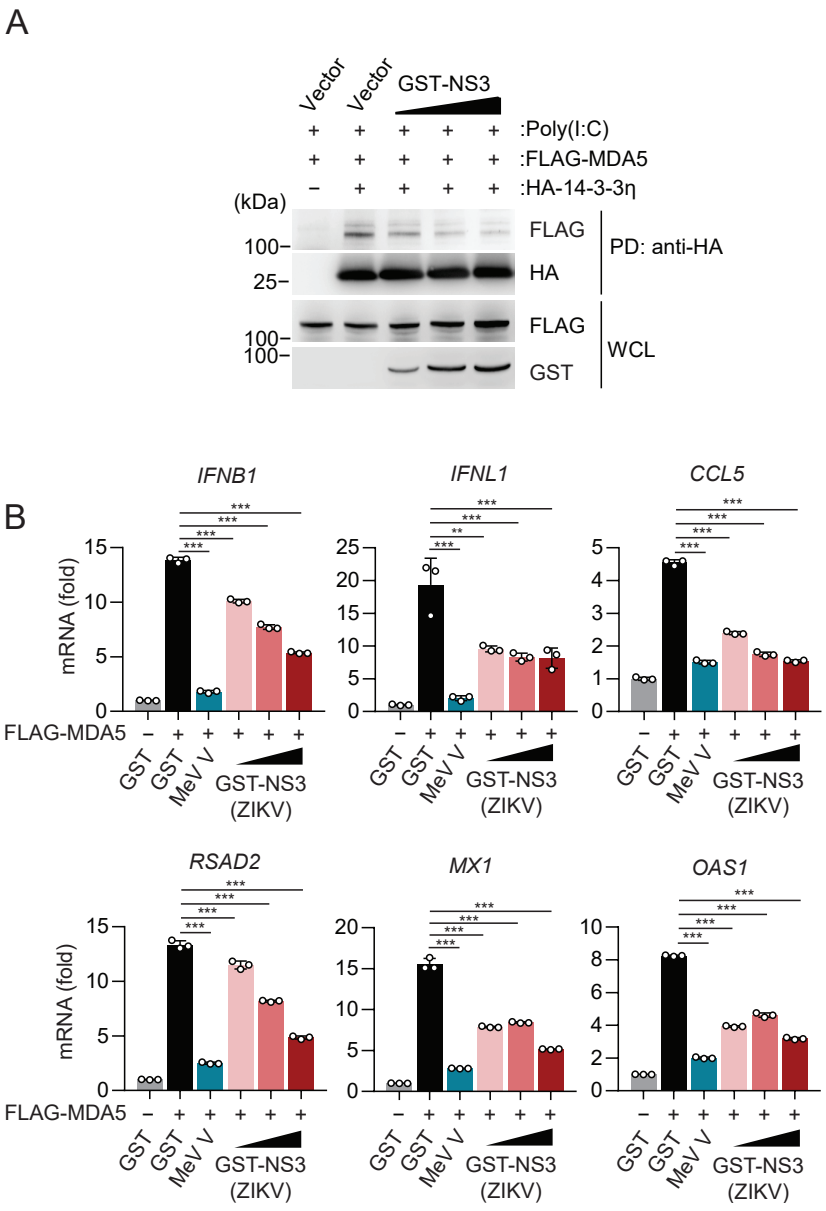

Figure 3.2 ZIKV NS3 competes for the MDA5-14-3-3η interaction to antagonize MDA5 signaling.

(A) Binding of HA-14-3-3η and FLAG-MDA5 in HEK293T cells transfected with HA-14-3-3η, FLAG-MDA5, and vector or increasing amounts of ZIKV GST-NS3 (BRA/2015) for 24 h then treated with 5μg/mL HMW-Poly(I:C)/Lyovec for 20 h, determined by HA pulldown and IB with the indicated antibodies.

(B) IFN, ISG, and cytokine transcript abundance in HeLa cells transfected with GST, MeV V, or ZIKV GST-NS3 and vector or FLAG-MDA5 for 24 h, assessed by qRT-PCR analysis. Data are expressed as means ± SD (n = 3). *p < 0.01, **p < 0.001, ***p < 0.0001 (ANOVA).

Because the phosphomimetic Rx(E/D)P motif necessary for the ZIKV NS3-14-3-3ϵ interaction is also conserved in DENV and WNV, we reasoned that these NS3 proteins similarly antagonize MDA5 signaling. Indeed, DENV and WNV NS3 proteins efficiently bound to 14-3-3η, and DENV NS3 showed the strongest binding affinity between the three NS3 proteins (Figure 3.3 A). Furthermore, we found that all three NS3 proteins blocked the the induction of IFN-β stimulated by MDA5-2CARD, the constitutively active form of MDA5[78] (Figure 3.3 B). Consistent with the binding data, DENV NS3 showed the strongest antagonism of MDA5-mediated IFN induction. Taken together, these results indicate that by sequestering 14-3-3η, ZIKV NS3 antagonizes MDA5 signaling, and that this immune escape mechanism is likely conserved in DENV and WNV NS3 proteins.

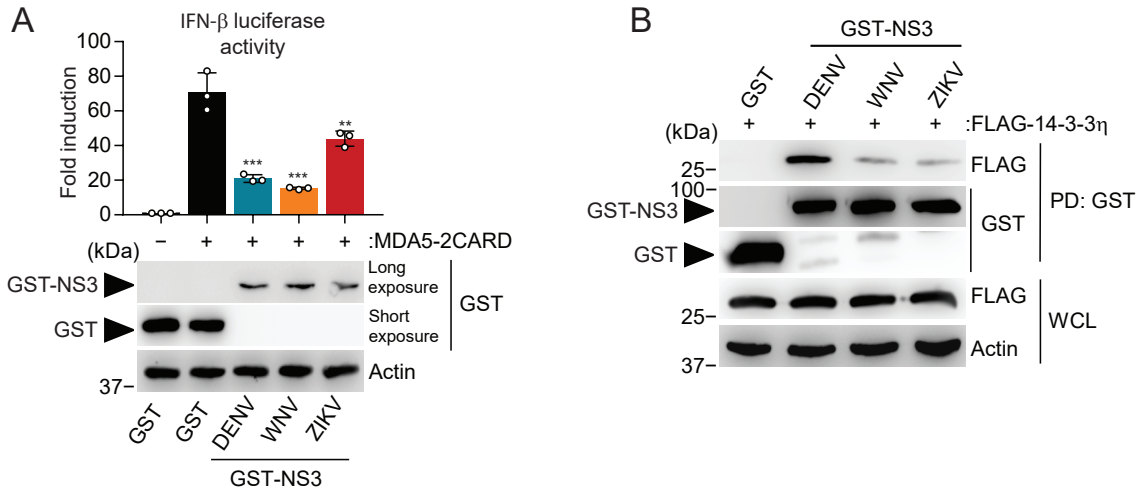

Figure 3.3 Flavivirus NS3 proteins antagonize MDA5 signaling by binding to 14-3-3η.
(A) Upper: IFN-β luciferase activity in HEK293T cells co-transfected to express a luciferase reporter under control of the IFN-β promoter, and MDA5-2CARD and GST or GST-NS3 from DENV (NGC), WNV (NY99) or ZIKV (BRA/2015) for 48 h. Luciferase activity was normalized to co-transfected β-Galactosidase. Data are presented relative to GST-expressing cells set to 1. Lower: IB analysis of WCL with anti-GST and anti-Actin (loading control).
(B) Interaction of GST or GST-NS3 of DENV (NGC), WNV (NY99), or ZIKV (BRA/2015) with FLAG-14-3-3η in HEK293T transfected to express those plasmids for 42 h, assessed by GST pulldown and subsequent immunoblot with the indicated antibodies.
Data are expressed as means ± SD (n = 3). **p < 0.001, ***p < 0.0001 (ANOVA).

3.3.2 ZIKV NS3 sequesters 14-3-3η to inhibit MDA5 cytosol -to- mitochondria translocation

Prior to interaction with and activation of MAVS, MDA5 must translocate to the site of the membrane-anchored MAVS protein—the mitochondrial associated membrane. This translocation is mediated by 14-3-3η, and MDA5 does not efficiently signal in the absence of 14-3-3η[86]. We then utilized the 14-3-3-protein-binding deficient virus, ZIKV(KIKP), we had previously generated (Figure 2.6) to evaluate whether loss of the NS3-14-3-3η

interaction attenuated ZIKV replication. Subcellular fractionation of astrocytes infected with mutant and wild-type viruses revealed that ZIKV(KIKP) elicits enhanced cytosol-to-mitochondria translocation of MDA5 in comparison to infection with ZIKV(WT) (Figure 3.4 A). Therefore, due to its inability to sequester 14-3-3η, ZIKV(KIKP) does not block the cytosol-to-mitochondria translocation of MDA5. Together with previous results regarding the RIG-I-14-3-3ϵ interaction, these data suggest that as a result of no longer binding to 14-3-3 proteins, ZIKV(KIKP) is attenuated by enhanced signaling through the RIG-I-like receptors RIG-I and MDA5.

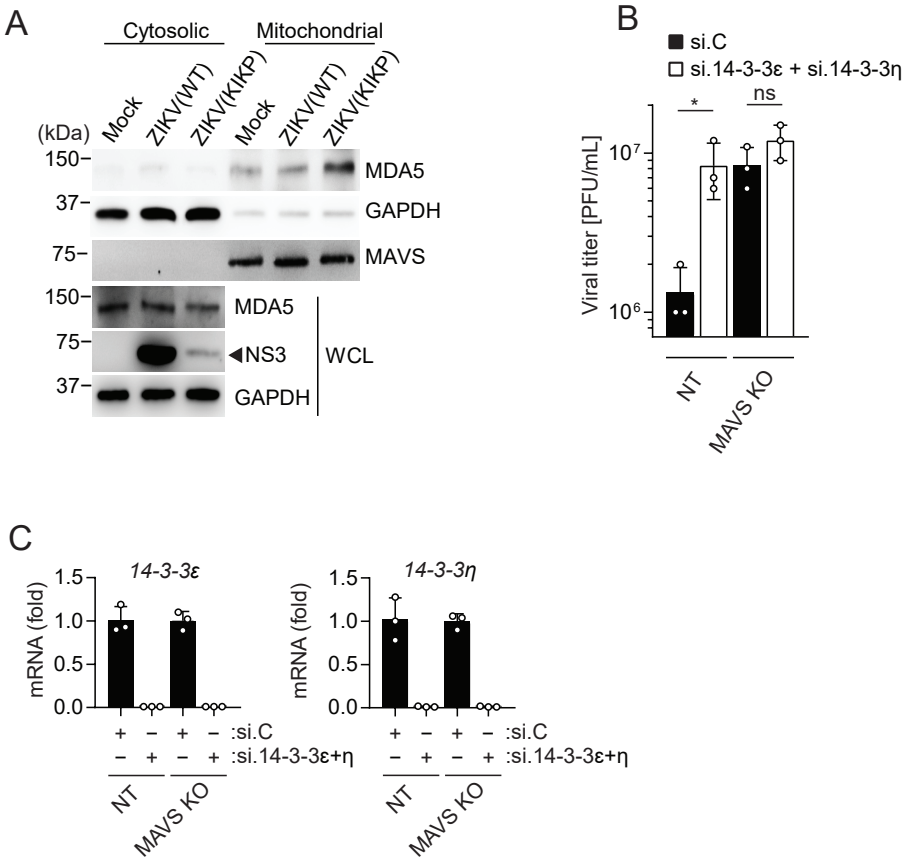

Figure 3.4 ZIKV(KIKP) shows diminished MDA5 antagonism via loss of NS3-14-3-3 interactions.

(A) Upper: IB analysis with anti-MDA5 antibody of cytosolic and mitochondrial fractions of SVGA cells mock-infected or infected with ZIKV(WT) or ZIKV(KIKP) (MOI 0.1) for 24 h. Purity of fractions was assessed by IB with anti-GAPDH or anti-MAVS antibodies. Lower: WCL was probed with anti-MDA5, anti-NS3, and anti-GAPDH.

(B) Viral titer in NT or *MAVS* KO SVGA cells transfected with si-Control (si.C) RNA or siRNA targeting 14-3-3ϵ and 14-3-3η for 30 h then infected with ZIKV(KIKP) (MOI 0.1) for 36 h, assessed by plaque assay and presented as PFU/mL.

(C) qRT-PCR-based knockdown efficiency of 14-3-3ϵ and 14-3-3η in SVGA cells transfected with siRNA targeting these transcripts for 3 days, for the experiment in (B).

Data are expressed as means ± SD (n = 3). *p < 0.05, **p < 0.01, ***p < 0.001 (Student's t test). ns, not statistically significant.

To formally assess whether 14-3-3 proteins mediate an enhanced antiviral signaling in response to ZIKV(KIKP) infection, we compared the replication capacity of ZIKV(KIKP) in

NT and *MAVS* KO SVGA cells transfected with control siRNA (si.C) or siRNA targeting 14-3-3ϵ and 14-3-3η. We found that ZIKV(KIKP) is attenuated in NT SVGA cells in comparison to *MAVS* KO SVGA cells, in agreement with the attenuation previously observed in A549 cells. However, silencing of the two 14-3-3 proteins in NT cells rescued ZIKV(KIKP) replication. Furthermore, infection of *MAVS* KO SVGA similarly rescued ZIKV(KIKP) replication, but infection of *MAVS* KO SVGA with both 14-3-3 proteins silenced did not enhance ZIKV(KIKP) infection (Figure 3.4 B and C). Together, these data confirm that ZIKV(KIKP) is attenuated because of its inability to sequester 14-3-3ϵ and 14-3-3η to antagonize RLR-MAVS signaling.

3.3.3 ZIKV(KIKP) is detected by both RIG-I and MDA5 in astrocytes

Multiple reports have demonstrated that in the A549 lung epithelial cell line, ZIKV is primarily detected by RIG-I, while another report found data indicating that ZIKV is detected by both RIG-I and MDA5 in human trophoblast cells[93–95]. Furthermore, data in mouse embryonic fibroblast cells infected with WNV has suggested that RIG-I and MDA5 act in a temporally distinct manner—RIG-I is necessary for initial induction of IFN during infection, while MDA5 signals at later time points[92]. We reasoned that infection of astrocyte cells with the mutant ZIKV(KIKP) virus would highlight the relevance of both of these pathways to ZIKV infection, and help elucidate the order in which these sensors act during ZIKV infection. We first knocked down either RIG-I, MDA5, or both RIG-I and MDA5 in SVGA cells using siRNA targeting these transcripts, then infected with ZIKV(KIKP). We found that ZIKV(KIKP) infection was enhanced in cells deficient in either RIG-I or MDA5, with greater enhancement of infection in cells with both sensors knocked down at once. Interestingly, both sensors enhanced ZIKV(KIKP) infection at each timepoint within the 60 hour time course, suggesting that both sensors are important for IFN induction in response to ZIKV infection at both early and later time points (Figure 3.5 A and B). Similarly, depletion of either 14-3-3ϵ or 14-3-3η alone increased ZIKV(KIKP) replication, while knockdown of both 14-3-3 proteins together enhanced ZIKV(KIKP) replication to a greater degree (Figure 3.5

C, D). All together, these data indicate that ZIKV(KIKP) is restricted by 14-3-3-mediated RLR signaling pathways at both early and late time points.

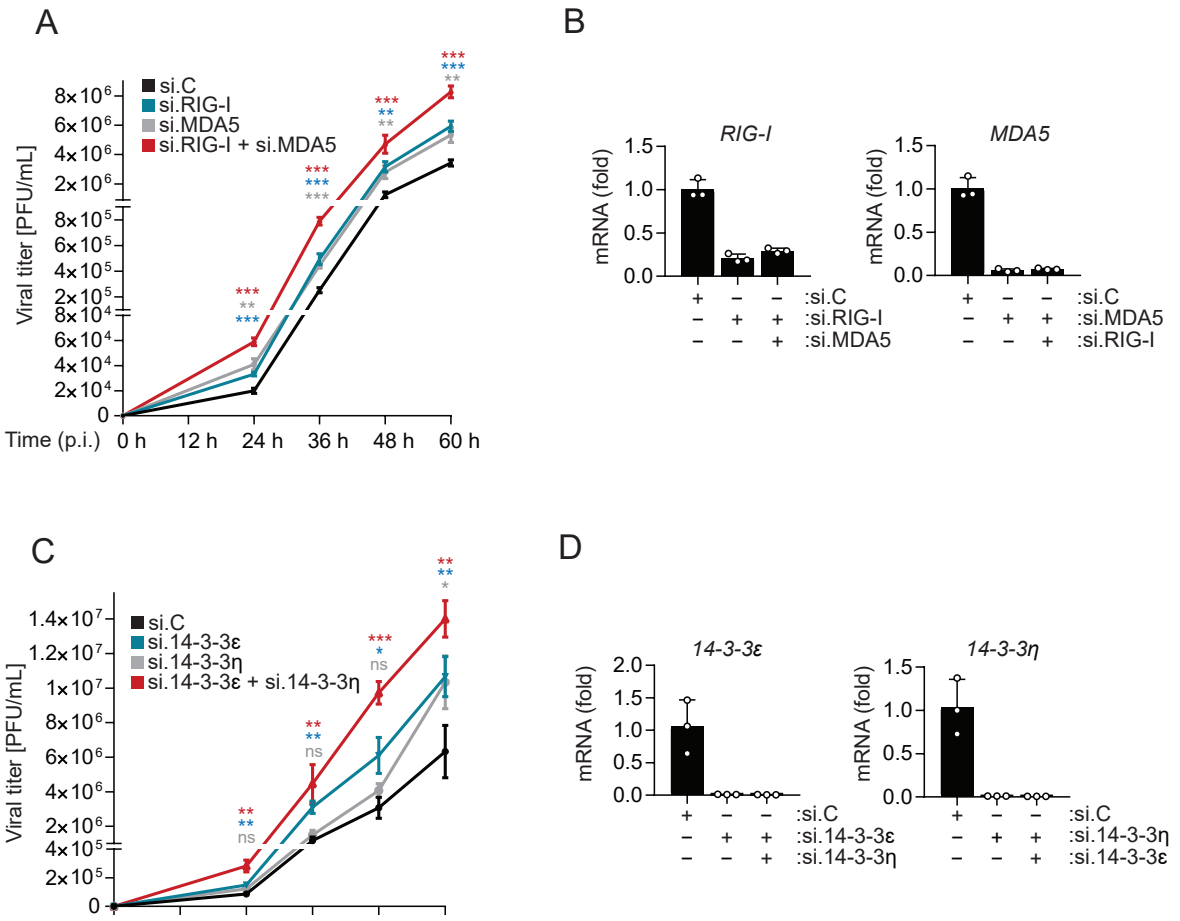

Figure 3.5 ZIKV(KIKP) is attenuated by RIG-I and MDA5 signaling in astrocytes.
(A) Viral titer in supernatant of SVGA cells transfected with si-Control (si.C) RNA or siRNA targeting RIG-I, MDA5, or RIG-I and MDA5 for 30 h infected with ZIKV (MOI 0.01) for the indicated times, assessed by plaque assay and presented as PFU/mL.
(B) qRT-PCR-based silencing efficiency of the indicated genes for experiment shown in (A).
(C) Viral titer in supernatant of SVGA cells transfected with si-Control (si.C) siRNA or siRNA targeting 14-3-3ϵ or 14-3-3η, or 14-3-3ϵ and 14-3-3η for 30 h infected with ZIKV (MOI 0.01) for the indicated times, assessed by plaque assay and presented as PFU/mL.
(D) qRT-PCR-based silencing efficiency of the indicated gens for the experiment shown in (C).
Data are expressed as means ± SD (n = 3). *p < 0.05, **p < 0.01, ***p < 0.001 (Student's t-test; pairwise comparisons to si.C). ns, not statistically significant.

3.4 Discussion

Multiple studies have implicated both RIG-I and MDA5 as important components in controlling flavivirus infection[74,92]. The 14-3-3 proteins 14-3-3ϵ and 14-3-3η have critical roles in redistributing active RIG-I and MDA5 to interact with MAVS at the mitochondria. Recently published work has shown that DENV and WNV antagonize RIG-I signaling by binding to a 14-3-3 protein, 14-3-3ϵ[102]. Our work in the previous chapter similarly established that ZIKV NS3 antagonizes RIG-I by binding to 14-3-3ϵ and blocking the cytosol-to-mitochondria translocation of activated RIG-I. Here, our work has demonstrated that ZIKV NS3 binds to 14-3-3η during infection of astrocyte cells, and that ZIKV NS3 antagonizes MDA5-mediated IFN induction. In the context of ZIKV infection, loss of the NS3-14-3-3η interaction resulted in enhanced MDA5 signaling and IFN induction. Similarly, we found that WNV and DENV NS3 bind to 14-3-3η and inhibit MDA5-mediated IFN induction. Whether DENV and WNV NS3 proteins antagonize MDA5 signaling during viral infection requires further study.

Previous studies have revealed that DENV and WNV are controlled by both RIG-I and MDA5 both *in vitro* and *in vivo*. Two recent studies identified RIG-I as the dominant sensor of ZIKV infection in A549 cells, while one study found that both RIG-I and MDA5 contribute to ZIKV-mediated IFN induction in trophoblast cells[93–95]. Using the ZIKV(KIKP) recombinant virus, we have found that in an astrocyte cell line both RIG-I and MDA5 are important in controlling ZIKV infection at early and late time points. Together, this group of studies indicates that ZIKV is controlled by RIG-I and MDA5 in a cell type dependent manner. It will be important to better understand how these two sensors function in concert to counter ZIKV infection in cell types relevant to disease to refine our view of how therapeutics should be developed and targeted.

The 14-3-3 protein family is made up of 7 members in humans (β, γ, ϵ, η, σ, θ, ζ). These proteins generally act as adaptor, scaffold, and chaperone proteins by altering the

conformation of target proteins, linking target proteins together, or blocking the interactions of a target protein[87]. While 14-3-3ϵ and 14-3-3η have been implicated in the RLR signaling pathways, 14-3-3 proteins have been associated with a number of other intracellular processes, including cellular metabolism, protein trafficking, and autophagy[87,113]. Interestingly, ZIKV NS3 binds to both 14-3-3ϵ and 14-3-3η to antagonize RLR-mediated innate immune induction, but does not bind to 14-3-3σ, suggesting some level of specificity for 14-3-3 proteins. Whether ZIKV NS3 specifically binds to other 14-3-3 proteins has yet to be determined. Furthermore, whether ZIKV NS3 modulates other 14-3-3-driven pathways merits a better understanding.

3.5 Methods

ZIKV strain Brazil Paraiba 2015 (BRA/2015)[119] was propagated in Vero cells following a protocol described previously[120]. ZIKV(KIKP) (strain MR 766) was generated based on a ZIKV strain MR 766 cDNA clone provided by Matthew Evans (Icahn School of Medicine, Mount Sinai) and previously described[121]. SeV (strain Cantell) was purchased from Charles River Laboratories.

Plasmids and transfections. FLAG-NS3 (ZIKV, strain H/PF/2013) was custom-synthesized by Invitrogen in the pcDNA3.1+ vector. GST-NS3 (ZIKV strain H/PF/2013) was generated by subcloning the FLAG-NS3 cDNA into the pEBG vector (encoding an N-terminal Glutathione S-transferase (GST)) using KpnI and NotI restriction sites. GST-NS3 (ZIKV, strain BRA/2015) was generated by introducing two silent mutations (nucleotide base positions 852 A $\rightarrow$G, 1734 C $\rightarrow$T) into GST-NS3 (ZIKV, strain H/PF/2013) by site-directed mutagenesis. FLAG-14-3-3η was generated by cloning human cDNA into pEF-BOS together with an N-terminal FLAG tag. HA-14-3-3η was generated by subcloning human 14-3-3η from the FLAG-14-3-3 construct into pQCXIP together with an N-terminal HA tag using the BamHI and NotI restriction sites. Plasmids encoding GST (pEBG), GST-NS3 (DENV, strain NGC), GST-NS3 (WNV, strain NY99), FLAG-14-3-3σ, IFN-β luciferase reporter plasmid and β-galactosidase-expressing plasmid (pGK-b-gal)[102], GST-MDA5 2CARD[80], FLAG-MDA5[78], HA- MeV V[124], have been described. All constructs were sequenced to verify the original sequence. Transfections were performed using Lipofectamine and Plus reagent (Life Technologies), linear polyethylenimine (1 mg/ mL solution in 20 mM Tris pH 6.8; Polysciences), or *Trans*IT-LT1 (Mirus Bio) following manufacturer's instructions.

Antibodies and reagents. These antibodies were used in immunoblotting: anti-GST (1:2,000, GST-2, Sigma), anti-FLAG (1:2,000, M2, Sigma), anti- HA (1:2,000, HA-7, Sigma), anti-14-3-3η (Santa Cruz, 6A12, Santa Cruz), anti-b-Actin (1:15,000, AC-15, Sigma), anti-GAPDH (1:40,000, CS204254, Millipore), anti-MAVS (1:1,000, 3993S, Cell Signaling Tech-

nology). A polyclonal anti-NS3 (ZIKV) antibody against the peptide CAALKSFKEFAAGKR was custom-generated by GenScript and was used for immunoblot analysis (1:1,500). A monoclonal anti-MDA5 antibody was purified from a mouse hybridoma cell line (1:500, Clone 17, provided by Jan Rehwinkel[94]). For immunoprecipitation of NS3, a polyclonal anti-NS3 (ZIKV) anti-body against the peptide CRRGRIGRNPNKPGD was custom-generated by GenScript and was used at a concentration of 2μg per sample.
Glutathione Sepharose 4B resin (GE Life Sciences), anti-HA magnetic beads (Thermo Scientific), or Dynabeads Protein G (Invitrogen) beads were used for respective pulldown or immunoprecipitation assays. Protease inhibitor cocktail (P2714, Sigma) was added at a concentration of 1:500 to cell lysates for all immunoblot and immunoprecipitation experiments. High-molecular weight (HMW)-poly(I:C) / LyoVec was purchased from InvivoGen.

Immunoblot analysis. Precipitated protein or cell lysates were resolved on 7% or 10% Bis-Tris SDS-PAGE gels (pH 6.4), and then transferred to a polyvinylidene difluoride (PVDF) membrane (Bio-Rad) using a Novex Semi-Dry Blotter (Invitrogen). Membranes were blocked with 5% (w/v) non-fat dry milk in PBS-T (PBS with 0.05% (v/v) Tween-20) for 30 min, and then probed with the indicated primary antibody in 2.5% (w/v) non-fat dry milk in PBS-T at 4 °C overnight. Following overnight incubation, membranes were probed with horseradish peroxidase (HRP)-conjugated secondary antibodies in 2.5% (w/v) non-fat dry milk in PBS-T for 1 h at room temperature. Proteins were visualized using SuperSignal West Pico or SuperSignal West Femto chemiluminescence reagents (Thermo Scientific) and detected by an ImageQuant LAS 4000 Chemiluminescent Image Analyzer (General Electric).

ZIKV infection and titration. SVGA cells were washed once with sterile PBS, then inoculated with FBS-free DMEM containing virus at 37 °C for 2 h at the indicated MOI. 2 h.p.i., supernatant was removed and cells were washed twice with PBS. Media was then replaced with DMEM (10% FBS) and incubated at 37 °C for 2 h for the incubated times. For plaque assay, samples were were serially diluted in DMEM with 1% penicillin-

streptomycin, then incubated on a confluent monolayer of Vero cells at 37 °C for 2 h. Infectious supernatant was removed and replaced with low-melting temperature agarose, then incubated for 3 days until plaque formation was visible. Cells were fixed in 1% (w/v) paraformaldehyde (PFA) (in PBS) for 1 h at room temperature, and then stained with crystal violet (VWR) in 20% (v/v) ethanol. Plaques were rinsed with water, counted, and virus titers calculated as described previously[120]. Briefly, dilution wells with distinct plaque formations were counted, and a plaque-forming unit per mL (PFU/mL) was calculated as (plaque count/well) x (dilution factor)/(volume of inoculum).

Cell lysis and immunoprecipitation. HEK293T and SVGA cells were lysed in Nonidet P-40 (NP-40) buffer (50 mM HEPES pH 7.4, 150 mM NaCl, 1% (v/v) NP-40, 1 mM EDTA, protease inhibitor cocktail) vortexed and centrifuged at 4 °C, 21,000 × g for 20 minutes. FLAG pull-downs, co-immunoprecipitations and western blot analyses were performed as previously described[80]. Briefly, lysates were subjected to pull-down with GST or FLAG beads for 4 h at 4 °C, or lysates were subjected to immunoprecipitation with 2μg primary antibody overnight at 4 °C followed by incubation with protein A/G agarose or Dynabeads Protein G beads for 2 h at 4 °C. A portion of the cell lysate was taken prior to pull-down or immunoprecipitation for analysis as a whole cell lysate (WCL) fraction. Elution of precipitated proteins was performed by heating samples in Laemmli SDS sample buffer at 95 °C for 5 minutes.

Luciferase reporter assays. HEK293T cells in 12-well plates were transfected with 300 ng of a β-galactosidase-expressing plasmid (pGK–gal), 200 ng of an IFN-β luciferase reporter plasmid, and 1.5μg of plasmid encoding the indicated GST-NS3 construct or GST-expressing pEBG vector. To stimulate IFN-β luciferase activity, cells were co-transfected with 100ng of GST-MDA5 2CARD. Cells were harvested at the indicated time point and luciferase activity (Promega) was measured alongside β-galactosidase activity. Luciferase values were normalized to β-galactosidase activity to control for transfection efficiency, and fold luciferase activity was calculated relative to values for control cells, set to 1.

Cytosol-Mitochondria fractionation assay. SVGA cells were infected with ZIKV(WT) or ZIKV(KIKP), and harvested 24 hours post infection in an Isotonic Mitochondrial Buffer (MIT1000, Merck Millipore). Cells were homogenized with a Dounce homogenizer and WCL was collected. Lysates were processed by low-speed centrifugation at 600 x g for 10 minutes to pellet nuclei and unbroken cells, which were then discarded. The supernatant was then centrifuged at 10,000 x g for 30 minutes at 4 $^{\circ}$C to pellet the mitochondrial fraction. The cytosolic (supernatant) and mitochondrial (pellet) fractions were subjected to a bicinchoninic acid (BCA) assay (Pierce), which was used to normalize protein amounts for SDS-PAGE and immunoblot analysis. Anti-GAPDH and anti-MAVS immunoblot analyses served as quality controls for relative cytosolic and mitochondrial fraction purity, respectively.

qRT-PCR. RNA was extracted from SVGA and HeLa cells using an RNA extraction kit (OMEGA Bio-Tek) following the manufacturer's instructions. Equal amounts of RNA (25-500ng) were used in a one-step qRT-PCR reaction using the SuperScript III Platinum One-Step qRT-PCR kit with ROX (Invitrogen) and FAM reporter dye primers, from IDT, for the genes analyzed. Gene expression was normalized to cellular GAPDH. The comparative CT method ($\triangle\ \triangle$ CT) was used to measure the induction of a target gene relative to its induction in mock-infected samples. All qRT-PCR reactions were performed using a 7500 FAST RT-PCR system (Applied Biosystems).

siRNA-mediated knockdown. SVGA cells were seeded (1 x 10^5) in 12 well plates and transfected with 50nM of gene-specific siGENOME SMARTpool siRNAs (Dharmacon) against RIG-I, MDA5, 14-3-3ϵ, 14-3-3η with RNAiMAX transfection reagent (Invitrogen) according to the manufacturer's instructions. As a control, non-targeting siRNA (siGENOME Non-Targeting siRNA Pool siGENOME Non-Targeting siRNA Pool 2, D-001206-14-05) was transfected. The following siRNAs were used: siRNAs targeting RIG-I (siGENOME SMARTpool M-012511-01-0005), MDA5 (siGENOME SMARTpool M-013041-00-0005), 14-3-3ϵ (siGENOME SMARTpool M-017302-03-005), or 14-3-3η (siGENOME SMART-

pool M-010626-01-0005) Silencing efficiency of these genes was determined by measuring transcript abundance at the indicated times by qRT-PCR using predesigned gene specific primers from IDT.

Statistical analysis. All data were presented as means ± SD and analyzed using GraphPad Prism software (version 7). An unpaired two-tailed Student's t-test ($p < 0.05$ was considered statistically significant), or a one-way ANOVA with Dunnett's multiple comparisons ($p < 0.01$ was considered statistically significant) was used as indicated in the legends. Pre-specified effect sizes were not assumed, and in general three biological replicates (n) for each condition were used within independent experiments.

CHAPTER 4

PHOSPHORYLATION-BASED FLAVIVIRAL EVASION OF 14-3-3-MEDIATED INNATE IMMUNITY

Attributions: WR performed and analyzed all experiments with the exception of all data related to mouse infection and WNV infection, as well as generation of mutant WNV, which was performed at ABSL-3 in collaboration with Ping Zhang, Qing Tan, Larissa Thackray and Michael Diamond at Washington University in St. Louis.

4.1 Abstract

14-3-3 protein family members facilitate the translocation of RIG-I and MDA5 to mitochondrial membranes to promote downstream RLR signaling, leading to the induction of type I IFNs. Our previous work has demonstrated that Zika (ZIKV), dengue (DENV), and West Nile (WNV) virus NS3 proteins bind to 14-3-3ϵ and 14-3-3η through a phosphomimetic RLDP motif to antagonize RIG-I and MDA5 signaling, respectively. Here, we demonstrate that loss of the RLDP-dependent 14-3-3 interaction motif attenuates WNV pathogenicity *in vivo*, and promotes the evolution of a compensatory phosphorylation-based NS3-14-3-3 interaction. Furthermore, we find that a naturally occurring phosphorylation-based NS3-14-3-3ϵ interaction motif is encoded in Powassan virus (POWV).

4.2 Introduction

Flaviviruses are members of the *Flaviviridae* family, and are made up of single-stranded positive-sense RNA viruses spread by arthropod vectors, a number of which are important to human health. Major flaviviruses spread by mosquitos include Yellow fever (YFV), Japanese encephalitis (JEV), DENV, ZIKV, and WNV. Flaviviruses can also be transmitted by ticks, and include Tick borne encephalitis (TBEV) and POWV.

The primary hosts of WNV are various avian species including those of the family Corvidae. WNV is spread between these birds via infected *Culex* mosquito species. Humans and horses can become infected with WNV as well, though infection in humans and horses typically leads to low level viremia. As such, humans and horses are considered terminal hosts and are unable to sustain high levels of disease within a population. Despite low levels of viremia in humans, WNV can cause disease in humans with symptoms including high fever, arthralgia, headache and fatigue. In some cases, WNV crosses the blood brain barrier and can cause encephalitis and meningitis[31,32].

POWV was first isolated in 1958 near the town of Powassan, Ontario, after the death

of a young child who had been infected with the virus[36]. POWV is transmitted via the bite of an infected *Ixodes* tick species, and has transmission routes through ticks to squirrels, skunks, and humans[37]. POWV circulates in North America and parts of Russia. In the US during the past decade, serological studies indicate that the number of human cases of POWV has increased in comparison to previous decades[37]. POWV crosses the blood brain barrier to cause encephalitic disease with a case fatality rate as high as 30%. In those who survive POWV infection, long-term neurological sequelae are not uncommon[38].

Many flaviviruses, including WNV, are controlled by type I IFN signaling[92]. Type I IFNs are induced in many cell types through recognition of viruses and other pathogens via pattern recognition receptors. Viruses are detected by intracellular sensors of nucleic acids, including the RIG-I like receptors (RLRs) RIG-I and MDA5 which detect cytosolic RNA. Binding to RNA activates the RLRs and initiates a set of reversible post translational modifications that enable interaction with other molecules involved in the signaling pathway[53]. For example, RIG-I is dephosphorylated in its CARD domains by cellular phosphatases, which enables RIG-I to adopt an open conformation and bind to the E3 ubiquitin ligase TRIM25, which ubiquitinates the CARD domain of RIG-I[52,78,80]. RIG-I and TRIM25 together with 14-3-3ϵ form a ternary translocon complex that shuttles RIG-I from the cytosol to the outer mitochondrial membrane and the mitochondrial associated membrane (MAM) to interact with the downstream signaling partner of RIG-I, the mitochondrial antiviral signaling (MAVS) protein. 14-3-3ϵ is critical for the re-distribution of activated RIG-I from the cytosol to the mitochondrial membranes[84,85]. MAVS is a membrane-anchored protein situated at the mitochondrial membrane, and interacts with RIG-I via CARD-CARD interactions[53,64]. These interactions serve to activate MAVS and stimulate oligomerization, spurring recruitment of TBK1 and IKKϵ[52]. This complex activates the cytosolic IRF3 and IRF7 transcription factors, that then translocate to the nucleus to induce the expression of type I IFNs, including IFN-β. Type I IFNs are secreted from the infected cell and bind to the IFNα/β receptor (IFNAR) in a paracrine and autocrine manner. Activated IFNAR amplifies antiviral signaling through activation of the intracellu-

lar JAK-STAT signaling pathway to induce the expression of IFN-stimulated genes (ISGs), a group of several hundred genes that encode proteins with antiviral signaling properties or direct antiviral activity[54,125]. Therefore, activation of the RLR signaling pathways activates type I IFN signaling to create an antiviral state in the infected cell as well as cells surrounding the infected cell.

WNV is controlled by type I IFN signaling in both *in vitro* cell culture models as well as *in vivo* mouse models[92]. Loss of either RIG-I or MDA5 results in diminished innate immune induction, while loss of both RIG-I and MDA5 results in a complete loss of innate immune signaling in a mouse model[92]. Therefore, the RLR-MAVS signaling axis is essential for control of WNV infection. Recent work from our lab has established that several flaviviruses, including DENV, ZIKV, and WNV encode a phosphomimetic motif that enables an interaction between NS3 and 14-3-3ϵ as well as 14-3-3η. By binding to these 14-3-3 proteins, NS3 blocks both RIG-I and MDA5 signaling pathways, thereby antagonizing induction of antiviral innate immunity. Generation of recombinant mutant DENV and ZIKV that harbor a mutated NS3-14-3-3 interaction motif revealed that these NS3-14-3-3 protein interactions are crucial for successful viral proliferation in an IFN-dependent manner in cell culture[102,126]. However, whether this NS3-mediated evasion of 14-3-3-driven innate immunity contributes to viral pathogenesis *in vivo* has not been determined as of yet.

The study of POWV as it relates to innate immunity has largely been neglected. It is unclear how POWV is detected by intracellular sensors, but because of its genetic similarity and similar mode of transmission is thought to behave similarly to TBEV[37]. MAVS is required for induction of IFN-β in response to TBEV infection in mouse embryonic fibroblasts and has been demonstrated to be important in neural tissue during infection of mice with TBEV[127–129].

Here, we evaluate whether the NS3-14-3-3 protein interaction affects pathogenicity

of WNV by generating a NS3 mutant recombinant WNV that harbors a mutated 14-3-3-binding motif. Our findings indicate that in a mouse model of infection, WNV encoding a mutated 14-3-3 protein interaction motif in NS3 (WNV(KIKP)) is strikingly attenuated due to the RLR-MAVS signaling axis. Furthermore, we find that WNV(KIKP) generates a compensatory mechanism to bind 14-3-3ϵ through a non-phosphomimetic-based method. We also find that another flavivirus species, POWV, encodes a non-phosphomimetic 14-3-3ϵ interaction motif in its NS3 protein that we conclude is reliant on phosphorylation via a cellular kinase. Our findings broaden our understanding of the importance of the NS3-14-3-3 protein interaction throughout members of *Flaviviridae*.

4.3 Results

4.3.1 WNV NS3 antagonizes RIG-I signaling in human and mouse cell lines

Recently published work from our laboratory has demonstrated that DENV, WNV, and ZIKV NS3 proteins bind to 14-3-3ϵ and 14-3-3η to antagonize RIG-I and MDA5 signaling, respectively[102,126]. Generation of mutant recombinant viruses deficient in this 14-3-3-protein interaction ability and infection of cell lines has shown binding to 14-3-3 proteins is important for immune evasion *in vitro*, and we hypothesize that the NS3-14-3-3 interaction is similarly critical during *in vivo* infection. Because immunocompetent mice generally do not display disease symptoms upon infection of ZIKV or DENV, we utilized a mouse model of WNV infection, which displays symptoms of disease relevant to human infection[122,130,131]. Furthermore, the amino acid sequence of 14-3-3ϵ is identical in human and mouse.

We first assessed whether WNV NS3 antagonizes RIG-I signaling in both human and mouse cells. In HEK293T, a human kidney cell line, WNV NS3 of three different strains (NY99, Kunjin, and B-956) all antagonized RIG-I-mediated induction of IFN stimulated by

SeV (Figure 4.1 A), in agreement with previous results. Similarly, ectopic expression of WNV NS3 proteins of the three strains tested antagonized RIG-I-mediated induction of IFN in Hepa1-6 cells, a mouse liver cell line (Figure 4.1 B). While the intensity of antagonism is overall lower in the mouse cell line, the general induction of IFN is also lower in the mouse cell line. Due to lower overall expression of plasmids in the mouse cell line than in the human HEK293T cells, which are readily transfectable, we believe this apparent diminished antagonism is technical in nature. Therefore, we conclude that WNV NS3 antagonizes RIG-I signaling in mouse cells as it does in human cells. Importantly, B-956 was the first isolated strain of WNV, while NY99 was much more recently isolated (1999). Because the antagonism of RIG-I signaling by NS3 was seen for all WNV strains we tested, we believe this suggests NS3 evasion of RIG-I signaling is a fundamental property of WNV, similar to what we observed for ZIKV[126].

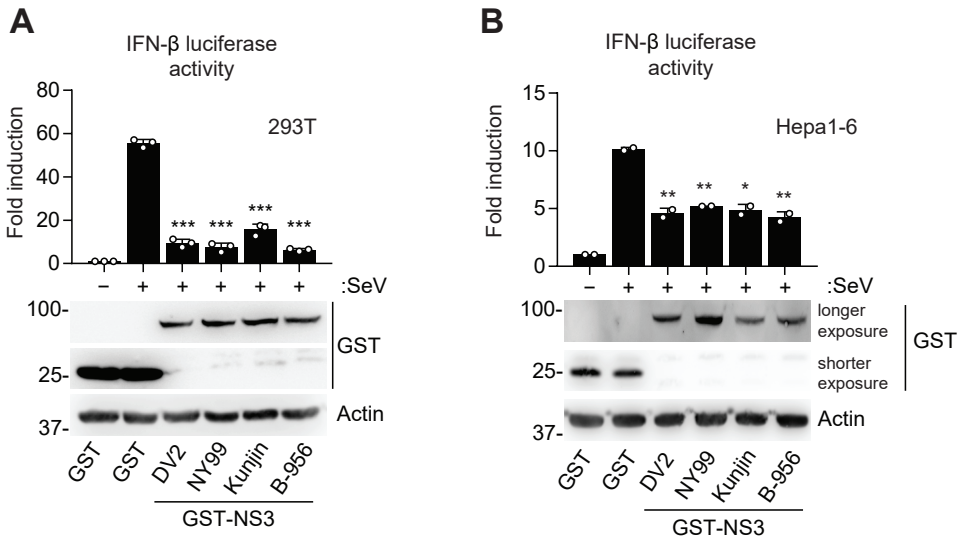

Figure 4.1 WNV NS3 antagonizes RIG-I signaling in human and mouse cells.
(A) Upper: IFN-β luciferase activity in HEK293T cells co-transfected to express a luciferase reporter under control of the IFN-β promoter, and GST or GST-NS3 from DENV (NGC), WNV (NY99), or WNV (Kunjin), or WNV (B-956) for 42 h. Cells were infected with SeV (50 HAU/mL) for 28 h, then harvested and luciferase activity was measured and normalized to co-transfected β-galactosidase. Values are presented relative to GST-expressing cells, set to 1. Lower: IB analysis of WCL with anti-GST and anti-Actin (loading control).
(B) IFN-β luciferase activity in Hepa1-6 transfected and assessed as in (A).
Data are expressed as means ± SD (n = 3). *p < 0.05, **p < 0.01, ***p < 0.001 (Student's t test).

4.3.2 The pathogenicity of WNV(KIKP) is attenuated in mice as compared to WT(WNV)

To assess the importance of the NS3-14-3-3 protein interaction *in vivo*, we generated a mutant WNV (strain NY99), termed hereafter WNV(KIKP), by introducing the mutations R64→K64, L65→I65, D66→K66 into NS3. We then infected 5 week old WT C57B6/J mice through footpad injection with WNV(WT) and WNV(KIKP) viruses and measured survival over a 30 day period. We found that mice were highly vulnerable to WNV(WT) but not WNV(KIKP); approximately 10% of the mice infected with WNV(WT) survived, in contrast to 50% survival in mice infected with WNV(KIKP) (Figure 4.2 A). Furthermore, infection

of MAVS$^{-/-}$ mice (C57BL/6J background) resulted in similar survival curves for the two viruses (Figure 4.2 B). Together, these data indicate that WNV(KIKP) is attenuated *in vivo* due to its inability to antagonize the RLR-MAVS signaling axis.

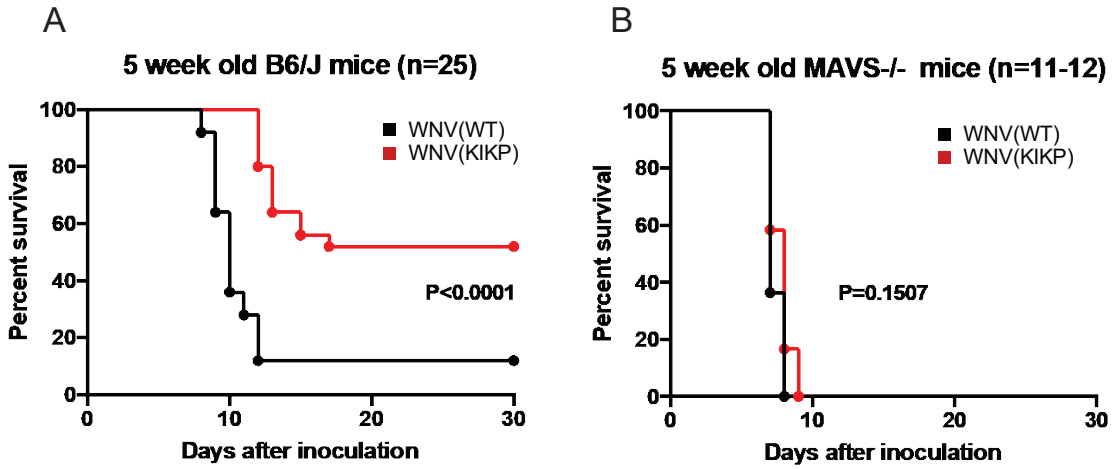

Figure 4.2 Pathogenicity of WNV(KIKP) is attenuated *in vivo*.
(A) Survival of 5-week old C57B6/J mice that were inoculated subcutaneously with 10^2 focus-forming units (FFU) of WNV(WT) or WNV(KIKP).
(B) Survival of 5-week old MAVS$^{-/-}$ mice that were inoculated subcutaneously with 10^2 FFU WNV(WT) or WNV(KIKP).

We then sequenced the virus from all WT mice infected with WNV(KIKP) that had succumbed to infection, and found that the virus had mutated from WNV(KIKP) to WNV(TIKP)—that is, K64→T64. We reasoned that this K64T mutation may enhance viral pathogenicity by re-establishing the NS3-14-3-3 interactions. However, upon re-sequencing viral stocks, we found that WNV(TIKP) had already existed prior to being introduced into mice. Therefore, stocks were re-generated and it was verified that the newly generated stocks contained either only WNV(WT) or WNV(KIKP). In addition, a WNV(TIKP) mutant recombinant virus was made.

4.3.3 WNV(KIKP), but not WNV(TIKP), is attenuated in HeLa and HEK293T

We first assessed how the three viruses (WT, KIKP, and TIKP) replicate in IFN-deficient cell culture. Upon infection of Vero cells, which do not secrete IFN[115], we found that the three viruses had similar replication kinetics over a 96 hour time course, although WNV(KIKP) was attenuated between 10 and 100 fold at 24 h post infection (Figure 4.3 A). Similarly, infection of C6/36 mosquito cells showed similar replication kinetics between WNV(WT) and WNV(TIKP), but WNV(KIKP) appeared to be attenuated by a 10-fold difference throughout the time series (Figure 4.3 B). We concluded that WNV(KIKP) had a slight growth-attenuation in comparison to WNV(WT), but the K64T mutation in WNV(TIKP) rescued any minor attenuation seen in WNV(KIKP).

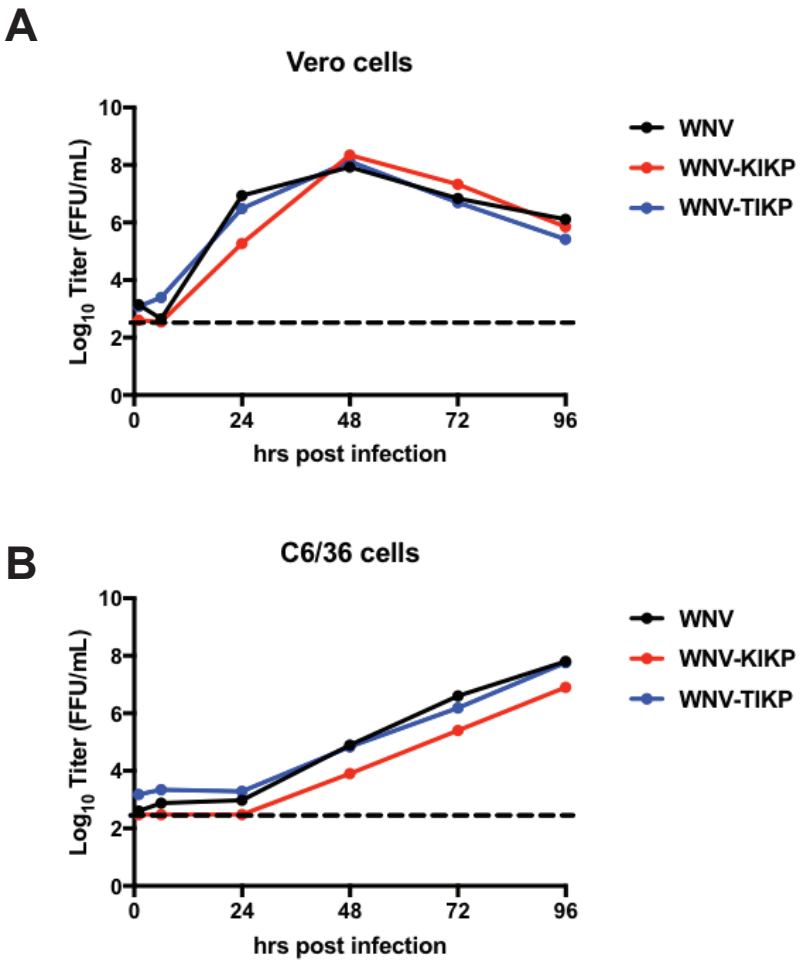

Figure 4.3 Replication of WNV(WT), WNV(KIKP), and WNV(TIKP) in IFN-deficient cell lines.

(A) Viral titer in the supernatant of Vero cells that were infected with WNV(WT), WNV(KIKP), or WNV(TIKP) (10^3 FFU for each) for the indicated times, determined by focus-forming assay, represented as FFU/mL. Dotted line indicates limit of detection.

(B) Viral titer in the supernatant of C6/36 cells that were infected with WNV(WT), WNV(KIKP), or WNV(TIKP) (10^3 FFU for each) for the indicated times, assessed by focus-forming assay and presented as FFU/mL. Dotted line indicates limit of detection.

We then assessed whether the mutant viruses are attenuated during infection of IFN-competent cells. In HeLa cells, WNV(WT) and WNV(TIKP) had similar replication kinetics over a 96 time course, but WNV(KIKP) was significantly attenuated by about 100 fold in comparison to WNV(WT) (Figure 4.4 A). Similarly, WNV(KIKP) had strongly diminished growth in HEK293T cells in comparison to WNV(WT), but WNV(TIKP) had a growth phenotype more similar to WNV(WT) (Figure 4.4 B). Together with the *in vivo* data, we conclude that WNV(KIKP) is attenuated primarily in an IFN-dependent manner, but WNV(TIKP) rescues this attenuation.

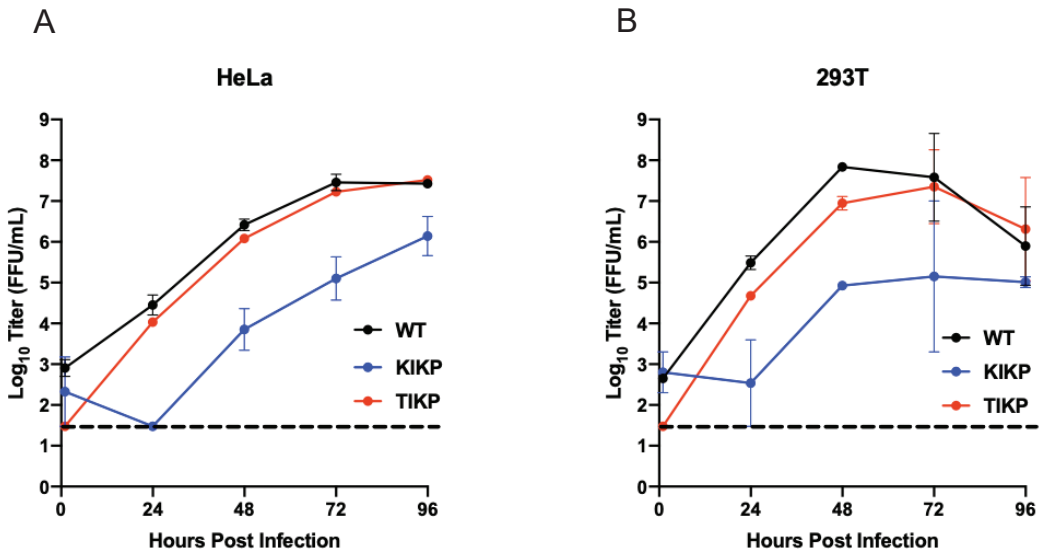

Figure 4.4 Replication of WNV(WT), WNV(KIKP), and WNV(TIKP) in human cell lines. **(A)** WNV(WT), WNV(KIKP), or WNV(TIKP)-infected HeLa cells at the indicated FFU. Supernatant was harvested at the indicated time points and viral titer was determined by focus-forming assay, presented here as FFU/mL. Dotted line indicates limit of detection. **(B)** Viral titer in the supernatant of HEK293T cells infected with WNV(WT), WNV(KIKP), or WNV(TIKP) at the indicated FFU. Supernatant was harvested at the indicated time points and assessed by focus forming assay and presented as FFU/mL. and assessed as in (A). Dotted line indicates limit of detection.

4.3.4 WNV NS3-TIKP restores the NS3-14-3-3ϵ interaction

Given that WNV(TIKP) appears to have similar pathogenicity to WNV(WT), we reasoned, we reasoned that NS3-TIKP restores binding to 14-3-3ϵ and therefore reinstates the ability of WNV to subvert RIG-I-mediated immunity. Therefore, we assessed the ability of the different WNV NS3 proteins (WT, KIKP, and TIKP) to bind to 14-3-3ϵ. We found that WNV NS3-TIKP binds to 14-3-3ϵ with a binding affinity similar to that of NS3-WT. In contrast, NS3-KIKP showed a near-complete loss of 14-3-3ϵ binding, in agreement with previously published results (Figure 4.5 A). We then evaluated whether WNV NS3-TIKP is capable of sequestering 14-3-3ϵ from the RIG-I-14-3-3ϵ interaction. We found that in the presence of NS3-WT and NS3-TIKP, the interaction between RIG-I and 14-3-3ϵ was strongly diminished. However, NS3-KIKP did not inhibit the RIG-I-14-3-3ϵ interaction (Figure 4.5 B). Therefore, the K64T mutation in WNV NS3 restores the ability of NS3 to bind to 14-3-3ϵ and compete for the RIG-I-14-3-3ϵ interaction. In this manner, WNV NS3-TIKP rescues the ability of WNV to subvert innate immune induction driven by RIG-I.

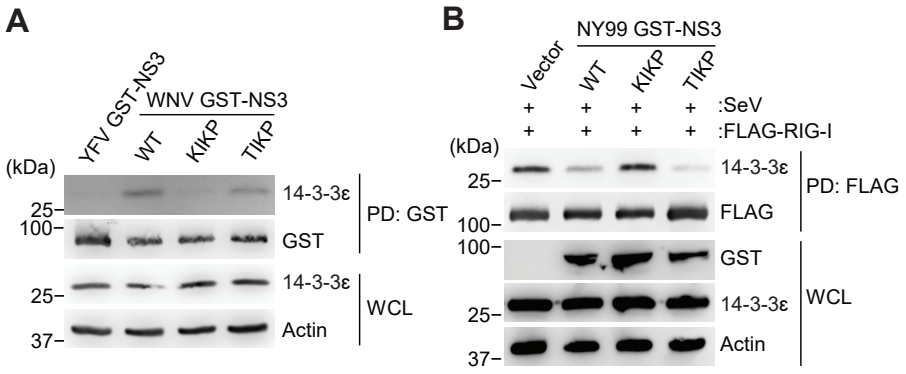

Figure 4.5 WNV NS3 (WT) and NS3(TIKP), but not NS3(KIKP), bind to and sequester 14-3-3ϵ.
(A) NS3-14-3-3ϵ interaction in HEK293T cells transfected for 42 h with YFV GST-NS3 (negative control), or WNV GST-NS3 (WT, KIKP, or TIKP), determined by GST-pulldown and IB with the indicated antibodies.
(B) Interaction between FLAG-RIG-I and endogenous 14-3-3ϵ in HEK293T cells that were transfected with FLAG-RIG-I together with either empty vector or WNV GST-NS3 (WT, KIKP, or TIKP) for 42 h and then infected with SeV (50 HAU/mL) for 20 h, assessed by FLAG-pulldown (PD: FLAG) and IB with the indicated antibodies.

4.3.5 WNV NS3-TIKP is phosphorylated

14-3-3 proteins typically bind to cellular proteins that encode a RxxpS/pTxP motif, which contains an essential phosphorylated serine or threonine residue[88]. In addition, other phosphorylated motifs have been identified to mediate 14-3-3 binding. We reasoned that WNV NS3-TIKP restores the NS3-14-3-3ϵ interaction through a similarly phosphorylated mode. We therefore assessed the phosphorylation of T64 in WNV NS3-TIKP. We compared the level of phosphorylation of WNV NS3-WT and NS3-TIKP in HEK293T cells, and found that NS3-TIKP was more highly phosphorylated than NS3-WT, despite encoding only one extra threonine residue (Figure 4.6 A). This suggested to us that NS3-TIKP is phosphorylated at T64. We then affinity-purified WNV NS3-TIKP and analyzed post-translational modification of NS3-TIKP using liquid chromatography and tandem mass spectrometry (LC-MS/MS). Analysis of the mass spectra indicated that NS3-TIKP is indeed phosphorylated at T64 (Figure 4.6 B). Together these data indicate that WNV NS3-TIKP is phosphorylated at T64, which restores the NS3-14-3-3ϵ interaction.

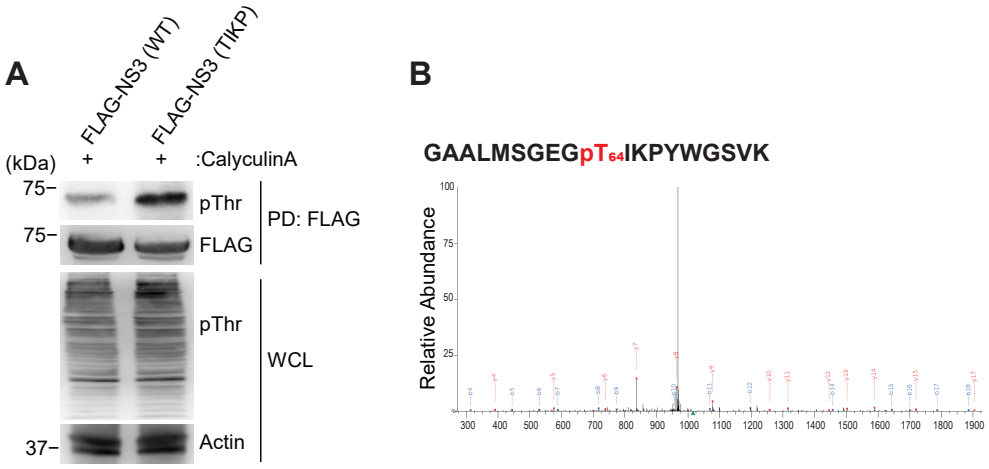

Figure 4.6 WNV NS3(TIKP) is phosphorylated at T64.
(A) Threonine phosphorylation of FLAG-tagged WNV NS3(WT) or NS3(TIKP) purified from HEK293T cells that were transfected for 42 h with those plasmids and then treated with phosphatase inhibitor Calyculin A for 45 min, assessed by FLAG-pulldown (PD: FLAG) and IB with a pan-pThreonine antibody (pThr) and FLAG antibodies. WCLs were further probed with anti-pThr and Actin (loading control) antibodies.
(B) Tandem mass spectra of the tryptic phosphopeptide GAALMSGEGpT$_{64}$IKPYWGSVK of affinity purified WNV NS3(TIKP) using anti-FLAG agarose from HEK293T cells that were transiently transfected for 48 h with this plasmid and then treated with Calyculin A for 45 min. Mass spectra identified phosphorylation at T64. b- and y-ion designations are shown.

4.3.6 POWV NS3 encodes a non-phosphomimetic 14-3-3ϵ interaction motif

We then sought to determine whether any naturally occurring flavivirus species encode a non-phosphomimetic 14-3-3ϵ interaction motif. We found that POWV NS3 encodes either a 67-TSGP-70 or 67-VSGP-70 motif at the location corresponding to the WNV/ZIKV 64-RLDP-67 NS3 motif (Figure 4.7 A). We reasoned that either T67 or S68 of the POWV motif could be phosphorylated and coordinate binding to 14-3-3ϵ. We therefore assessed whether NS3 of either POWV subtype could bind to 14-3-3ϵ. Immunoprecipitation of POWV NS3 of two unique strains showed that POWV NS3 (strain LB), encoding

67-TSGP-70, binds to 14-3-3ϵ. However, POWV NS3 (strain Spooner), encoding 67-VSGP-70, only minimally binds to 14-3-3ϵ (Figure 4.7 B). To determine whether T67 is necessary for the LB NS3-14-3-3ϵ interaction, we generated a plasmid encoding LB NS3 67-KSGP-70. We found that LB NS3-KSGP had a strongly diminished binding to 14-3-3ϵ, in comparison to DENV NS3 and LB NS3-WT (Figure 4.7 C). Together, these data suggest that T67 is necessary for the NS3-14-3-3ϵ interaction.

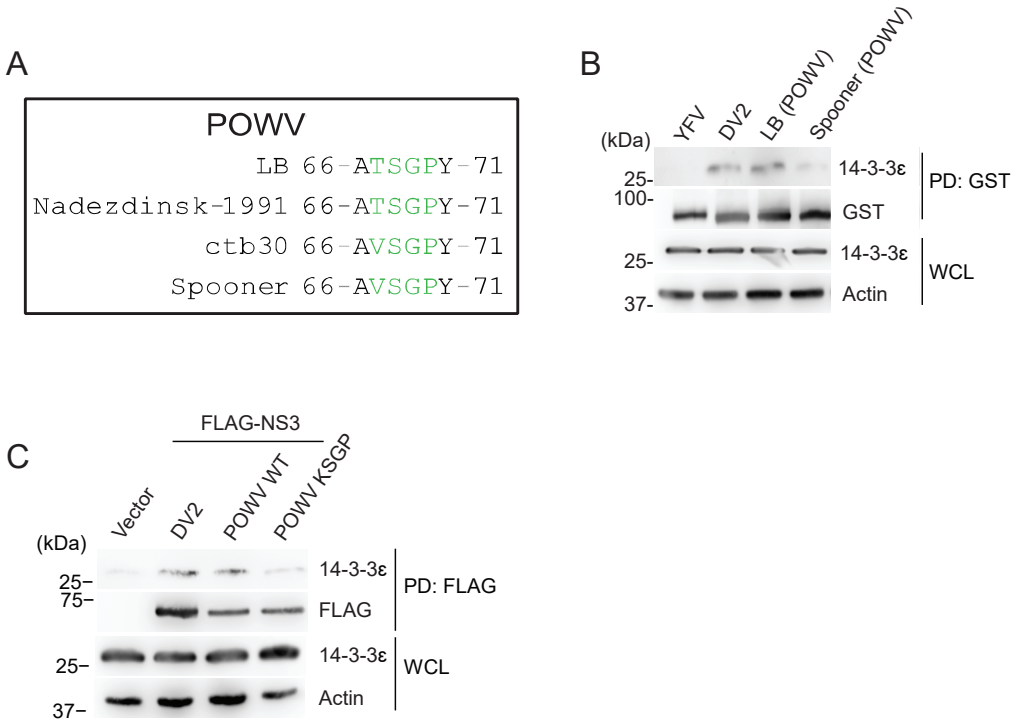

Figure 4.7 POWV NS3 binds to 14-3-3ϵ via a non-phosphomimetic motif.
(A) Amino acid sequence of the POWV NS3 region from the indicated strains that corresponds to phosphomimetic RxE/DP motif found in other flaviviruses.
(B) NS3-14-3-3ϵ interaction in HEK293T cells transfected with GST-NS3 of YFV (17D), DENV (NGC), POWV (LB), or POWV (Spooner), assessed by GST-pulldown (PD: GST) and IB with the indicated antibodies.
(C) NS3-14-3-3ϵ interaction in HEK293T cells transfected with FLAG-tagged NS3 from DENV (NGC) or POWV (LB) FLAG-NS3 WT or KSGP mutant, assessed by FLAG-pulldown (PD: FLAG) and IB with the indicated antibodies.

4.3.7 POWV NS3 is phosphorylated

Similar to the WNV NS3-TIKP interaction with 14-3-3ϵ, we reasoned that phosphorylation of the 67-TSGP-70 motif at T67 might promote an interaction between POWV NS3 (strain LB) and 14-3-3ϵ. We therefore affinity purified POWV NS3 (strain LB) and subjected it to LC-MS/MS (Figure 4.8 A). Based on the mass spectra for the peptide containing 67-TSGP-70 (RGAALSVEGATSGPYWADVRE), we found that this peptide is indeed phosphorylated at one single site (Figure 4.8 B). However, analysis of the mass spectra cannot determine which residue in this peptide is phosphorylated. Therefore, we utilized the Phos-tag system to visualize phosphorylation by immunoblot. Phos-tag is a functional molecule that binds to phosphorylated proteins and slows their migration through an SDS-PAGE gel[132]. Therefore, more highly phosphorylated proteins have slower migration in a gel. When we compared the gel shift of POWV NS3-WT to POWV NS3-KSGP using Phos-tag, we found that the WT NS3 but not NS3-KSGP has a band that migrates more slowly in the gel (Figure 4.8 C). This suggests that either T67 is indeed phosphorylated, or that T67 is important for phosphorylation of the RGAALSVEGATSGPYWADVRE peptide within LB NS3.

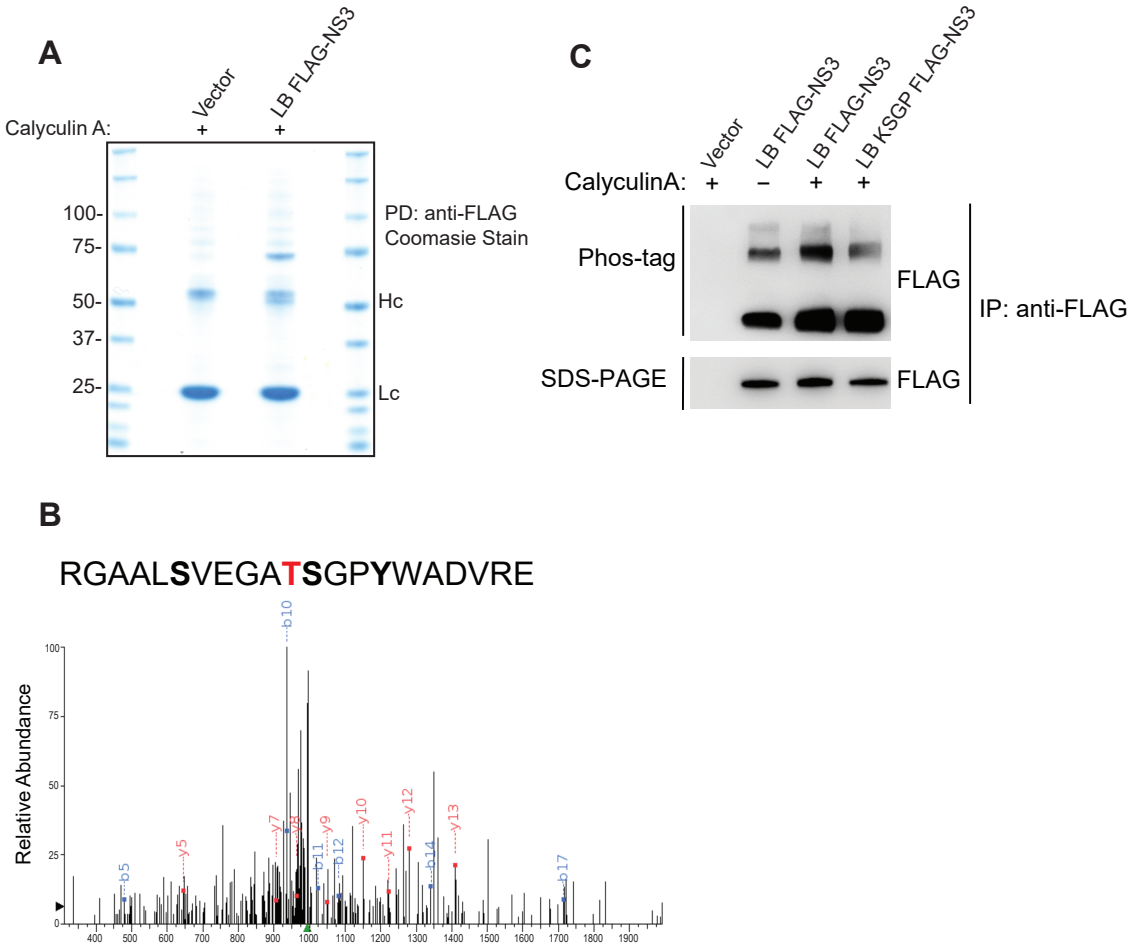

Figure 4.8 Phosphorylation of POWV LB NS3.

(A) Coomassie-stained complexes of affinity-purified POWV (LB) FLAG-NS3 affinity-purified using anti-FLAG agarose from HEK293T cells that were transfected for 48 h with this plasmid and then treated with Calyculin A for 45 min. Cells transfected with empty vector served as a negative control. An asterisk denotes the FLAG-NS3 protein. Hc, antibody heavy chain. Lc, antibody light chain.

(B) Tandem mass spectra of tryptic phosphopeptide RGAALSVEGATSGPYWADVRE derived from POWV (LB) NS3 WT identified a single phosphorylation site at either S59, T64, S65, or Y68. b- and y-ion designations are shown.

(C) Phosphorylation of POWV LB NS3 in HEK293T cells that were transfected for 42 h with either empty vector or POWV FLAG-NS3 (WT or KSGP) and then treated with Calyculin A for 45 min, assessed by FLAG-pulldown (PD: FLAG) and Phos-tag or SDS-PAGE, followed by IB with anti-FLAG antibody.

4.4 Discussion

Together, our data demonstrates that the flavivirus NS3-14-3-3ϵ and NS3-14-3-3η interactions are critical for evading antiviral innate immune signaling via the RLR-MAVS signaling axis *in vivo*. Moreover, evasion of the RLR signaling pathways appears to be the major attenuating feature of WNV-KIKP, suggesting that any speculative loss of other 14-3-3-driven pathways that NS3 may modulate are less detrimental than an inability to evade type I IFN responses. Interestingly, during infection of C6/36 mosquito cells, we found that WNV(KIKP) is consistently attenuated. This may indicate that WNV replication relies in part on 14-3-3-driven pathways outside of RLR-based innate immunity during infection of mosquito cells. Previous studies did not examine replication kinetics of DENV(KIKP) or ZIKV(KIKP) in mosquito cells[102,126]. Our results also show the appearance of a compensatory mutation in the WNV(KIKP) virus that rescues its inability to bind to 14-3-3ϵ. This suggests that even in cell culture, where the T64 mutant virus arose, WNV(KIKP) is under high evolutionary pressure to regain the NS3-14-3-3 protein interaction. In this case, WNV(KIKP) mutated to WNV(TIKP), which we found binds to and sequesters 14-3-3ϵ from RIG-I after being phosphorylated by a cellular kinase. Interestingly, WNV(TIKP) no longer binds 14-3-3ϵ via a phosphomimetic motif, but rather through a phosphorylatable threonine residue. However, the phosphorylated T64 of NS3-TIKP is still able to compete for the 14-3-3ϵ interaction with RIG-I. We suggest that because it is an artificial sequence, 64-TIKP-67 is not regulated by a phosphatase, and instead remains in a constitutive binding 'on' state and therefore is able to compete with RIG-I for the 14-3-3ϵ interaction.

Our findings also demonstrate that interactions between flavivirus NS3 and 14-3-3 proteins are not limited to mosquito-borne flaviviruses. A number of strains of POWV, a tick-borne flavivirus responsible for a sometimes lethal encephalitic infection, encode a non-phosphomimetic 14-3-3ϵ interaction motif. It is unclear why only some NS3 proteins of different POWV strains encode this 14-3-3 interaction motif, when others encode instead 67-VSGP-70. Because 14-3-3 proteins are present in different forms within different spe-

cies, it is interesting to speculate that this differential 14-3-3ϵ binding ability affects host tropisms between strains. More work will have to be done to understand the evolutionary history of POWV strains, as well as if other non-structural proteins bind to 14-3-3ϵ and could therefore compensate for the loss of this ability.

Our data demonstrates that LB NS3 is phosphorylated in the peptide encompassing the 67-TSGP-70 motif. Furthermore, the binding data we collected suggest that T67 is critical for binding to 14-3-3ϵ. Together, we believe these data support a model wherein T67 is phosphorylated by a cellular kinase, thereby allowing POWV LB NS3 to compete for the RIG-I-14-3-3ϵ interaction, though this has yet to be experimentally addressed. This is further supported by our WNV NS3-TIKP binding data, wherein we found that phosphorylation-based competition is sufficient to sequester 14-3-3ϵ from RIG-I and therefore is an efficient mode of antagonism. The identity of the cellular kinase that enables the POWV NS3-14-3-3ϵ interaction has yet to be determined, but may make a tantalizing cellular target for anti-POWV therapeutics.

We expect that through binding to 14-3-3ϵ, POWV NS3 antagonizes RIG-I mediated IFN induction, although further study will be needed to experimentally verify this. If true, this natural occurrence of a non-phosphomimetic interaction motif highlights the need flaviviruses have of subverting RLR signaling. Moreover, the non-phosphomimetic antagonism of 14-3-3ϵ-driven RIG-I signaling and the phosphomimetic-based antagonism are examples of convergent evolution within *Flaviviridae*.

4.5 Methods

Cell culture and viruses. HEK293T, Vero, and HeLa cells were cultured in Dulbecco's Modified Eagle's Medium (DMEM, Gibco) supplemented with 10% FBS (v/v) (Gibco) and 1% penicillin-streptomycin (v/v) (Gibco). C6/36 and Hepa1-6 were cultured in Eagle's Minimum Essential Medium (Gibco) supplemented with 10% (v/v) FBS and 1% (v/v) penicillin-streptomycin. All cells were cultured under standard culture conditions.

WNV(KIKP) and WNV(TIKP) were generated using a NY99 cDNA plasmid previously described[133]. Site-directed mutagenesis by PCR was used to generate mutant NY99 cDNA clones encoding the substitutions R64K, L65I, and D66K in the gene encoding NS3. *In vitro*-transcribed RNA generated from the WT and mutant infectious clone plasmids was electroporated into BHK21 cells. Viral supernatant was collected 3 days post electroporation when cytopathic effect was evident, and the WT and mutant viruses were amplified in BHK21 cells. Supernatants containing amplified recombinant WNV(KIKP), WNV(TIKP) or the parental virus were serially diluted and titers were determined by focus-forming assay on Vero cells.

The WNV strain (NY99) was propagated in Vero cells and quantified as previously described in detail[120]. SeV (strain Cantell) was purchased from Charles Rivers Laboratories.

Mouse experiments. C57BL/6J wild-type mice were commercially obtained (Jackson Laboratories, Bar Harbor, ME). MAVS$^{-/-}$ were generated in the C57BL/6J background by Michael Gale (University of Washington) and were bred at Washington University. Male and female 5 week-old mice were used for all *in vivo* studies. 10^2 FFU of WNV was diluted in PBS and inoculated by subcutaneous footpad injection in a volume of 50μL.

Plasmids and transfections. pEBG, WNV GST-NS3 (strain NY99), DV2 GST-NS3 (strain NGC), YFV GST-NS3 (strain 17D), FLAG-RIG-I, IFN-β luciferase construct, and pGK-b-

gal have been described previously[102]. WNV GST-NS3 (strains Kunjin, B-956) constructs were made by cloning Kunjin and B-956 NS3 into the pEBG vector. WNV FLAG-NS3 (strains NY99, Kunjin, B-956) were made by subcloning pEBG-NS3 (respective strains) into the pEF-BOS vector using PCR. WNV FLAG-NS3-TIKP was generated using site-directed mutagenesis by PCR. POWV GST-NS3 (strains LB, Spooner) constructs were made by cloning gBlock (IDT) sequences encoding the respective NS3 sequence into the pEBG vector using Gibson assembly. POWV FLAG-NS3 (strain LB) was generated by subcloning pEBG-NS3 (LB) into pEF-BOS using KpnI and NotI restriction sites. POWV FLAG-NS3-KSGP was generated using site-directed mutagenesis by PCR.

All constructs were sequenced to verify 100% agreement with the original sequence. Transfections were performed using the calcium phosphate method, or Lipofectamine and Plus reagent (Life Technologies), or linear polyethylenimine (1 mg/mL solution in 20mM Tris pH 6.8; Polysciences).

Antibodies and reagents. For immunoblot analysis, the following antibodies were used: anti-GST (1:2,000, GST-2, Sigma), anti-FLAG (1:2,000, M2, Sigma), anti–Actin (1:15,000, AC-15, Sigma), anti-14-3-3 (1:1,500, N1C3, Genetex). Anti-mouse or anti-rabbit-horseradish peroxidase (HRP) conjugated secondary antibodies (both 1:2,000) were purchased from Cell Signaling Technology (7076S and 7074S, respectively).

Anti-FLAG M2 magnetic beads, (Sigma), Glutathione Sepharose 4B resin (GE Life Sciences), or Dynabeads Protein G (Invitrogen) beads were used for respective pull-downs and immunoprecipitations. Calyculin A was purchased from Invitrogen and used at a dilution of 1:250 for 45 minutes at 37 °C. Protease inhibitor cocktail (P2714) was purchased from Sigma and used at a concentration of 1:500 in all immunoprecipitation experiments.

Immunoblot analysis. Protein samples were separated on 10% Bis-Tris SDS-PAGE gels (pH 6.4), and then transferred to a Polyvinylidene difluoride (PVDF) membrane (Bio-Rad) using a semi-dry transfer method. Membranes were blocked with 5% (w/v) non-fat dry

milk in PBS-T (PBS with 0.05% (v/v) Tween-20) for 30 minutes at room temperature, and then probed with the indicated antibody overnight in 2.5% (w/v) non-fat dry milk in PBS-T at 4 °C. The next day, membranes were washed in PBS-T for 30 minutes, then probed with HRP-linked secondary antibodies in 2.5% non-fat dry milk in PBS-T at room temperature for 1 h before being washed in PBS-T again. Protein bands were visualized using SuperSignal West Pico or Femto chemiluminescence reagents (Pieree) and detected with an ImageQuant LAS 4000 Chemiluminescent Image Analyzer (GE).

Cell lysis and immunoprecipitation. HEK293T or Hepa1-6 cells were lysed in NP-40 buffer (Nonidet P-40) containing 50 mM HEPES pH 7.4, 150 mM NaCl, 1% (v/v) NP-40, 1 mM EDTA, protease inhibitor cocktail, then vortexed and centrifuged at 4 °C, 21,000 × g for 20 minutes. GST or FLAG-pulldowns and western blot analyses were performed as previously described[80]. A portion of cell lysate was taken prior to pull-down for analysis as a whole cell lysate (WCL). Elution of protein was done by heating samples in Laemmli SDS sample buffer for 5 minutes at 95 °C.

Luciferase reporter assays. HEK293T cells were seeded into 12 well plates at a density of 10^5. The following day, they were transfected with 300ng of pGK-b-gal (β-galactosidase-expression plasmid), 200ng of IFN-β luciferase reporter plasmid, as well as 1.5μg of plasmid encoding the indicated GST-NS3 constructs or the GST-expressing pEBG vector. Hepa1-6 cells were seeded into 10-cm dishes at a density of about 2.5 × 10^6. The next day, cells were transfected with 2.4μg IFN-β luciferase reporter plasmid, 3.6μg pGK-b-gal , and 204μg of plasmid encoding the indicated GST-NS3 constructs or the pEBG vector. IFN-β luciferase was induced by infecting cells with SeV (50 HAU/mL) 42 h after transfection. At the indicated time points, cells were washed once using sterile PBS, then harvested using a luciferase lysis buffer, and luciferase activity was measured (Promega). Luciferase values were normalized to β-galactosidase activity to control for transfection efficiency, and fold luciferase activity was calculated relative to values for control cells, set to 1.

Phos-tag phosphorylation analysis. 30μL Dynabeads were conjugated with 3μL FLAG antibody (ms) in PBS-T with rotation for 2 hours at 4 $^{\circ}$C, and then incubated with Calyculin A-treated cell lysate with rotation for 2 h at 4 $^{\circ}$C. Beads were washed under stringent conditions using RIPA buffer (150mM NaCl, 1% (v/v) NP-40, 1% (w/v) deoxycholic acid, 0.01% (w/v) SDS, 20mM Tris (pH 8.0), and protease inhibitor cocktail) to remove non-specific binding proteins. Zn^{2+}-Phos-tag SDS PAGE gels were prepared according to manufacturer's instructions, using 75 μM Phos-tag reagent in each gel preparation. 10μL of precipitated protein sample was diluted in 1x Laemmli sample buffer to a total volume of 25μL and run using a neutral MOPS buffer for 2 h 15 m at 0.03 mA, and further processed by immunoblot as described above.

POWV NS3 sequence analysis. Alignment tools and and the flavivirus database at viprbrc.org were used to align the amino acid sequences of Powassan virus strains, and NS3 sequences were analyzed for the presence of 14-3-3-interaction motifs at the region corresponding to ZIKV, DENV, and WNV NS3 phosphomimetic motifs as described before.

Statistical Analysis. All data were presented as means ± SD and analyzed using GraphPad Prism software (version 7). An unpaired two-tailed Student's t-test ($p < 0.05$ was considered statistically significant) was used as indicated.

CHAPTER 5

CONCLUSIONS

5.1 Overview of results

In this dissertation, we have demonstrated that ZIKV NS3 encodes a 14-3-3 protein interaction motif to antagonize RIG-I and MDA5 signaling during viral infection. Furthermore, this 14-3-3 protein interaction is conserved in several flavivirus species, and is essential for successful viral pathogenicity in an animal model. Specifically, we have shown:

In Chapter II, we described a mechanism by which ZIKV NS3 binds to 14-3-3ϵ to antagonize antiviral signaling through the RIG-I innate immune induction pathway.

- Induction of type I IFN during ZIKV infection of astrocytes is dependent upon both RIG-I and MDA5, as well as the 14-3-3 proteins associated with their respective signaling pathways, 14-3-3ϵ and 14-3-3η.

- ZIKV NS3 encodes a phosphomimetic motif, 64-RLDP-67, which enables binding to 14-3-3ϵ. Mutation of this motif to 64-KIKP-67 results in a loss of the NS3-14-3-3ϵ interaction.

- ZIKV NS3 antagonizes RIG-I-mediated IFN induction through sequestration of 14-3-3ϵ.

- Generation of a mutant recombinant ZIKV deficient in the NS3-14-3-3ϵ interaction, ZIKV(KIKP), revealed that this interaction is important for the evasion of the type I IFN response by ZIKV and thereby for ZIKV replication.

- ZIKV(KIKP) elicits enhanced RIG-I cytosol-to-mitochondria translocation. Moreover, loss of the NS3-14-3-3ϵ interaction attenuates ZIKV replication due to enhanced cytokine and ISG induction.

In Chapter III, we demonstrated that ZIKV, DENV, and WNV NS3 antagonize MDA5 signaling through an interaction with 14-3-3η.

- ZIKV NS3 utilizes its phosphomimetic 64-RLDP-67 motif to interact with 14-3-3η. Mutation of this motif to 64-KIKP-67 results in a loss of the NS3-14-3-3η interaction.

- The NS3 proteins of DENV and WNV also bind to 14-3-3η. All three flavivirus NS3 proteins antagonize induction of IFN mediated by MDA5.

- Loss of the NS3-14-3-3η interaction elicits enhanced innate immune induction during ZIKV infection due to an inability to block the cytosol-to-mitochondria translocation of MDA5.

- The replication of ZIKV(KIKP) is attenuated as compared to ZIKV(WT) in a MAVS- and 14-3-3ϵ/η-dependent manner.

- ZIKV(KIKP) replication is controlled by both RIG-I and MDA5 in a non-redundant fashion in astrocytes. ZIKV(KIKP) is similarly controlled by both 14-3-3ϵ and 14-3-3η.

In Chapter IV, we found that WNV(KIKP) has diminished pathogenicity in mice as compared to WNV(WT), and that loss of the NS3-14-3-3 protein interaction pressures WNV to evolve a compensatory 14-3-3-binding mechanism that is dependent on phosphorylation. Furthermore, we found that a similar 14-3-3ϵ binding mechanism naturally occurs in POWV.

- The pathogenicity of WNV(KIKP) is attenuated as compared to WNV(WT) during infection of WT mice (C57BL/6J) , but not MAVS$^{-/-}$ mice (C57BL/6J).

- WNV(KIKP) experiences selective pressure to create a compensatory 14-3-3-binding mutation, 64-TIKP-67. Our data demonstrate that WNV(TIKP) arose to enable the NS3-14-3-3ϵ interaction. Phosphorylation of T64 enables NS3-TIKP to bind and sequester 14-3-3ϵ from the RIG-I-14-3-3ϵ interaction.

- The NS3 protein of POWV (strain LB) binds to 14-3-3ϵ utilizing a phosphorylated

peptide, a binding mode that is similar to that of the WNV NS3-TIKP protein.

Taken together, our results demonstrate that evasion of the RLR proteins RIG-I and MDA5 by certain flaviviruses is mediated by a phosphomimetic 14-3-3-binding motif in their NS3 protein. The NS3-14-3-3-interaction enables evasion of RLR signaling pathways in cell culture during ZIKV infection and in a mouse model of WNV infection. Furthermore, a related NS3-14-3-3ϵ interaction is conserved in certain strains of the tick-borne POWV. Together, these results highlight the importance of RLR subversion for successful replication of multiple members of *Flaviviridae*.

5.2 Concluding remarks and perspectives

5.2.1 Emerging flaviviruses and human health

Although we now recognize DENV, WNV, and ZIKV as hazards to human health, these viruses have only been recently identified as such. These, and other yet unidentified emerging and re-emerging arthropod-borne flaviviruses, present a major problem to human health and economic stability given their potential to re-emerge in naïve populations. Without proper treatment options, these viruses have epidemic potential to cause a significant burden on global health. This conserved emergent potential warrants intensive study of their underlying biology and pathogenesis.

ZIKV has only recently been identified as a public health threat. The virus was first identified in 1947 through a YFV surveillance program[9]. Between the first identification of the virus and the year 2000, there were less than 20 instances of human disease recorded[3]. In the mid-to-late 2000s, the virus caused two larger instances of epidemic disease in the South Pacific. Very quickly the virus gained international attention when it caused a major epidemic spanning over 50 countries in South and Central America between 2014-2016[3]. Moreover, the symptoms of ZIKV disease broadened to reflect the neurotropic nature of the virus during these more recent outbreaks—i.e., Guillain-Barre syndrome in

adults and congenital ZIKV syndrome in newborn infants vertically infected[16]. The reason for this broadening of symptoms associated with ZIKV infection is not entirely understood, and could be attributed to alterations of viral genetics, characteristics of the naïve populations to which the virus was introduced, or the scale of the ZIKV outbreaks in the 21st century. Although herd immunity slowed the 2016 outbreak to a halt, the distinct possibility of epidemic ZIKV reemergence remains a threat. Furthermore, ZIKV was relatively unheard of prior to 2015. Similarly, a great number of other flaviviruses have not yet caused outbreaks of disease, but their emergent potential dictates that shared mechanisms of pathogenesis should be carefully evaluated and targeted for treatment.

WNV was first identified in 1937 and caused several epidemics of febrile disease in humans before an absence of disease between 1975 and 1993. In the late 1990s, several epidemics occurred that included encephalitic WNV infection, most notably the outbreak in 1999 in New York, but similar epidemics also occurred in North Africa, Europe, and the Middle East[31]. WNV has since been endemic in the United States, and is prevalent even in many urban areas of the world. Therefore, in a short amount of time, WNV has become endemic to many parts of the world, and remains a significant threat to human health.

Incidence of febrile DENV disease has been recorded for over 200 years, but more severe symptoms (e.g. hemorrhagic fever and shock syndrome) were not recorded until the 1950s[134]. DENV is a re-emerging pathogen, with an increasing number of regions becoming hyperendemic with multiple serotypes. This virus remains a perennial threat, as roughly half of the world's population inhabits DENV-endemic regions[23,26]. Therefore, it remains of grave importance to study the mechanisms of viral pathogenesis associated with this virus. This becomes particularly difficult due to the fact that immunocompetent mice do not display DENV disease symptoms. However, WNV readily infects and causes relevant disease symptoms in mice, thereby highlighting a need to study shared mechanisms of viral pathogenesis between members of *Flaviviridae*.

To date, POWV has not caused large outbreaks of disease, though POWV disease can be fatal in the rare number of incidences that occur each year. Unfortunately, this tickborne virus has shown increased incidence of transmission in the past decade in comparison to earlier decades[37,38]. Previous examples of shifts in flavivirus epidemiology and disease indicate that new strains of POWV that are more pathogenic, or introduction of extant strains to more susceptible populations, have the potential to cause great disease burdens in human populations. Therefore, to ward off the increasing threat of flaviviral disease, it is of paramount importance to understand the underlying biology of these viruses. With this knowledge, better therapeutics can be generated before epidemics of disease can gain a foothold.

5.2.2 14-3-3-specific protein antagonism by flaviviruses

Both RIG-I and MDA5 detect RNA within the cytosol of infected cells, but a number of studies, as well as research in this dissertation, have demonstrated that both are critical and non-redundant in controlling DENV, WNV, and ZIKV infection[74,92,95,126]. Our work has found that by antagonizing 14-3-3 protein interactions with RIG-I and MDA5 enables these viruses to subvert innate immune induction to promote their replication. This successful competition for 14-3-3 proteins with RLRs is mediated by a phosphomimetic motif in NS3 that appears to have a higher binding affinity than the RLR-14-3-3 interactions that are expected to be regulated by phosphorylation and dephosphorylation. Although it is expected that RIG-I and MDA5 bind to 14-3-3ϵ and 14-3-3η via a phosphorylated motif, such a motif has never been identified in either sensor. Previous studies have identified the N-terminal CARD regions of RIG-I and MDA5 as sufficient for binding to the associated 14-3-3 protein, but future work should further define the 14-3-3 interaction site in each sensor[84,86]. Limited examples have been found wherein cellular proteins bind to 14-3-3 proteins via non-phosphorylated interaction motifs, and the possibility remains that RIG-I and MDA5 bind to 14-3-3ϵ and 14-3-3η as such[113]. Moreover, identification of the 14-3-3 interaction site in these sensors would further elucidate the mechanisms regulat-

ing RLR-14-3-3 interactions—-regulatable phosphorylation and dephosphorylation events mediated by cellular kinases and phosphatases, or conformational change unmasking 14-3-3 interaction sites are two distinct possibilities of regulation.

Intriguingly, we found that a phosphorylation-based NS3-14-3-3ϵ interaction is utilized by WNV NS3-TIKP to antagonize the RIG-I-14-3-3ϵ interaction, suggesting that NS3 can outcompete RLR-14-3-3ϵ protein interactions even without a phosphomimetic motif. Along these lines, we found that POWV NS3 (strain LB) encodes a phosphorylatable 14-3-3ϵ-interaction motif. We suggest that this phosphorylation-based mode of binding to 14-3-3ϵ is again sufficient to compete for RIG-I-14-3-3ϵ interaction, and thereby antagonize RIG-I signaling. However, future work will have to determine if POWV is indeed detected by the RLR signaling pathways, and furthermore whether POWV utilizes its 14-3-3ϵ interaction motif to antagonize RLR-mediated innate immune induction.

An NS3-14-3-3 interaction via a phosphorylated residue implies a level of regulation subject to dynamic phosphorylation and dephosphorylation by cellular kinases and phosphatases. However, in the absence of any phosphatase inhibitor, we did not detect a major loss of POWV NS3 (strain LB) phosphorylation; this suggests that cellular phosphatases do not efficiently dephosphorylate POWV NS3. If it is true that cellular phosphatases do not act on POWV NS3 (strain LB)—or, by extension of this logic, the WNV(TIKP) motif—it follows that these NS3 proteins can efficiently antagonize RIG-I and MDA5 signaling due to a high baseline phosphorylation of their 14-3-3-interaction motifs. Given that these interactions are mediated by phosphorylated residues—in contrast to the phosphomimetic motifs of DENV, WNV, and ZIKV—POWV NS3 and WNV NS3(TIKP) are very likely reliant on the activity of cellular kinases to sequester 14-3-3 proteins and subvert RLR-mediated immunity. Therefore, the identification of these cellular kinases that phosphorylate NS3 and enable immune evasion should be of great interest to future work that seeks to attenuate POWV infection through targeting cellular components.

A recurring puzzle that arises from the work in this dissertation is that flaviviruses target 14-3-3 proteins rather than directly targeting the RLRs. One possible explanation for this is that flavivirus NS3 proteins also modulate other 14-3-3-driven processes. For example, 14-3-3 proteins are involved in a number of different intracellular pathways aside from innate immunity, including cellular metabolism, protein trafficking, and autophagy, and DNA replication[87–89]. Flaviviruses could therefore antagonize other intracellular processes to enhance replication, in addition to evasion of innate immune induction. For example, the HCV core protein binds to a 14-3-3 protein to activate the Raf-1 cellular kinase involved in the MAPK cell signaling pathway[116]. NS3-14-3-3 protein interactions could modulate intracellular pathways in a cell-type dependent manner, as well. While ZIKV infection of astrocytes is controlled by RIG-I and MDA5, other research has shown that in A549 cells, detection of ZIKV is predominantly through RIG-I[93,94]. Because certain cellular pathways have cell-type dependent importance to cellular function, it follows that other 14-3-3-driven pathways can play a greater role in other cell types, and thus have a greater role in viral replication in other cell types.

Another explanation for antagonism of 14-3-3 proteins rather than direct antagonism of RLR proteins relates to the host tropism of these viruses. While mosquitos do not have type I IFN or associated nucleic acid sensors RIG-I or MDA5, the genomes of mosquito and tick species encode for two 14-3-3 proteins. It is conceivable that the NS3 proteins of flaviviruses target 14-3-3-driven pathways in arthropod species. Whether this is related to Dicer-mediated immunity or other intracellular pathways should be experimentally evaluated.

5.2.3 Targeting flavivirus NS3-14-3-3 interaction for therapeutics

While the catalytic protease activity of flaviviral NS2B-3 proteins provides a tantalizing target for the development of antiviral drugs given its essential function in the viral life cycle, it has proven a challenge to develop effective inhibitors. This is in part due to

the superficial and solvent exposed substrate pocket of the protease domain[135]. Our work in identifying 14-3-3 proteins as major players in the flaviviral innate immune strategy provides a druggable cellular target during infection, and provides the idea that targeting the 14-3-3 interaction motif in NS3 may prove a useful tool in targeting flaviviral infection with antiviral drugs. Given that POWV appears to bind to 14-3-3ϵ through a phosphorylated residue, we expect that a cellular kinase phosphorylates POWV NS3. While the identity of this cellular kinase must be revealed by future work, we propose that this kinase can be similarly targeted by a chemical inhibitor to quell POWV evasion of innate immunity.

REFERENCES

1. Chong, H. Y.; Leow, C. Y.; Abdul Majeed, A. B.; Leow, C. H. Flavivirus infection-A review of immunopathogenesis, immunological response, and immunodiagnosis. *Virus Res* **2019**, *274*, 197770.

2. Lindenbach, H. R. C., Brett; Thiel Flaviviridae: The viruses and their replication. *Fields Virology* **2007**, 1101–1151.

3. Song, B. H.; Yun, S. I.; Woolley, M.; Lee, Y. M. Zika virus: History, epidemiology, transmission, and clinical presentation. *J Neuroimmunol* **2017**, *308*, 50–64.

4. Miller, J. L.; de Wet, B. J.; Martinez-Pomares, L.; Radcliffe, C. M.; Dwek, R. A.; Rudd, P. M.; Gordon, S. The mannose receptor mediates dengue virus infection of macrophages. *PLoS Pathog* **2008**, *4*, e17.

5. Meertens, L.; Labeau, A.; Dejarnac, O.; Cipriani, S.; Sinigaglia, L.; Bonnet-Madin, L.; Le Charpentier, T.; Hafirassou, M. L.; Zamborlini, A.; Cao-Lormeau, V. M.; Coulpier, M.; Misse, D.; Jouvenet, N.; Tabibiazar, R.; Gressens, P.; Schwartz, O.; Amara, A. Axl Mediates ZIKA Virus Entry in Human Glial Cells and Modulates Innate Immune Responses. *Cell Rep* **2017**, *18*, 324–333.

6. Neufeldt, C. J.; Cortese, M.; Acosta, E. G.; Bartenschlager, R. Rewiring cellular networks by members of the Flaviviridae family. *Nat Rev Microbiol* **2018**, *16*, 125–142.

7. Apte-Sengupta, S.; Sirohi, D.; Kuhn, R. J. Coupling of replication and assembly in flaviviruses. *Curr Opin Virol* **2014**, *9*, 134–42.

8. Welsch, S.; Miller, S.; Romero-Brey, I.; Merz, A.; Bleck, C. K.; Walther, P.; Fuller, S. D.; Antony, C.; Krijnse-Locker, J.; Bartenschlager, R. Composition and three-dimensional architecture of the dengue virus replication and assembly sites. *Cell Host Microbe* **2009**, *5*, 365–75.

9. Dick, G. W.; Kitchen, S. F.; Haddow, A. J. Zika virus. I. Isolations and serological specificity. *Trans R Soc Trop Med Hyg* **1952**, *46*, 509–20.

10. Robert S. Lanciotti, J. J. L. J. O. V. A. J. L. A. J. J. S. M. S. M. R. D., Olga L. Kosoy Genetic and Serologic Properties of Zika Virus Associated with an Epidemic, Yap State, Micronesia, 2007. *Emerging Infectious Diseases* **2008**, *Vol. 14*.

11. Faria, N. R.; Azevedo, R.; Kraemer, M. U. G.; Souza, R.; Cunha, M. S.; Hill, S. C.; Theze, J.; Bonsall, M. B.; Bowden, T. A.; Rissanen, I.; Rocco, I. M.; Nogueira, J. S.; Maeda, A. Y.; Vasami, F.; Macedo, F. L. L.; Suzuki, A.; Rodrigues, S. G.; Cruz, A. C. R.; Nunes, B. T.; Medeiros, D. B. A.; Rodrigues, D. S. G.; Queiroz, A. L. N.; da Silva, E. V. P.; Henriques, D. F.; da Rosa, E. S. T.; de Oliveira, C. S.; Martins, L. C.; Vasconcelos, H. B.; Casseb, L. M. N.; Simith, D. B.; Messina, J. P.; Abade, L.; Lourenco, J.; Alcantara, L. C. J.; de Lima, M. M.; Giovanetti, M.; Hay, S. I.; de Oliveira, R. S.; Lemos, P. D. S.; de Oliveira, L. F.; de Lima, C. P. S.; da Silva, S. P.;

de Vasconcelos, J. M.; Franco, L.; Cardoso, J. F.; Vianez-Junior, J.; Mir, D.; Bello, G.; Delatorre, E.; Khan, K.; Creatore, M.; Coelho, G. E.; de Oliveira, W. K.; Tesh, R.; Pybus, O. G.; Nunes, M. R. T.; Vasconcelos, P. F. C. Zika virus in the Americas: Early epidemiological and genetic findings. *Science* **2016**, *352*, 345–349.

12. Pierson, T. C.; Diamond, M. S. The emergence of Zika virus and its new clinical syndromes. *Nature* **2018**, *560*, 573–581.

13. Messina, J. P.; Kraemer, M. U.; Brady, O. J.; Pigott, D. M.; Shearer, F. M.; Weiss, D. J.; Golding, N.; Ruktanonchai, C. W.; Gething, P. W.; Cohn, E.; Brownstein, J. S.; Khan, K.; Tatem, A. J.; Jaenisch, T.; Murray, C. J.; Marinho, F.; Scott, T. W.; Hay, S. I. Mapping global environmental suitability for Zika virus. *Elife* **2016**, *5*.

14. Vasilakis, N.; Weaver, S. C. Flavivirus transmission focusing on Zika. *Curr Opin Virol* **2017**, *22*, 30–35.

15. Foy, B. D.; Kobylinski, K. C.; Chilson Foy, J. L.; Blitvich, B. J.; Travassos da Rosa, A.; Haddow, A. D.; Lanciotti, R. S.; Tesh, R. B. Probable non-vector-borne transmission of Zika virus, Colorado, USA. *Emerg Infect Dis* **2011**, *17*, 880–2.

16. Miner, J. J.; Diamond, M. S. Zika Virus Pathogenesis and Tissue Tropism. *Cell Host Microbe* **2017**, *21*, 134–142.

17. Oliveira Melo, A. S.; Malinger, G.; Ximenes, R.; Szejnfeld, P. O.; Alves Sampaio, S.; Bispo de Filippis, A. M. Zika virus intrauterine infection causes fetal brain abnormality and microcephaly: tip of the iceberg? *Ultrasound Obstet Gynecol* **2016**, *47*, 6–7.

18. Gao, D.; Lou, Y.; He, D.; Porco, T. C.; Kuang, Y.; Chowell, G.; Ruan, S. Prevention and Control of Zika as a Mosquito-Borne and Sexually Transmitted Disease: A Mathematical Modeling Analysis. *Sci Rep* **2016**, *6*, 28070.

19. Li, C.; Xu, D.; Ye, Q.; Hong, S.; Jiang, Y.; Liu, X.; Zhang, N.; Shi, L.; Qin, C. F.; Xu, Z. Zika Virus Disrupts Neural Progenitor Development and Leads to Microcephaly in Mice. *Cell Stem Cell* **2016**, *19*, 120–6.

20. Tang, H.; Hammack, C.; Ogden, S. C.; Wen, Z.; Qian, X.; Li, Y.; Yao, B.; Shin, J.; Zhang, F.; Lee, E. M.; Christian, K. M.; Didier, R. A.; Jin, P.; Song, H.; Ming, G. L. Zika Virus Infects Human Cortical Neural Progenitors and Attenuates Their Growth. *Cell Stem Cell* **2016**, *18*, 587–90.

21. Bhatnagar, J.; Rabeneck, D. B.; Martines, R. B.; Reagan-Steiner, S.; Ermias, Y.; Estetter, L. B.; Suzuki, T.; Ritter, J.; Keating, M. K.; Hale, G.; Gary, J.; Muehlenbachs, A.; Lambert, A.; Lanciotti, R.; Oduyebo, T.; Meaney-Delman, D.; Bolanos, F.; Saad, E. A.; Shieh, W. J.; Zaki, S. R. Zika Virus RNA Replication and Persistence in Brain and Placental Tissue. *Emerg Infect Dis* **2017**, *23*, 405–414.

22. Huang, W. C.; Abraham, R.; Shim, B. S.; Choe, H.; Page, D. T. Zika virus infection during the period of maximal brain growth causes microcephaly and corticospinal neuron apoptosis in wild type mice. *Sci Rep* **2016**, *6*, 34793.

23. Gubler, D. J. Dengue and dengue hemorrhagic fever. *Clin Microbiol Rev* **1998**, *11*, 480–96.

24. Bhatt, S.; Gething, P. W.; Brady, O. J.; Messina, J. P.; Farlow, A. W.; Moyes, C. L.; Drake, J. M.; Brownstein, J. S.; Hoen, A. G.; Sankoh, O.; Myers, M. F.; George, D. B.; Jaenisch, T.; Wint, G. R.; Simmons, C. P.; Scott, T. W.; Farrar, J. J.; Hay, S. I. The global distribution and burden of dengue. *Nature* **2013**, *496*, 504–7.

25. St John, A. L.; Abraham, S. N.; Gubler, D. J. Barriers to preclinical investigations of anti-dengue immunity and dengue pathogenesis. *Nat Rev Microbiol* **2013**, *11*, 420–6.

26. Guzman, M. G.; Harris, E. Dengue. *Lancet* **2015**, *385*, 453–65.

27. Katzelnick, L. C.; Gresh, L.; Halloran, M. E.; Mercado, J. C.; Kuan, G.; Gordon, A.; Balmaseda, A.; Harris, E. Antibody-dependent enhancement of severe dengue disease in humans. *Science* **2017**, *358*, 929–932.

28. Kyle, J. L.; Beatty, P. R.; Harris, E. Dengue virus infects macrophages and dendritic cells in a mouse model of infection. *J Infect Dis* **2007**, *195*, 1808–17.

29. Schmid, M. A.; Harris, E. Monocyte recruitment to the dermis and differentiation to dendritic cells increases the targets for dengue virus replication. *PLoS Pathog* **2014**, *10*, e1004541.

30. John, D. V.; Lin, Y. S.; Perng, G. C. Biomarkers of severe dengue disease - a review. *J Biomed Sci* **2015**, *22*, 83.

31. Campbell, G. L.; Marfin, A. A.; Lanciotti, R. S.; Gubler, D. J. West Nile virus. *Lancet Infect Dis* **2002**, *2*, 519–29.

32. Samuel, M. A.; Diamond, M. S. Pathogenesis of West Nile Virus infection: a balance between virulence, innate and adaptive immunity, and viral evasion. *J Virol* **2006**, *80*, 9349–60.

33. Brault, A. C. Changing patterns of West Nile virus transmission: altered vector competence and host susceptibility. *Vet Res* **2009**, *40*, 43.

34. Byrne, S. N.; Halliday, G. M.; Johnston, L. J.; King, N. J. Interleukin-1beta but not tumor necrosis factor is involved in West Nile virus-induced Langerhans cell migration from the skin in C57BL/6 mice. *J Invest Dermatol* **2001**, *117*, 702–9.

35. Maximova, O. A.; Pletnev, A. G. Flaviviruses and the Central Nervous System: Revisiting Neuropathological Concepts. *Annu Rev Virol* **2018**, *5*, 255–272.

36. Mc, L. D.; Donohue, W. L. Powassan virus: isolation of virus from a fatal case of encephalitis. *Can Med Assoc J* **1959**, *80*, 708–11.

37. Kemenesi, G.; Banyai, K. Tick-Borne Flaviviruses, with a Focus on Powassan Virus. *Clin Microbiol Rev* **2019**, *32*.

38. Fatmi, S. S.; Zehra, R.; Carpenter, D. O. Powassan Virus-A New Reemerging Tick-Borne Disease. *Front Public Health* **2017**, *5*, 342.

39. Ebel, G. D.; Kramer, L. D. Short report: duration of tick attachment required for transmission of powassan virus by deer ticks. *Am J Trop Med Hyg* **2004**, *71*, 268–71.

40. Hermance, M. E.; Thangamani, S. Proinflammatory cytokines and chemokines at the skin interface during Powassan virus transmission. *J Invest Dermatol* **2014**, *134*, 2280–2283.

41. Hermance, M. E.; Santos, R. I.; Kelly, B. C.; Valbuena, G.; Thangamani, S. Immune Cell Targets of Infection at the Tick-Skin Interface during Powassan Virus Transmission. *PLoS One* **2016**, *11*, e0155889.

42. Beasley, D. W.; Suderman, M. T.; Holbrook, M. R.; Barrett, A. D. Nucleotide sequencing and serological evidence that the recently recognized deer tick virus is a genotype of Powassan virus. *Virus Res* **2001**, *79*, 81–9.

43. Kuno, G.; Artsob, H.; Karabatsos, N.; Tsuchiya, K. R.; Chang, G. J. Genomic sequencing of deer tick virus and phylogeny of powassan-related viruses of North America. *Am J Trop Med Hyg* **2001**, *65*, 671–6.

44. Ebel, G. D. Update on Powassan virus: emergence of a North American tick-borne flavivirus. *Annu Rev Entomol* **2010**, *55*, 95–110.

45. Tavakoli, N. P.; Wang, H.; Dupuis, M.; Hull, R.; Ebel, G. D.; Gilmore, E. J.; Faust, P. L. Fatal case of deer tick virus encephalitis. *N Engl J Med* **2009**, *360*, 2099–107.

46. Benelli, G. Spread of Zika virus: The key role ofmosquito vector control. *Asian Pac J Trop Biomed* **2016**, *6*, 468–471.

47. Lees, R. S.; Gilles, J. R.; Hendrichs, J.; Vreysen, M. J.; Bourtzis, K. Back to the future: the sterile insect technique against mosquito disease vectors. *Curr Opin Insect Sci* **2015**, *10*, 156–162.

48. Collins, M. H.; Metz, S. W. Progress and Works in Progress: Update on Flavivirus Vaccine Development. *Clin Ther* **2017**, *39*, 1519–1536.

49. Capeding, M. R.; Tran, N. H.; Hadinegoro, S. R.; Ismail, H. I.; Chotpitayasunondh, T.; Chua, M. N.; Luong, C. Q.; Rusmil, K.; Wirawan, D. N.; Nallusamy, R.; Pitisuttithum, P.; Thisyakorn, U.; Yoon, I. K.; van der Vliet, D.; Langevin, E.; Laot, T.; Hutagalung, Y.; Frago, C.; Boaz, M.; Wartel, T. A.; Tornieporth, N. G.; Saville, M.;

Bouckenooghe, A.; Group, C. Y. D. S. Clinical efficacy and safety of a novel tetravalent dengue vaccine in healthy children in Asia: a phase 3, randomised, observer-masked, placebo-controlled trial. *Lancet* **2014**, *384*, 1358–65.

50. Villar, L.; Dayan, G. H.; Arredondo-Garcia, J. L.; Rivera, D. M.; Cunha, R.; Deseda, C.; Reynales, H.; Costa, M. S.; Morales-Ramirez, J. O.; Carrasquilla, G.; Rey, L. C.; Dietze, R.; Luz, K.; Rivas, E.; Miranda Montoya, M. C.; Cortes Supelano, M.; Zambrano, B.; Langevin, E.; Boaz, M.; Tornieporth, N.; Saville, M.; Noriega, F.; Group, C. Y. D. S. Efficacy of a tetravalent dengue vaccine in children in Latin America. *N Engl J Med* **2015**, *372*, 113–23.

51. Bardina, S. V.; Bunduc, P.; Tripathi, S.; Duehr, J.; Frere, J. J.; Brown, J. A.; Nachbagauer, R.; Foster, G. A.; Krysztof, D.; Tortorella, D.; Stramer, S. L.; Garcia-Sastre, A.; Krammer, F.; Lim, J. K. Enhancement of Zika virus pathogenesis by preexisting antiflavivirus immunity. *Science* **2017**, *356*, 175–180.

52. Chow, K. T.; Gale, J., M.; Loo, Y. M. RIG-I and Other RNA Sensors in Antiviral Immunity. *Annu Rev Immunol* **2018**, *36*, 667–694.

53. Rehwinkel, J.; Gack, M. U. RIG-I-like receptors: their regulation and roles in RNA sensing. *Nat Rev Immunol* **2020**,

54. Schneider, W. M.; Chevillotte, M. D.; Rice, C. M. Interferon-stimulated genes: a complex web of host defenses. *Annu Rev Immunol* **2014**, *32*, 513–45.

55. Medzhitov, R. Recognition of microorganisms and activation of the immune response. *Nature* **2007**, *449*, 819–26.

56. Gay, N. J.; Gangloff, M. Structure and function of Toll receptors and their ligands. *Annu Rev Biochem* **2007**, *76*, 141–65.

57. Sun, L.; Wu, J.; Du, F.; Chen, X.; Chen, Z. J. Cyclic GMP-AMP synthase is a cytosolic DNA sensor that activates the type I interferon pathway. *Science* **2013**, *339*, 786–91.

58. Wu, J.; Sun, L.; Chen, X.; Du, F.; Shi, H.; Chen, C.; Chen, Z. J. Cyclic GMP-AMP is an endogenous second messenger in innate immune signaling by cytosolic DNA. *Science* **2013**, *339*, 826–30.

59. Xiao, T. S.; Fitzgerald, K. A. The cGAS-STING pathway for DNA sensing. *Mol Cell* **2013**, *51*, 135–9.

60. Aguirre, S.; Luthra, P.; Sanchez-Aparicio, M. T.; Maestre, A. M.; Patel, J.; Lamothe, F.; Fredericks, A. C.; Tripathi, S.; Zhu, T.; Pintado-Silva, J.; Webb, L. G.; Bernal-Rubio, D.; Solovyov, A.; Greenbaum, B.; Simon, V.; Basler, C. F.; Mulder, L. C.; Garcia-Sastre, A.; Fernandez-Sesma, A. Dengue virus NS2B protein targets cGAS for degradation and prevents mitochondrial DNA sensing during infection. *Nat Microbiol* **2017**, *2*, 17037.

61. Ding, Q.; Gaska, J. M.; Douam, F.; Wei, L.; Kim, D.; Balev, M.; Heller, B.; Ploss, A. Species-specific disruption of STING-dependent antiviral cellular defenses by the Zika virus NS2B3 protease. *Proc Natl Acad Sci U S A* **2018**, *115*, E6310–E6318.

62. Sun, B.; Sundstrom, K. B.; Chew, J. J.; Bist, P.; Gan, E. S.; Tan, H. C.; Goh, K. C.; Chawla, T.; Tang, C. K.; Ooi, E. E. Dengue virus activates cGAS through the release of mitochondrial DNA. *Sci Rep* **2017**, *7*, 3594.

63. Zheng, Y.; Liu, Q.; Wu, Y.; Ma, L.; Zhang, Z.; Liu, T.; Jin, S.; She, Y.; Li, Y. P.; Cui, J. Zika virus elicits inflammation to evade antiviral response by cleaving cGAS via NS1-caspase-1 axis. *EMBO J* **2018**, *37*.

64. Meylan, E.; Curran, J.; Hofmann, K.; Moradpour, D.; Binder, M.; Bartenschlager, R.; Tschopp, J. Cardif is an adaptor protein in the RIG-I antiviral pathway and is targeted by hepatitis C virus. *Nature* **2005**, *437*, 1167–72.

65. Hornung, V.; Ellegast, J.; Kim, S.; Brzozka, K.; Jung, A.; Kato, H.; Poeck, H.; Akira, S.; Conzelmann, K. K.; Schlee, M.; Endres, S.; Hartmann, G. 5'-Triphosphate RNA is the ligand for RIG-I. *Science* **2006**, *314*, 994–7.

66. Pichlmair, A.; Schulz, O.; Tan, C. P.; Naslund, T. I.; Liljestrom, P.; Weber, F.; Reis e Sousa, C. RIG-I-mediated antiviral responses to single-stranded RNA bearing 5'-phosphates. *Science* **2006**, *314*, 997–1001.

67. Liu, G.; Park, H. S.; Pyo, H. M.; Liu, Q.; Zhou, Y. Influenza A Virus Panhandle Structure Is Directly Involved in RIG-I Activation and Interferon Induction. *J Virol* **2015**, *89*, 6067–79.

68. Rehwinkel, J.; Tan, C. P.; Goubau, D.; Schulz, O.; Pichlmair, A.; Bier, K.; Robb, N.; Vreede, F.; Barclay, W.; Fodor, E.; Reis e Sousa, C. RIG-I detects viral genomic RNA during negative-strand RNA virus infection. *Cell* **2010**, *140*, 397–408.

69. Kato, H.; Takeuchi, O.; Sato, S.; Yoneyama, M.; Yamamoto, M.; Matsui, K.; Uematsu, S.; Jung, A.; Kawai, T.; Ishii, K. J.; Yamaguchi, O.; Otsu, K.; Tsujimura, T.; Koh, C. S.; Reis e Sousa, C.; Matsuura, Y.; Fujita, T.; Akira, S. Differential roles of MDA5 and RIG-I helicases in the recognition of RNA viruses. *Nature* **2006**, *441*, 101–5.

70. Saito, T.; Owen, D. M.; Jiang, F.; Marcotrigiano, J.; Gale, J., M. Innate immunity induced by composition-dependent RIG-I recognition of hepatitis C virus RNA. *Nature* **2008**, *454*, 523–7.

71. Malathi, K.; Dong, B.; Gale, J., M.; Silverman, R. H. Small self-RNA generated by RNase L amplifies antiviral innate immunity. *Nature* **2007**, *448*, 816–9.

72. Chiang, J. J.; Sparrer, K. M. J.; van Gent, M.; Lassig, C.; Huang, T.; Osterrieder, N.; Hopfner, K. P.; Gack, M. U. Viral unmasking of cellular 5S rRNA pseudogene transcripts induces RIG-I-mediated immunity. *Nat Immunol* **2018**, *19*, 53–62.

73. Dias Junior, A. G.; Sampaio, N. G.; Rehwinkel, J. A Balancing Act: MDA5 in Antiviral Immunity and Autoinflammation. *Trends Microbiol* **2019**, *27*, 75–85.

74. Loo, Y. M.; Fornek, J.; Crochet, N.; Bajwa, G.; Perwitasari, O.; Martinez-Sobrido, L.; Akira, S.; Gill, M. A.; Garcia-Sastre, A.; Katze, M. G.; Gale, J., M. Distinct RIG-I and MDA5 signaling by RNA viruses in innate immunity. *J Virol* **2008**, *82*, 335–45.

75. Gack, M. U.; Nistal-Villan, E.; Inn, K. S.; Garcia-Sastre, A.; Jung, J. U. Phosphorylation-mediated negative regulation of RIG-I antiviral activity. *J Virol* **2010**, *84*, 3220–9.

76. Nistal-Villan, E.; Gack, M. U.; Martinez-Delgado, G.; Maharaj, N. P.; Inn, K. S.; Yang, H.; Wang, R.; Aggarwal, A. K.; Jung, J. U.; Garcia-Sastre, A. Negative role of RIG-I serine 8 phosphorylation in the regulation of interferon-beta production. *J Biol Chem* **2010**, *285*, 20252–61.

77. Sun, Z.; Ren, H.; Liu, Y.; Teeling, J. L.; Gu, J. Phosphorylation of RIG-I by casein kinase II inhibits its antiviral response. *J Virol* **2011**, *85*, 1036–47.

78. Wies, E.; Wang, M. K.; Maharaj, N. P.; Chen, K.; Zhou, S.; Finberg, R. W.; Gack, M. U. Dephosphorylation of the RNA sensors RIG-I and MDA5 by the phosphatase PP1 is essential for innate immune signaling. *Immunity* **2013**, *38*, 437–49.

79. Gack, M. U.; Kirchhofer, A.; Shin, Y. C.; Inn, K. S.; Liang, C.; Cui, S.; Myong, S.; Ha, T.; Hopfner, K. P.; Jung, J. U. Roles of RIG-I N-terminal tandem CARD and splice variant in TRIM25-mediated antiviral signal transduction. *Proc Natl Acad Sci U S A* **2008**, *105*, 16743–8.

80. Gack, M. U.; Shin, Y. C.; Joo, C. H.; Urano, T.; Liang, C.; Sun, L.; Takeuchi, O.; Akira, S.; Chen, Z.; Inoue, S.; Jung, J. U. TRIM25 RING-finger E3 ubiquitin ligase is essential for RIG-I-mediated antiviral activity. *Nature* **2007**, *446*, 916–920.

81. Oshiumi, H.; Matsumoto, M.; Hatakeyama, S.; Seya, T. Riplet/RNF135, a RING finger protein, ubiquitinates RIG-I to promote interferon-beta induction during the early phase of viral infection. *J Biol Chem* **2009**, *284*, 807–17.

82. Oshiumi, H.; Miyashita, M.; Matsumoto, M.; Seya, T. A distinct role of Riplet-mediated K63-Linked polyubiquitination of the RIG-I repressor domain in human antiviral innate immune responses. *PLoS Pathog* **2013**, *9*, e1003533.

83. Sanchez, J. G.; Sparrer, K. M. J.; Chiang, C.; Reis, R. A.; Chiang, J. J.; Zurenski, M. A.; Wan, Y.; Gack, M. U.; Pornillos, O. TRIM25 Binds RNA to Modulate Cellular Anti-viral Defense. *J Mol Biol* **2018**, *430*, 5280–5293.

84. Liu, H. M.; Loo, Y. M.; Horner, S. M.; Zornetzer, G. A.; Katze, M. G.; Gale, J., M. The mitochondrial targeting chaperone 14-3-3epsilon regulates a RIG-I translocon that mediates membrane association and innate antiviral immunity. *Cell Host Microbe* **2012**, *11*, 528–37.

85. Horner, S. M.; Liu, H. M.; Park, H. S.; Briley, J.; Gale, J., M. Mitochondrial-associated endoplasmic reticulum membranes (MAM) form innate immune synapses and are targeted by hepatitis C virus. *Proc Natl Acad Sci U S A* **2011**, *108*, 14590–5.

86. Lin, J. P.; Fan, Y. K.; Liu, H. M. The 14-3-3eta chaperone protein promotes antiviral innate immunity via facilitating MDA5 oligomerization and intracellular redistribution. *PLoS Pathog* **2019**, *15*, e1007582.

87. Pennington, K. L.; Chan, T. Y.; Torres, M. P.; Andersen, J. L. The dynamic and stress-adaptive signaling hub of 14-3-3: emerging mechanisms of regulation and context-dependent protein-protein interactions. *Oncogene* **2018**, *37*, 5587–5604.

88. Johnson, C.; Crowther, S.; Stafford, M. J.; Campbell, D. G.; Toth, R.; MacKintosh, C. Bioinformatic and experimental survey of 14-3-3-binding sites. *Biochem J* **2010**, *427*, 69–78.

89. Nomura, M.; Shimizu, S.; Sugiyama, T.; Narita, M.; Ito, T.; Matsuda, H.; Tsujimoto, Y. 14-3-3 Interacts directly with and negatively regulates pro-apoptotic Bax. *J Biol Chem* **2003**, *278*, 2058–65.

90. Runge, S.; Sparrer, K. M.; Lassig, C.; Hembach, K.; Baum, A.; Garcia-Sastre, A.; Soding, J.; Conzelmann, K. K.; Hopfner, K. P. In vivo ligands of MDA5 and RIG-I in measles virus-infected cells. *PLoS Pathog* **2014**, *10*, e1004081.

91. Sanchez David, R. Y.; Combredet, C.; Sismeiro, O.; Dillies, M. A.; Jagla, B.; Coppee, J. Y.; Mura, M.; Guerbois Galla, M.; Despres, P.; Tangy, F.; Komarova, A. V. Comparative analysis of viral RNA signatures on different RIG-I-like receptors. *Elife* **2016**, *5*, e11275.

92. Errett, J. S.; Suthar, M. S.; McMillan, A.; Diamond, M. S.; Gale, J., M. The essential, nonredundant roles of RIG-I and MDA5 in detecting and controlling West Nile virus infection. *J Virol* **2013**, *87*, 11416–25.

93. Esser-Nobis, K.; Aarreberg, L. D.; Roby, J. A.; Fairgrieve, M. R.; Green, R.; Gale, J., M. Comparative Analysis of African and Asian Lineage-Derived Zika Virus Strains Reveals Differences in Activation of and Sensitivity to Antiviral Innate Immunity. *J Virol* **2019**, *93*.

94. Hertzog, J.; Dias Junior, A. G.; Rigby, R. E.; Donald, C. L.; Mayer, A.; Sezgin, E.; Song, C.; Jin, B.; Hublitz, P.; Eggeling, C.; Kohl, A.; Rehwinkel, J. Infection with a Brazilian isolate of Zika virus generates RIG-I stimulatory RNA and the viral NS5 protein blocks type I IFN induction and signaling. *Eur J Immunol* **2018**, *48*, 1120–1136.

95. Ma, J.; Ketkar, H.; Geng, T.; Lo, E.; Wang, L.; Xi, J.; Sun, Q.; Zhu, Z.; Cui, Y.; Yang, L.; Wang, P. Zika Virus Non-structural Protein 4A Blocks the RLR-MAVS Signaling. *Front Microbiol* **2018**, *9*, 1350.

96. Serman, T. M.; Gack, M. U. Evasion of Innate and Intrinsic Antiviral Pathways by the Zika Virus. *Viruses* **2019**, *11*.

97. Chazal, M.; Beauclair, G.; Gracias, S.; Najburg, V.; Simon-Loriere, E.; Tangy, F.; Komarova, A. V.; Jouvenet, N. RIG-I Recognizes the 5' Region of Dengue and Zika Virus Genomes. *Cell Rep* **2018**, *24*, 320–328.

98. Uchida, L.; Espada-Murao, L. A.; Takamatsu, Y.; Okamoto, K.; Hayasaka, D.; Yu, F.; Nabeshima, T.; Buerano, C. C.; Morita, K. The dengue virus conceals double-stranded RNA in the intracellular membrane to escape from an interferon response. *Sci Rep* **2014**, *4*, 7395.

99. Bradrick, S. S. Causes and Consequences of Flavivirus RNA Methylation. *Front Microbiol* **2017**, *8*, 2374.

100. Chang, D. C.; Hoang, L. T.; Mohamed Naim, A. N.; Dong, H.; Schreiber, M. J.; Hibberd, M. L.; Tan, M. J. A.; Shi, P. Y. Evasion of early innate immune response by 2'-O-methylation of dengue genomic RNA. *Virology* **2016**, *499*, 259–266.

101. Chan, Y. K.; Gack, M. U. Viral evasion of intracellular DNA and RNA sensing. *Nat Rev Microbiol* **2016**, *14*, 360–73.

102. Chan, Y. K.; Gack, M. U. A phosphomimetic-based mechanism of dengue virus to antagonize innate immunity. *Nat Immunol* **2016**, *17*, 523–30.

103. He, Z.; Zhu, X.; Wen, W.; Yuan, J.; Hu, Y.; Chen, J.; An, S.; Dong, X.; Lin, C.; Yu, J.; Wu, J.; Yang, Y.; Cai, J.; Li, J.; Li, M. Dengue Virus Subverts Host Innate Immunity by Targeting Adaptor Protein MAVS. *J Virol* **2016**, *90*, 7219–7230.

104. Li, X. D.; Sun, L.; Seth, R. B.; Pineda, G.; Chen, Z. J. Hepatitis C virus protease NS3/4A cleaves mitochondrial antiviral signaling protein off the mitochondria to evade innate immunity. *Proc Natl Acad Sci U S A* **2005**, *102*, 17717–22.

105. Manokaran, G.; Finol, E.; Wang, C.; Gunaratne, J.; Bahl, J.; Ong, E. Z.; Tan, H. C.; Sessions, O. M.; Ward, A. M.; Gubler, D. J.; Harris, E.; Garcia-Blanco, M. A.; Ooi, E. E. Dengue subgenomic RNA binds TRIM25 to inhibit interferon expression for epidemiological fitness. *Science* **2015**, *350*, 217–21.

106. Chang, R. Y.; Hsu, T. W.; Chen, Y. L.; Liu, S. F.; Tsai, Y. J.; Lin, Y. T.; Chen, Y. S.; Fan, Y. H. Japanese encephalitis virus non-coding RNA inhibits activation of interferon by blocking nuclear translocation of interferon regulatory factor 3. *Vet Microbiol* **2013**, *166*, 11–21.

107. Donald, C. L.; Brennan, B.; Cumberworth, S. L.; Rezelj, V. V.; Clark, J. J.; Cordeiro, M. T.; Freitas de Oliveira Franca, R.; Pena, L. J.; Wilkie, G. S.; Da Silva Filipe, A.; Davis, C.; Hughes, J.; Varjak, M.; Selinger, M.; Zuvanov, L.; Owsianka, A. M.; Patel, A. H.; McLauchlan, J.; Lindenbach, B. D.; Fall, G.; Sall, A. A.; Biek, R.; Rehwinkel, J.; Schnettler, E.; Kohl, A. Full Genome Sequence and sfRNA Interferon Antagonist Activity of Zika Virus from Recife, Brazil. *PLoS Negl Trop Dis* **2016**, *10*, e0005048.

108. Schuessler, A.; Funk, A.; Lazear, H. M.; Cooper, D. A.; Torres, S.; Daffis, S.; Jha, B. K.; Kumagai, Y.; Takeuchi, O.; Hertzog, P.; Silverman, R.; Akira, S.; Barton, D. J.; Diamond, M. S.; Khromykh, A. A. West Nile virus noncoding subgenomic RNA contributes to viral evasion of the type I interferon-mediated antiviral response. *J Virol* **2012**, *86*, 5708–18.

109. Dalrymple, N. A.; Cimica, V.; Mackow, E. R. Dengue Virus NS Proteins Inhibit RIG-I/MAVS Signaling by Blocking TBK1/IRF3 Phosphorylation: Dengue Virus Serotype 1 NS4A Is a Unique Interferon-Regulating Virulence Determinant. *mBio* **2015**, *6*, e00553–15.

110. Wu, Y.; Liu, Q.; Zhou, J.; Xie, W.; Chen, C.; Wang, Z.; Yang, H.; Cui, J. Zika virus evades interferon-mediated antiviral response through the co-operation of multiple nonstructural proteins in vitro. *Cell Discov* **2017**, *3*, 17006.

111. Xia, H.; Luo, H.; Shan, C.; Muruato, A. E.; Nunes, B. T. D.; Medeiros, D. B. A.; Zou, J.; Xie, X.; Giraldo, M. I.; Vasconcelos, P. F. C.; Weaver, S. C.; Wang, T.; Rajsbaum, R.; Shi, P. Y. An evolutionary NS1 mutation enhances Zika virus evasion of host interferon induction. *Nat Commun* **2018**, *9*, 414.

112. Anglero-Rodriguez, Y. I.; Pantoja, P.; Sariol, C. A. Dengue virus subverts the interferon induction pathway via NS2B/3 protease-IkappaB kinase epsilon interaction. *Clin Vaccine Immunol* **2014**, *21*, 29–38.

113. Tzivion, G.; Avruch, J. 14-3-3 proteins: active cofactors in cellular regulation by serine/threonine phosphorylation. *J Biol Chem* **2002**, *277*, 3061–4.

114. Hamel, R.; Dejarnac, O.; Wichit, S.; Ekchariyawat, P.; Neyret, A.; Luplertlop, N.; Perera-Lecoin, M.; Surasombatpattana, P.; Talignani, L.; Thomas, F.; Cao-Lormeau, V. M.; Choumet, V.; Briant, L.; Despres, P.; Amara, A.; Yssel, H.; Misse, D. Biology of Zika Virus Infection in Human Skin Cells. *J Virol* **2015**, *89*, 8880–96.

115. Desmyter, J.; Melnick, J. L.; Rawls, W. E. Defectiveness of interferon production and of rubella virus interference in a line of African green monkey kidney cells (Vero). *J Virol* **1968**, *2*, 955–61.

116. Aoki, H.; Hayashi, J.; Moriyama, M.; Arakawa, Y.; Hino, O. Hepatitis C virus core protein interacts with 14-3-3 protein and activates the kinase Raf-1. *J Virol* **2000**, *74*, 1736–41.

117. Trujillo-Ocampo, A.; Cazares-Raga, F. E.; Del Angel, R. M.; Medina-Ramirez, F.; Santos-Argumedo, L.; Rodriguez, M. H.; Hernandez-Hernandez, F. C. Participation of 14-3-3epsilon and 14-3-3zeta proteins in the phagocytosis, component of cellular immune response, in Aedes mosquito cell lines. *Parasit Vectors* **2017**, *10*, 362.

118. Major, E. O.; Miller, A. E.; Mourrain, P.; Traub, R. G.; de Widt, E.; Sever, J. Establishment of a line of human fetal glial cells that supports JC virus multiplication. *Proc Natl Acad Sci U S A* **1985**, *82*, 1257–61.

119. Sapparapu, G.; Fernandez, E.; Kose, N.; Bin, C.; Fox, J. M.; Bombardi, R. G.; Zhao, H.; Nelson, C. A.; Bryan, A. L.; Barnes, T.; Davidson, E.; Mysorekar, I. U.; Fremont, D. H.; Doranz, B. J.; Diamond, M. S.; Crowe, J. E. Neutralizing human antibodies prevent Zika virus replication and fetal disease in mice. *Nature* **2016**, *540*, 443–447.

120. Brien, J. D.; Lazear, H. M.; Diamond, M. S. Propagation, quantification, detection, and storage of West Nile virus. *Curr Protoc Microbiol* **2013**, *31*, 15D 3 1–15D 3 18.

121. Schwarz, M. C.; Sourisseau, M.; Espino, M. M.; Gray, E. S.; Chambers, M. T.; Tortorella, D.; Evans, M. J. Rescue of the 1947 Zika Virus Prototype Strain with a Cytomegalovirus Promoter-Driven cDNA Clone. *mSphere* **2016**, *1*.

122. Lazear, H. M.; Govero, J.; Smith, A. M.; Platt, D. J.; Fernandez, E.; Miner, J. J.; Diamond, M. S. A Mouse Model of Zika Virus Pathogenesis. *Cell Host Microbe* **2016**, *19*, 720–30.

123. Zust, R.; Toh, Y. X.; Valdes, I.; Cerny, D.; Heinrich, J.; Hermida, L.; Marcos, E.; Guillen, G.; Kalinke, U.; Shi, P. Y.; Fink, K. Type I interferon signals in macrophages and dendritic cells control dengue virus infection: implications for a new mouse model to test dengue vaccines. *J Virol* **2014**, *88*, 7276–85.

124. Davis, M. E.; Wang, M. K.; Rennick, L. J.; Full, F.; Gableske, S.; Mesman, A. W.; Gringhuis, S. I.; Geijtenbeek, T. B.; Duprex, W. P.; Gack, M. U. Antagonism of the phosphatase PP1 by the measles virus V protein is required for innate immune escape of MDA5. *Cell Host Microbe* **2014**, *16*, 19–30.

125. Schoggins, J. W.; Rice, C. M. Interferon-stimulated genes and their antiviral effector functions. *Curr Opin Virol* **2011**, *1*, 519–25.

126. Riedl, W.; Acharya, D.; Lee, J. H.; Liu, G.; Serman, T.; Chiang, C.; Chan, Y. K.; Diamond, M. S.; Gack, M. U. Zika Virus NS3 Mimics a Cellular 14-3-3-Binding Motif to Antagonize RIG-I- and MDA5-Mediated Innate Immunity. *Cell Host Microbe* **2019**, *26*, 493–503 e6.

127. Kurhade, C.; Zegenhagen, L.; Weber, E.; Nair, S.; Michaelsen-Preusse, K.; Spanier, J.; Gekara, N. O.; Kroger, A.; Overby, A. K. Type I Interferon response in olfactory bulb, the site of tick-borne flavivirus accumulation, is primarily regulated by IPS-1. *J Neuroinflammation* **2016**, *13*, 22.

128. Lindqvist, R.; Upadhyay, A.; Overby, A. K. Tick-Borne Flaviviruses and the Type I Interferon Response. *Viruses* **2018**, *10*.

129. Overby, A. K.; Popov, V. L.; Niedrig, M.; Weber, F. Tick-borne encephalitis virus delays interferon induction and hides its double-stranded RNA in intracellular membrane vesicles. *J Virol* **2010**, *84*, 8470–83.

130. Graham, J. B.; Swarts, J. L.; Lund, J. M. A Mouse Model of West Nile Virus Infection. *Curr Protoc Mouse Biol* **2017**, *7*, 221–235.

131. Na, W.; Yeom, M.; Choi, I. K.; Yook, H.; Song, D. Animal models for dengue vaccine development and testing. *Clin Exp Vaccine Res* **2017**, *6*, 104–110.

132. Kinoshita, E.; Kinoshita-Kikuta, E.; Takiyama, K.; Koike, T. Phosphate-binding tag, a new tool to visualize phosphorylated proteins. *Mol Cell Proteomics* **2006**, *5*, 749–57.

133. Kinney, R. M.; Huang, C. Y.; Whiteman, M. C.; Bowen, R. A.; Langevin, S. A.; Miller, B. R.; Brault, A. C. Avian virulence and thermostable replication of the North American strain of West Nile virus. *J Gen Virol* **2006**, *87*, 3611–22.

134. Gould, E. A.; Solomon, T. Pathogenic flaviviruses. *Lancet* **2008**, *371*, 500–9.

135. Luo, D.; Vasudevan, S. G.; Lescar, J. The flavivirus NS2B-NS3 protease-helicase as a target for antiviral drug development. *Antiviral Res* **2015**, *118*, 148–58.